

## Small Polarons in Two-Dimensional Pnictogens: A First-Principles Study

Vasilii Vasilchenko, Sergey Levchenko, Vasili Perebeinos, and Andriy Zhugayevych\*



Cite This: *J. Phys. Chem. Lett.* 2021, 12, 4674–4680



Read Online

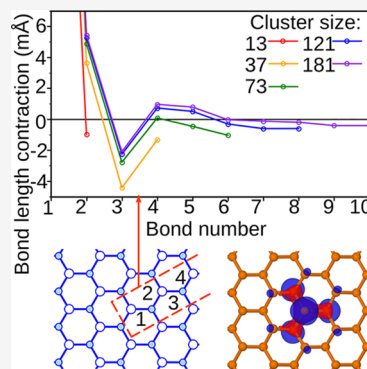
ACCESS |

Metrics & More

Article Recommendations

Supporting Information

**ABSTRACT:** We report the first-principles study of small polarons in the most stable two-dimensional pnictogen allotropes: blue and black phosphorene and arsenene. While both cations and anions of small hydrogen-passivated clusters show charge localization and local lattice distortions, only the hole polaron in the blue allotrope is stable in the infinite size cluster limit. The adiabatic polaron relaxation energy is found to be 0.1 eV for phosphorene and 0.15 eV for arsenene. The polaron is localized on lone-pair orbitals with half of the extra charge distributed among 13 atoms. In the blue phosphorene, these orbitals form the valence band's top with a relatively flat band dispersion. However, in the black phosphorene, lone-pair orbitals hybridize with bonding orbitals, which explains the difference in hole localization strength between the two topologically equivalent allotropes. The polaron's adiabatic barriers for motion are small compared to the most strongly coupled phonon frequency, implying the polaron barrierless motion.



Nowadays, several electronically different classes of two-dimensional (2D) semiconductors are well studied both theoretically and experimentally<sup>1–4</sup> including the graphene family, transition metal dichalcogenides,<sup>5,6</sup> and pnictogens<sup>7,8</sup> especially phosphorene.<sup>9–12</sup> Pnictogens belong to the group of average valence five materials known to have distinctive properties in three dimensions.<sup>13–15</sup> The electronic structure of 2D pnictogens has been intensively investigated with density functional theory (DFT),<sup>16–23</sup> and also charge carrier transport in the weak electron–phonon scattering regime has been considered.<sup>24–27</sup> However, to our knowledge, small-polaron effects have not been studied, which is the subject of the present work.

Polaron effects are ubiquitous in insulators<sup>28</sup> because of omnipresent electron–phonon interaction and no phase transition in simple models to rigorously differentiate polarons and free carriers<sup>29,30</sup> (such as localization in a static disorder). At the same time, the small adiabatic polaron is well-defined as a dynamically stable localized lattice deformation, and in the present work, we will use the “polaron” term in this context. Thus, defined polarons exist in organic semiconductors including molecular crystals,<sup>31–33</sup> halide perovskites,<sup>34</sup> transition metal oxides,<sup>35–37</sup> and ionic solids<sup>38</sup> and affect not only optoelectronic properties but also nonelectronic phenomena such as ion transport.<sup>39</sup> In 2D semiconductors, there is an experimental signature of large polarons in transition metal dichalcogenides<sup>40</sup> supported by the presence of strong electron–phonon coupling in these materials.<sup>41</sup> In 2D geometry, polarons can be additionally stabilized by interaction with polar substrates<sup>42</sup> and static disorder induced by adatoms<sup>43</sup> or dielectric disorder.<sup>44</sup> No polarons exist in

graphene due to highly dispersive electronic bands, in contrast to  $\pi$ -conjugated polymers whose unique properties originate from the reduced dimensionality.<sup>45,46</sup> In pnictogens and other electron-rich semiconductors<sup>15,47</sup> nonbonding electrons at the top of the valence band might facilitate polaron formation (as in many oxides<sup>37</sup>), which will be investigated in the present work.

Pnictogens, even if limited to P and As, form a variety of stable systems of any dimensionality from molecules to solids with electronic properties ranging from insulator to metal. Geometrically, most of the structures can be obtained as cuts and deformations of the simple cubic lattice.<sup>15,48</sup> The driving force of the distortion is a complex interplay of  $pp\sigma$  dimerization,  $pp\pi$  interaction, and  $sp$  hybridization.<sup>49</sup> In a bottom-up approach, using the pyramids as building blocks and taking into account  $pp\pi$  interaction, an additional set of low-energy fully covalent structures can be obtained.<sup>50</sup> At ambient conditions the most stable are black-phosphorus (A17) and  $\alpha$ -arsenic (A7), transforming into the parent simple cubic structure (via A7) at higher pressure.<sup>51</sup> Both crystals consists of 2D layers: “blue” allotrope for A7 and “black” allotrope for A17 (see Figure 1). Both these 2D allotropes are dynamically stable and very close in energy for P and As.<sup>7</sup> Many other 2D structures have been theoretically pre-

Received: March 22, 2021

Accepted: May 11, 2021

Published: May 12, 2021



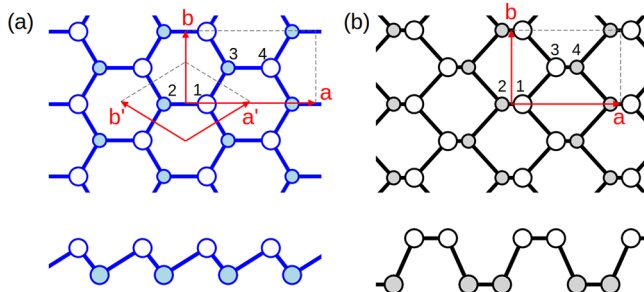


**Figure 1.** Structure of the most stable two-dimensional forms of pnictogens. Both “blue” (a) and “black” (b) allotropes have the same interatomic connectivity and puckered structure where half of the atoms are situated above the middle plane and half are below as illustrated in the figure by larger and shaded smaller disks. The difference is in opposite orderings of atoms 3 and 4. Both structures have common rectangular four-atom unit cell (vectors  $\vec{a}$ ,  $\vec{b}$ ), although the primitive cell of the “blue” allotrope is 2 times smaller (vectors  $\vec{a}'$ ,  $\vec{b}'$ ).

dicted,<sup>7,52</sup> but only for blue and black allotropes is there a consensus in formation energy between various calculations, and only these two forms were obtained experimentally for phosphorene.<sup>7</sup> For these reasons we consider only these two allotropes.

Several approaches can be employed for first-principle studies of small adiabatic polaron in insulators.<sup>34–36,38,53–57</sup> In this work we will perform calculations for hydrogen-passivated phosphorene and arsenene clusters (see Section S1 in the Supporting Information) and extrapolate the results to the infinite monolayer. This approach works well for nonpolar nanocrystalline and organic semiconductors.<sup>57–59</sup> In addition, very close values of electronegativity of H, P, and As should minimize any charge distribution disbalance. The geometry of clusters is fully optimized. It is natural to expect simple scaling of the key physical properties:<sup>56,59</sup> if  $N$  is the number of pnictogen atoms in a cluster, then the ionization potential can be presented as a (generally asymptotic) power series in  $N^{-1/2}$ . Detailed analysis of size convergence of cluster calculations is given in Section S2. The results are not sensitive to the choice of cluster passivation and whether the perimeter is fixed or relaxed; see Section S16.

Polaron relaxation (binding) energy is calculated by the formula

$$E^{\text{polaron}} = \Delta E^{\text{charged}} \equiv \epsilon^{\text{polaron}} - \Delta E^{\text{neutral}} \quad (1)$$

where  $\Delta E^{\text{charged}}$  and  $\Delta E^{\text{neutral}}$  are total energy differences between polaron and undistorted geometries in the charged and neutral states, respectively (as defined in Figure 4b), and  $\epsilon^{\text{polaron}}$  is the pure electronic polaron energy defined as the energy required to move electron/hole from the localized state to the fully delocalized one. The latter quantity can be approximated by one-electron energy calculated for neutral system, which in case of the hole polaron reads

$$\epsilon^{\text{polaron}} \approx \epsilon_{\text{HOMO}}^{\text{polaron}} - \epsilon_{\text{HOMO}}^{\text{undistorted}} \quad (2)$$

where  $\epsilon_{\text{HOMO}}$  is the energy of the highest occupied molecular orbital (HOMO). For an exact DFT functional, eq 2 would be exact. Typically, for an approximate DFT functional exchange–correlation error in  $\Delta E^{\text{charged}}$  is larger than the error of eq 2; therefore, the latter formula is more reliable for estimation of the polaron energy unless the density functional is well tuned.<sup>60</sup>

DFT calculations of clusters are performed in the Gaussian 16 program.<sup>61</sup> Among several basis sets tested (see Section S3), def2-TZVP<sup>62</sup> has been selected due to a good balance of accuracy and feasibility (we came to the same conclusion also for organic  $\pi$ -conjugated molecules<sup>63</sup>). In addition, for infinite monolayers this basis set gives results close to those obtained with plane waves (Table S5). The def2-SVP basis set shows qualitatively the same results and thus we use it for calculations of the largest considered clusters. Several density functionals have been tested: PBE,<sup>64</sup> B3LYP,<sup>65</sup> HSE06,<sup>66</sup> PBE0,<sup>67</sup> APF,<sup>68</sup> CAM-B3LYP,<sup>69</sup> and  $\omega$ B97X.<sup>70</sup> All these functionals show comparable accuracy if benchmarked against CCSD for small clusters (Section S4), although for fine features such functionals as PBE0, HSE06, and APF clearly show a better agreement with CCSD, whereas PBE is an outlier (Table S4). To differentiate methods more rigorously and for larger clusters, we use Koopman’s theorem for the ionization potential (IP).<sup>60,71</sup> For PBE0 the sum IP +  $\epsilon_{\text{HOMO}}$  is closest to zero for large clusters (Section S5); consequently, the main results are discussed for PBE0 functional. DFT calculations of translationally invariant systems are performed in Gaussian 16 with localized basis sets and in VASP 5.4 with plane waves using projector augmented-wave (PAW) method.<sup>72</sup> Localized molecular orbitals (LMO) are generated by orthogonal projection of the corresponding natural bond orbitals (NBO) onto the valence band or lower part of the conduction band (see details in Figure S12).

We start with discussion of undistorted monolayers. The main structural and electronic properties are summarized in Table 1 and Figure 2 with details given in Section S6. Overall,

**Table 1. Main Parameters of Blue and Black Pnictogen Monolayers and Hole Polaron in the Blue Allotrope Calculated with PBE0/TZVP<sup>a</sup>**

system	bond, Å	angle, deg	gap, eV	o-gap, eV	$\Delta E$ , meV
black-P	2.234	96.4	2.28	1.7	
	2.202	104.2			
blue-P	2.241	93.2	3.40	2.7	+10
	2.187	104.2	0.47		88
black-As	2.461	94.6	2.21	1.6	+29
	2.461	101.7			
blue-As	2.473	92.3	3.40	2.7	
	2.424	102.1	0.45		144

<sup>a</sup>Two bond length values for black allotrope correspond to the longer out-of-plane and shorter in-plane bonds. The “gap” is the HOMO–LUMO gap for undistorted monolayers and midgap level separation for polaron given by Eq 2. The “o-gap” is the optical gap (see Figure S38). The  $\Delta E$  for undistorted monolayers is the energy penalty per atom of the less stable allotrope; for polaron it is adiabatic polaron relaxation energy.

the functional PBE0 selected by the above-described methodology accurately predicts these properties for well studied black-phosphorene: the fundamental gap is 2.28 vs 2.4 eV by the quantum Monte Carlo method,<sup>58</sup> and the optical gap is 1.7 vs 1.77 eV from experiment.<sup>73</sup> Because the two allotropes have the same topology of interconnections and similar local structure, their electronic properties are also similar, whereas the differences are due to a gentle balance of multiple factors. For example, the lower parts of the valence bands are similar, whereas frontier orbitals differ substantially. The valence band of the pnictogen layers is composed of two types of LMO

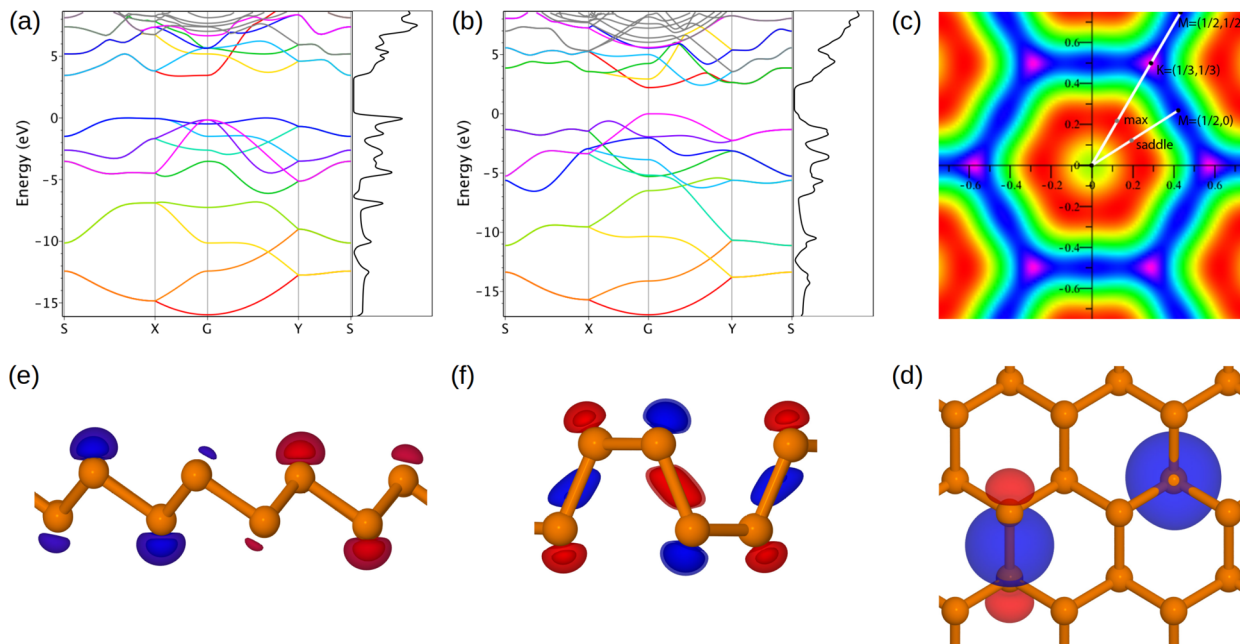


**Figure 2.** Electronic structure of the considered systems calculated for the rectangular cell shown in Figure 1: (a) blue-P and (b) black-P. Colored are the 20 lowest bands corresponding to four valence orbitals per atom. Gray-colored bands are not fully converged. The flat top valence subband with the pronounced density of states peak in the blue-P is responsible for polaron stability in this polymorph. (c) Isosurface of the top of the valence band for the blue-P showing a ring of nearly degenerate states (see Figure S13 for notations). (d) Two LMOs composing the valence band of pnictogen layers:  $\sigma$ -bond and lone pair. (e, f) The HOMO of blue-P (e) is composed primarily of lone pairs whereas in black-P (f) the two LMO types are intermixed.

shown in Figure 2d: lone pair and  $\sigma$ -bond. Because they are close in energy, small changes in these energies and interorbital couplings might produce substantial changes in canonical molecular orbitals that is observed for the case of blue-P vs black-P whose HOMOs are shown in Figure 2e,f. The lower part of the conduction band is composed of antibonding orbitals (colored in Figure 2a,b) with little mixing with the next-shell atomic orbitals (see Figure S12). From Figure 2a it should be noted that the top of the blue-P valence band has a complex structure with bands crowding at the  $\Gamma$ -point and a flat band; see Figure 2c.

To study polarons we begin with small hydrogen-passivated clusters of various shapes to determine possible charge localization patterns. It turns out that there are only four possible lattice deformations: one per charge per system (all four are shown in Figure S20, and the hole polaron in blue-P is shown also in Figure 4a). Positive extra charge is localized on lone pair LMOs that are atom-centered, resulting in a contraction of bonds around the atom. A negative charge is localized on antibonding orbitals that are bond-centered, leading to a bond elongation. Interestingly, in the black allotrope the negative charge is localized on out-of-plane antibonding orbitals, and no localization on in-plane bonds is observed. Already at the level of small clusters, it is easy to observe various degrees of wave function localization for different systems: “hole” in blue-P (Figure 4a) is the most localized and “hole” in black-P is the most delocalized (Figure S20).

To determine stability of these hypothetical small polarons with respect to delocalization, we study convergence of the polaron wave function and lattice deformation with increasing cluster size. Analysis of spatial distribution of extra charge and bond length contraction/elongation shows that only for hole polaron in blue-P we obtain a spatial pattern converging with

cluster size (Figures S21–S26). More rigorous extrapolation of polaron parameters confirms this picture as summarized in Figure 3. In particular, the polaron electronic wave function

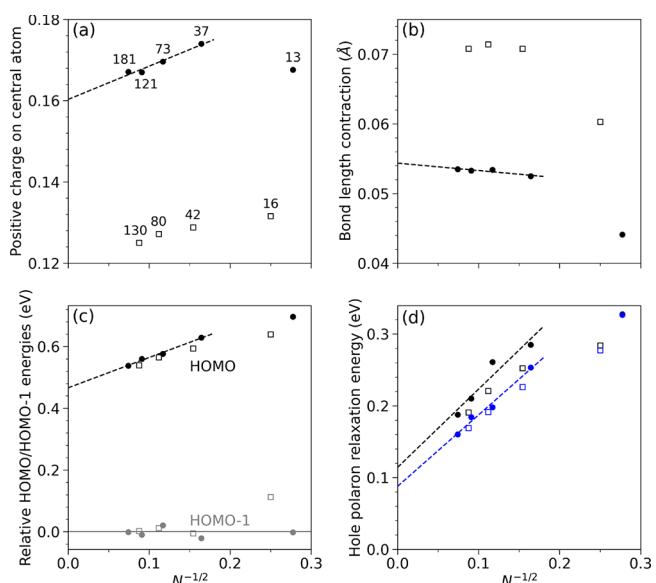


**Figure 3.** Cluster size convergence of the hole polaron parameters in blue-P for two series of clusters: atom-centered (black dots) and bond-centered (white squares),  $N$  is the number of pnictogen atoms (labeled explicitly in the first panel). (a) Excessive charge on central atom(s) shows that the wave function converges quickly with increasing cluster size. (b) Contraction of the length of central bond(s) shows that the lattice deformation converges even faster. (c) The polaron electronic level is deep inside the gap. (d) Polaron relaxation energy calculated by eq 1 (black colored) and with approximation given by eq 2 (blue colored).

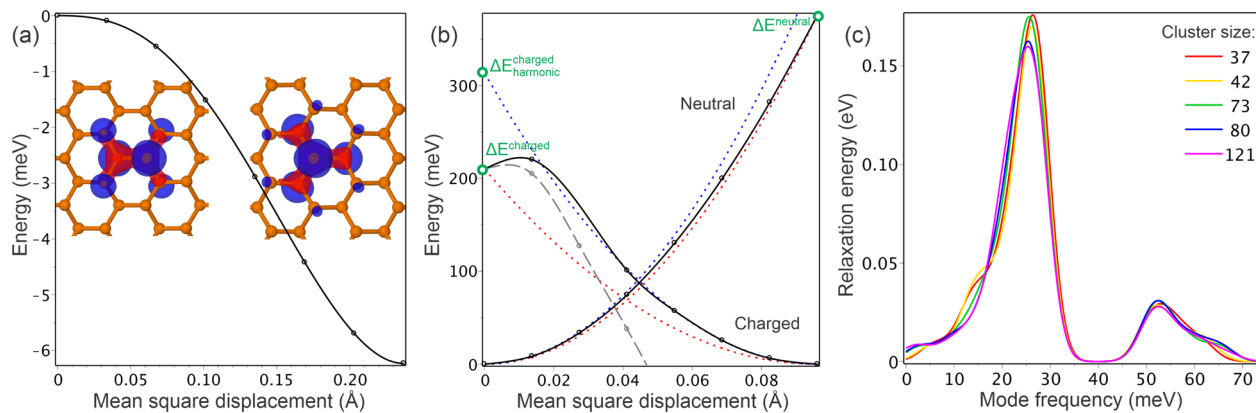


**Figure 4.** (a) Wave function (natural orbital) of the adiabatic hole polaron in blue-P at two stable configurations and the linear potential energy scan between them (130-atom cluster). (b) Potential energy scan between neutral and cation geometry for 121-atom cluster. Blue dotted lines show harmonic approximation, whereas red dotted lines correspond to quadratic curves between end points. The gray line shows the HOMO energy shifted by a constant value to match  $\Delta E_{\text{harmonic}}^{\text{charged}}$  at zero displacement. (c) Phonon spectral decomposition of the polaron harmonic relaxation energy  $\Delta E_{\text{harmonic}}^{\text{charged}}$  for a series of clusters of various size and shape.

converges quickly with increasing cluster size, as evidenced by the convergence of the excessive charge on central atoms; see Figure 3a (calculated as difference of NBO charges of the fully relaxed cation and fully relaxed neutral cluster). The lattice deformation converges even faster: the calculated difference of bond lengths of the fully relaxed cation and fully relaxed neutral cluster is nearly size-independent for clusters larger than the polaron core containing about 13 atoms; see Figure 3b. In addition, the electronic level of the polaron calculated by eq 2 stays deep inside the gap with the energy independent of the cluster shape as illustrated in Figure 3c where HOMO and HOMO-1 energies of the neutral system in the polaron geometry relative to the HOMO energy of the perfect geometry are calculated. The size convergence of the hole polaron in blue-P is achieved also for other considered functionals except for PBE (see Section S9).

The above analysis proves the existence of an adiabatic small polaron in blue-P, and now we need to calculate its energy to compare with a large polaron or free carrier.<sup>30</sup> Such computations are more challenging because the polaron energy computed directly by eq 1 strongly depends on the density functional. However, use of eq 2 removes the uncertainty and all the considered methods except for PBE predict absolute stability of the polaron with its energy converging to about 90 meV for PBE0, HSE06, and B3LYP functionals (see Section S9 and Table S7). Importantly, in the case of the PBE0 functional both formulas give nearly the same energy well converging with cluster size, as shown in Figure 3d.

Finally, we speculate on dynamic properties of the hole polaron in the blue allotrope, not going into details of nonadiabatic dynamics. The adiabatic barrier for polaron motion is the main property of the potential energy surface influencing the dynamics. Since the polaron is atom-centered, the saddle point is located at the bond-centered polaron configuration. The energy profile between these two polaron positions is shown in Figure 4a (calculated for linearly interpolated geometry because the path is too shallow for such approaches as intrinsic reaction coordinate). The barrier is of the order of several millielectronvolts, implying a barrierless motion of the polaron.<sup>29</sup> Another important property determining charge carrier mobility is the strength of electron–phonon interaction and the nature of strongly coupled phonons. To this end we calculate electron–phonon

couplings to the polaron state assuming the displaced harmonic oscillator model commonly used for organic semiconductors;<sup>33</sup> see details in Section S10. Indeed, potential energy scans between undistorted and polaron geometries (Figure 4b) show a perfect quadratic curve for the neutral system and a substantial range of validity of harmonic approximation for the charged system with little asymmetry between the two states. There is also a barrier between small and large polarons in this linear-interpolation scan. To estimate electron–phonon couplings for the polaron state, we decompose the polaron harmonic relaxation energy into contributions from individual normal modes:  $\Delta E_{\text{harmonic}}^{\text{charged}} = \sum_{\omega} S_{\omega} \hbar \omega$ , where  $S_{\omega}$  are Huang–Rhys factors (squared couplings). The result is shown in Figure 4c, where Gaussian broadening with unit prefactor is applied, so that the height of bands does not depend on their width but the integral over the mode frequency should be divided by  $\sqrt{2\pi\sigma^2}$  to obtain  $\Delta E_{\text{harmonic}}^{\text{charged}}$ . We see that the main contribution to the polaron energy originates from the high-frequency acoustic modes.

Considering other quasiparticles, we find that triplet exciton is localized in blue-P, as expected from its interpretation as a bound electron–hole pair. Calculations show that the triplet is well localized on a broken bond with large relaxation energy (see Section S12). In black-P the distorted geometry with localized wave function is stable but the relaxation energy vanishes in the limit of infinite monolayer (Figure S42).

Properties of blue and black arsenic monolayers are similar to those of phosphorus. The key difference is that the blue allotrope is more stable and its hole polaron has higher relaxation energy, approximately 0.15 eV (see Section S13 for details). For heavier pnictogens effects of spin–orbit coupling (SOC) might be critical preventing their robust study within the methodology of this work. Nevertheless, to see how polaron effects change across the pnictogen group, we consider antimony in Section S14. Our calculations show that in the PBE0/SVP method the polaron in blue-Sb is not stable because the top of the valence band consists of  $\sigma$ -bond LMOs, whereas the polaron wave function is the same as for lighter pnictogens. However, SOC is large enough for antimony to change the energy of valence orbitals substantially; therefore, a more accurate study is required.

To understand why the adiabatic polaron exists and why it exists only for holes in the blue allotrope, we need to consider two competing factors: electron–phonon couplings and intersite electronic couplings. Phonon couplings to the singly occupied molecular orbital of charged clusters are of the same magnitude for all considered systems except for holes in black-P ([Figures S33 and S34](#)). The difference is observed in electronic couplings whose values determine the electronic bandwidth: only holes in blue-P have a narrow enough subband at the top of the valence band visible by both flat dispersion and narrow density of states peak in [Figure 2a](#). This indicates localization of the states at the top of the valence band, whose character is inherited by the polaron state. The ring-like structure in [Figure 2c](#) spans an energy range of only 50 meV (energy difference between “max” and “saddle”  $k$ -points), and the  $\Gamma$  point is only 150 meV lower than the valence band edge, which is substantially smaller than the polaron harmonic relaxation energy of about 300 meV ([Figure 4b](#)). It should be noted that hole band dispersion along the  $\Gamma$ –Y direction in black-P is also flat, but this only results in high anisotropy of the mobility and not in the formation of small polaron, in part because of weak electron–phonon couplings. The latter is also the main reason why PBE functional is unable to localize hole polaron in blue-P; see [Figure S35](#).

To conclude, we have shown that in the blue-allotrope of pnictogen monolayers, holes form a small polaron in the adiabatic limit. That polaron is more stable than a free charge carrier. It spans many lattice sites, has a low migration barrier, and should be mobile, similar to polarons in a perfect conjugated polymer. In contrast to large polarons, this small but mobile polaron should be more sensitive to local defects and environment, which is similar to conjugated polymers whose intrinsic high mobility is hard to achieve in real devices due to imperfections.

## ■ ASSOCIATED CONTENT

### SI Supporting Information

The following files are available free of charge: The Supporting Information is available free of charge at <https://pubs.acs.org/doi/10.1021/acs.jpcllett.1c00929>.

Tables and figures of considered clusters, size convergence studies of undistorted clusters and hole polaron in blue-P, benchmarking basis sets and density functionals, calculated parameters and electronic structure of monolayers, polaron wave-function and lattice deformation, potential energy surfaces and electron-phonon couplings, excited states, triplet exciton, results for arsenic and antimony, reference atomic data for pnictogens, dependence on cluster passivation ([PDF](#))

Atomic coordinates of considered phosphorus monolayers and clusters (listed in [Section S1](#)) and natural orbitals of small clusters in Gaussian log-file format readable by Jmol program ([Figure S20](#), [Figure 4a](#), [Figure S39](#)) ([ZIP](#))

## ■ AUTHOR INFORMATION

### Corresponding Author

Andriy Zhugayevych – Skolkovo Institute of Science and Technology, Moscow 143026, Russia; [orcid.org/0000-0003-4713-1289](https://orcid.org/0000-0003-4713-1289); Email: [a.zhugayevych@skoltech.ru](mailto:a.zhugayevych@skoltech.ru)

## Authors

Vasilii Vasilchenko – Skolkovo Institute of Science and Technology, Moscow 143026, Russia

Sergey Levchenko – Skolkovo Institute of Science and Technology, Moscow 143026, Russia

Vasili Perebeinos – Department of Electrical Engineering, University at Buffalo, Buffalo, New York 14260, United States; [orcid.org/0000-0002-0234-8188](https://orcid.org/0000-0002-0234-8188)

Complete contact information is available at:  
<https://pubs.acs.org/10.1021/acs.jpcllett.1c00929>

## Notes

The authors declare no competing financial interest.

## ■ ACKNOWLEDGMENTS

S.L. acknowledges financial support from RFBR and INSF, project number 20-53-56065. V.P. acknowledges support from the Vice President for Research and Economic Development (VPRED) at the University at Buffalo.

## ■ REFERENCES

- (1) Briggs, N.; Subramanian, S.; Lin, Z.; Li, X.; Zhang, X.; Zhang, K.; Xiao, K.; Geoghegan, D.; Wallace, R.; Chen, L.-Q.; et al. A Roadmap for Electronic Grade 2D Materials. *2D Mater.* **2019**, *6*, 022001.
- (2) Sangwan, V. K.; Hersam, M. C. Electronic Transport in Two-Dimensional Materials. *Annu. Rev. Phys. Chem.* **2018**, *69*, 299–325.
- (3) Yang, S.; Zhang, P.; Nia, A.; Feng, X. Emerging 2D Materials Produced via Electrochemistry. *Adv. Mater.* **2020**, *32*, 1907857.
- (4) Li, X.; Tao, L.; Chen, Z.; Fang, H.; Li, X.; Wang, X.; Xu, J.; Zhu, H. Graphene and Related Two-Dimensional Materials: Structure-Property Relationships for Electronics and Optoelectronics. *Appl. Phys. Rev.* **2017**, *4*, 021306.
- (5) Radislavljevic, B.; Radenovic, A.; Brivio, J.; Giacometti, V.; Kis, A. Single-Layer MoS<sub>2</sub> Transistors. *Nat. Nanotechnol.* **2011**, *6*, 147–150.
- (6) Mak, K. F.; Lee, C.; Hone, J.; Shan, J.; Heinz, T. F. Atomically Thin MoS<sub>2</sub>: A New Direct-Gap Semiconductor. *Phys. Rev. Lett.* **2010**, *105*, 136805.
- (7) Ersan, F.; Kecik, D.; Ozcelik, V. O.; Kadioglu, Y.; Durgun, E.; Akturk, E.; Ciraci, S. Two-Dimensional Pnictogens: A Review of Recent Progresses and Future Research Directions. *Appl. Phys. Rev.* **2019**, *6*, 021308.
- (8) Liu, X.; Zhang, S.; Guo, S.; Cai, B.; Yang, S. A.; Shan, F.; Pumera, M.; Zeng, H. Advances of 2D Bismuth in Energy Sciences. *Chem. Soc. Rev.* **2020**, *49*, 263–285.
- (9) Li, L.; Yu, Y.; Ye, G. J.; Ge, Q.; Ou, X.; Wu, H.; Feng, D.; Chen, X. H.; Zhang, Y. Black Phosphorus Field-Effect Transistors. *Nat. Nanotechnol.* **2014**, *9*, 372–377.
- (10) Liu, H.; Neal, A. T.; Zhu, Z.; Luo, Z.; Xu, X.; Tomanek, D.; Ye, P. D. Phosphorene: An Unexplored 2D Semiconductor with a High Hole Mobility. *ACS Nano* **2014**, *8*, 4033–4041.
- (11) Xia, F.; Wang, H.; Hwang, J.; Neto, A.; Yang, L. Black Phosphorus and Its Isoelectronic Materials. *Nat. Rev. Phys.* **2019**, *1*, 306–317.
- (12) Zhang, Y.; Wang, J.; Liu, Q.; Gu, S.; Sun, Z.; Chu, P. K.; Yu, X. The Electrical, Thermal, and Thermoelectric Properties of Black Phosphorus. *APL Mater.* **2020**, *8*, 120903.
- (13) Wuttig, M.; Deringer, V. L.; Gonze, X.; Bichara, C.; Raty, J.-Y. Incipient Metals: Functional Materials with a Unique Bonding Mechanism. *Adv. Mater.* **2018**, *30*, 1803777.
- (14) Jones, R. O. Bonding in Phase Change Materials: Concepts and Misconceptions. *J. Phys.: Condens. Matter* **2018**, *30*, 153001.
- (15) Zhugayevych, A.; Lubchenko, V. Electronic Structure and the Glass Transition in Pnictide and Chalcogenide Semiconductor Alloys. I. The Formation of the  $p\pi\sigma$ -network. *J. Chem. Phys.* **2010**, *133*, 234503.

- (16) Rodin, A. S.; Carvalho, A. Strain-Induced Gap Modification in Black Phosphorus. *Phys. Rev. Lett.* **2014**, *112*, 176801.
- (17) Rudenko, A. N.; Katsnelson, M. I. Quasiparticle Band Structure and Tight-Binding Model for Single- and Bilayer Black Phosphorus. *Phys. Rev. B: Condens. Matter Mater. Phys.* **2014**, *89*, 201408.
- (18) Zhu, Z.; Tomanek, D. Semiconducting Layered Blue Phosphorus: A Computational Study. *Phys. Rev. Lett.* **2014**, *112*, 176802.
- (19) Kamal, C.; Ezawa, M. Arsenene: Two-Dimensional Buckled and Puckered Honeycomb Arsenic Systems. *Phys. Rev. B: Condens. Matter Mater. Phys.* **2015**, *91*, 085423.
- (20) Kou, L.; Ma, Y.; Tan, X.; Frauenheim, T.; Du, A.; Smith, S. Structural and Electronic Properties of Layered Arsenic and Antimony Arsenide. *J. Phys. Chem. C* **2015**, *119*, 6918–6922.
- (21) Xiao, J.; Long, M.; Zhang, X.; Ouyang, J.; Xu, H.; Gao, Y. Theoretical Predictions on the Electronic Structure and Charge Carrier Mobility in 2D Phosphorus Sheets. *Sci. Rep.* **2015**, *5*, 09961.
- (22) Mogulkoc, A.; Mogulkoc, Y.; Rudenko, A. N.; Katsnelson, M. I. Polaronic Effects in Monolayer Black Phosphorus on Polar Substrates. *Phys. Rev. B: Condens. Matter Mater. Phys.* **2016**, *93*, 085417.
- (23) Mogulkoc, Y.; Modarresi, M.; Mogulkoc, A.; Ciftci, Y. O. Electronic and Optical Properties of Bilayer Blue Phosphorus. *Comput. Mater. Sci.* **2016**, *124*, 23–29.
- (24) Trushkov, Y.; Perebeinos, V. Phonon-Limited Carrier Mobility in Monolayer Black Phosphorus. *Phys. Rev. B: Condens. Matter Mater. Phys.* **2017**, *95*, 075436.
- (25) Cheng, L.; Zhang, C.; Liu, Y. The Optimal Electronic Structure for High-Mobility 2D Semiconductors: Exceptionally High Hole Mobility in 2D Antimony. *J. Am. Chem. Soc.* **2019**, *141*, 16296–16302.
- (26) Jamdagni, P.; Thakur, A.; Kumar, A.; Ahluwalia, P. K.; Pandey, R. Two Dimensional Allotropes of Arsenene with a Wide Range of High and Anisotropic Carrier Mobility. *Phys. Chem. Chem. Phys.* **2018**, *20*, 29939–29950.
- (27) Brahma, M.; Kabiraj, A.; Bescond, M.; Mahapatra, S. Phonon Limited Anisotropic Quantum Transport in Phosphorene Field Effect Transistors. *J. Appl. Phys.* **2019**, *126*, 114502.
- (28) Franchini, C.; Reticcioli, M.; Setvin, M.; Diebold, U. Polarons in Materials. *Nat. Rev. Mater.* **2021**, DOI: [10.1038/s41578-021-00289-w](https://doi.org/10.1038/s41578-021-00289-w).
- (29) Alexandrov, A. S.; Devreese, J. T. *Advances in Polaron Physics*; Springer: Berlin, 2010.
- (30) Emin, D. *Polarons*; Cambridge University Press: New York, 2013.
- (31) Ghosh, R.; Spano, F. C. Excitons and Polarons in Organic Materials. *Acc. Chem. Res.* **2020**, *53*, 2201–2211.
- (32) Giannini, S.; Carof, A.; Ellis, M.; Yang, H.; Ziogos, O. G.; Ghosh, S.; Blumberger, J. Quantum Localization and Delocalization of Charge Carriers in Organic Semiconducting Crystals. *Nat. Commun.* **2019**, *10*, 3843.
- (33) Zhugayevych, A.; Tretiak, S. Theoretical Description of Structural and Electronic Properties of Organic Photovoltaic Materials. *Annu. Rev. Phys. Chem.* **2015**, *66*, 305–330.
- (34) Ghosh, D.; Welch, E.; Neukirch, A. J.; Zakhidov, A.; Tretiak, S. Polarons in Halide Perovskites: A Perspective. *J. Phys. Chem. Lett.* **2020**, *11*, 3271–3286.
- (35) Smart, T. J.; Pham, T. A.; Ping, Y.; Ogitsu, T. Optical Absorption Induced By Small Polaron Formation in Transition Metal Oxides: The Case of Co<sub>3</sub>O<sub>4</sub>. *Phys. Rev. Mater.* **2019**, *3*, 102401.
- (36) Brunin, G.; Rignanese, G.-M.; Hautier, G. High-Performance Transparent Conducting Oxides Through Small-Polaron Transport. *Phys. Rev. Mater.* **2019**, *3*, 064602.
- (37) Lany, S. Semiconducting Transition Metal Oxides. *J. Phys.: Condens. Matter* **2015**, *27*, 283203.
- (38) Perebeinos, V.; Allen, P. B.; Weinert, M. First-Principles Calculations of the Self-Trapped Exciton in Crystalline NaCl. *Phys. Rev. B: Condens. Matter Mater. Phys.* **2000**, *62*, 12589–12592.
- (39) Dathar, G. K. P.; Sheppard, D.; Stevenson, K. J.; Henkelman, G. Calculations of Li-Ion Diffusion in Olivine Phosphates. *Chem. Mater.* **2011**, *23*, 4032–4037.
- (40) Kang, M.; Jung, S.; Shin, W.; Sohn, Y.; Ryu, S.; Kim, T.; Hoesch, M.; Kim, K. Holstein Polaron in a Valley-Degenerate Two-Dimensional Semiconductor. *Nat. Mater.* **2018**, *17*, 676–680.
- (41) Sohier, T.; Calandra, M.; Mauri, F. Two-Dimensional Frohlich Interaction in Transition-Metal Dichalcogenide Monolayers: Theoretical Modeling and First-Principles Calculations. *Phys. Rev. B: Condens. Matter Mater. Phys.* **2016**, *94*, 085415.
- (42) Rodin, A.; Trushin, M.; Carvalho, A. Collective Excitations in 2D Materials. *Nat. Rev. Phys.* **2020**, *2*, 524–537.
- (43) Zhang, L.; Vasenko, A. S.; Zhao, J.; Prezhdo, O. V. Mono-Elemental Properties of 2D Black Phosphorus Ensure Extended Charge Carrier Lifetimes under Oxidation: Time-Domain Ab Initio Analysis. *J. Phys. Chem. Lett.* **2019**, *10*, 1083–1091.
- (44) Raja, A.; Waldecker, L.; Zipfel, J.; Cho, Y.; Brem, S.; Ziegler, J. D.; Kulig, M.; Taniguchi, T.; Watanabe, K.; Malic, E.; et al. Dielectric Disorder in Two-Dimensional Materials. *Nat. Nanotechnol.* **2019**, *14*, 832–837.
- (45) Giamarchi, T. *Quantum Physics in One Dimension*; Clarendon Press: Oxford, 2003.
- (46) Campbell, D. K. Polarons in a Diatomic Polymer. *Phys. Rev. Lett.* **1983**, *50*, 865.
- (47) Papoian, G. A.; Hoffmann, R. Hypervalent Bonding in One, Two, and Three Dimensions: Extending the Zintl-Klemm Concept to Nonclassical Electron-Rich Networks. *Angew. Chem., Int. Ed.* **2000**, *39*, 2408–2448.
- (48) Burdett, J. K.; Lee, S. Peierls Distortions in Two and Three Dimensions and the Structures of AB Solids. *J. Am. Chem. Soc.* **1983**, *105*, 1079–1083.
- (49) Seo, D.-K.; Hoffmann, R. What Determines the Structures of the Group 15 Elements? *J. Solid State Chem.* **1999**, *147*, 26–37.
- (50) Bocker, S.; Hoser, M. Covalent Structures of Phosphorus: A Comprehensive Theoretical Study. *Z. Anorg. Allg. Chem.* **1995**, *621*, 258–286.
- (51) Laniel, D.; Winkler, B.; Fedotenko, T.; Pakhomova, A.; Chariton, S.; Milman, V.; Prakapenka, V.; Dubrovinsky, L.; Dubrovinskaia, N. High-Pressure Polymeric Nitrogen Allotrope with the Black Phosphorus Structure. *Phys. Rev. Lett.* **2020**, *124*, 216001.
- (52) Zhang, S.; Xie, M.; Li, F.; Yan, Z.; Li, Y.; Kan, E.; Liu, W.; Chen, Z.; Zeng, H. Semiconducting Group 15 Monolayers: A Broad Range of Band Gaps and High Carrier Mobilities. *Angew. Chem., Int. Ed.* **2016**, *55*, 1666–1669.
- (53) Reticcioli, M.; Diebold, U.; Kresse, G.; Franchini, C. In *Handbook of Materials Modeling: Applications: Current and Emerging Materials*; Andreoni, W., Yip, S., Eds.; Springer International Publishing: Cham, 2020; pp 1035–1073.
- (54) Sio, W. H.; Verdi, C.; Ponc  , S.; Giustino, F. Ab Initio Theory of Polarons: Formalism and Applications. *Phys. Rev. B: Condens. Matter Mater. Phys.* **2019**, *99*, 235139.
- (55) Zhou, Z.; Long, R.; Prezhdo, O. V. Why Silicon Doping Accelerates Electron Polaron Diffusion in Hematite. *J. Am. Chem. Soc.* **2019**, *141*, 20222–20233.
- (56) Kokott, S.; Levchenko, S. V.; Rinke, P.; Scheffler, M. First-Principles Supercell Calculations of Small Polarons with Proper Account for Long-Range Polarization Effects. *New J. Phys.* **2018**, *20*, 033023.
- (57) Nayyar, I. H.; Batista, E. R.; Tretiak, S.; Saxena, A.; Smith, D. L.; Martin, R. L. Role of Geometric Distortion and Polarization in Localizing Electronic Excitations in Conjugated Polymers. *J. Chem. Theory Comput.* **2013**, *9*, 1144–1154.
- (58) Frank, T.; Derian, R.; Tok  , K.; Mitas, L.; Fabian, J.; Stich, I. Many-Body Quantum Monte Carlo Study of 2D Materials: Cohesion and Band Gap in Single-Layer Phosphorene. *Phys. Rev. X* **2019**, *9*, 011018.
- (59) Chelikowsky, J. R.; Tiago, M. L.; Saad, Y.; Zhou, Y. Algorithms for the Evolution of Electronic Properties in Nanocrystals. *Comput. Phys. Commun.* **2007**, *177*, 1–5.

- (60) Pinheiro, M.; Caldas, M. J.; Rinke, P.; Blum, V.; Scheffler, M. Length Dependence of Ionization Potentials of Transacetylenes: Internally Consistent DFT/GW Approach. *Phys. Rev. B: Condens. Matter Mater. Phys.* **2015**, *92*, 195134.
- (61) Frisch, M. J.; Trucks, G. W.; Schlegel, H. B.; Scuseria, G. E.; Robb, M. A.; Cheeseman, J. R.; Scalmani, G.; Barone, V.; Petersson, G. A.; Nakatsuji, H.; et al. *Gaussian 16*, Revision A.03; Gaussian Inc.: Wallingford, CT, 2016.
- (62) Weigend, F.; Ahlrichs, R. Balanced Basis Sets of Split Valence, Triple Zeta Valence and Quadruple Zeta Valence Quality for H to Rn: Design and Assessment of Accuracy. *Phys. Chem. Chem. Phys.* **2005**, *7*, 3297–3305.
- (63) Tukachev, N. V.; Maslennikov, D. R.; Sosorev, A. Y.; Tretiak, S.; Zhugayevych, A. Ground-State Geometry and Vibrations of Polyphenylenevinylene Oligomers. *J. Phys. Chem. Lett.* **2019**, *10*, 3232–3239.
- (64) Perdew, J. P.; Burke, K.; Ernzerhof, M. Generalized Gradient Approximation Made Simple. *Phys. Rev. Lett.* **1996**, *77*, 3865–3868.
- (65) Becke, A. D. Density-functional Thermochemistry. III. The Role of Exact Exchange. *J. Chem. Phys.* **1993**, *98*, 5648–5652.
- (66) Kruckau, A. V.; Vydrov, O. A.; Izmaylov, A. F.; Scuseria, G. E. Influence of the Exchange Screening Parameter on the Performance of Screened Hybrid Functionals. *J. Chem. Phys.* **2006**, *125*, 224106.
- (67) Adamo, C.; Barone, V. Toward Reliable Density Functional Methods without Adjustable Parameters: The PBE0Model. *J. Chem. Phys.* **1999**, *110*, 6158–6170.
- (68) Austin, A.; Petersson, G. A.; Frisch, M. J.; Dobek, F. J.; Scalmani, G.; Throssell, K. A Density Functional with Spherical Atom Dispersion Terms. *J. Chem. Theory Comput.* **2012**, *8*, 4989–5007.
- (69) Yanai, T.; Tew, D. P.; Handy, N. C. A New Hybrid Exchange-Correlation Functional Using the Coulomb-Attenuating Method (CAM-B3LYP). *Chem. Phys. Lett.* **2004**, *393*, 51–57.
- (70) Chai, J.-D.; Head-Gordon, M. Long-Range Corrected Hybrid Density Functionals with Damped Atom-Atom Dispersion Corrections. *Phys. Chem. Chem. Phys.* **2008**, *10*, 6615–6620.
- (71) Autschbach, J.; Srebro, M. Delocalization Error and “Functional Tuning” in Kohn–Sham Calculations of Molecular Properties. *Acc. Chem. Res.* **2014**, *47*, 2592–2602.
- (72) Kresse, G.; Furthmüller, J. Efficient Iterative Schemes for Ab Initio Total-Energy Calculations Using a Plane-Wave Basis Set. *Phys. Rev. B: Condens. Matter Mater. Phys.* **1996**, *54*, 11169–11186.
- (73) Huang, S.; Wang, F.; Zhang, G.; Song, C.; Lei, Y.; Xing, Q.; Wang, C.; Zhang, Y.; Zhang, J.; Xie, Y.; et al. From Anomalous to Normal: Temperature Dependence of the Band Gap in Two-Dimensional Black Phosphorus. *Phys. Rev. Lett.* **2020**, *125*, 156802.

# Supporting Information for

## “Small Polarons in Two-Dimensional Pnictogens: A First-Principles Study”

Vasilii Vasilchenko,<sup>†</sup> Sergey Levchenko,<sup>†</sup> Vasili Perebeinos,<sup>‡</sup> Andriy Zhugayevych<sup>†</sup>

<sup>†</sup> Skolkovo Institute of Science and Technology, Moscow 143026, Russia

<sup>‡</sup> Department of Electrical Engineering, University at Buffalo, NY 14260, USA

E-mail: a.zhugayevych@skoltech.ru

May 11, 2021

S1	Considered clusters . . . . .	S2
S2	Size convergence of calculations of undistorted clusters . . . . .	S4
S3	Benchmarking basis sets . . . . .	S8
S4	Benchmarking density functionals against CCSD . . . . .	S10
S5	Benchmarking density functionals by Koopman’s theorem . . . . .	S13
S6	Main parameters of blue- and black-P monolayers . . . . .	S14
S7	Electronic structure of monolayers . . . . .	S17
S8	Polaron wave-function and lattice deformation . . . . .	S23
S9	Size convergence studies of hole polaron in blue-P . . . . .	S28
S10	Potential energy surfaces . . . . .	S33
S11	Excited states . . . . .	S38
S12	Triplet exciton . . . . .	S39
S13	Results for arsenic . . . . .	S41
S14	Results for antimony . . . . .	S44
S15	Atomic data for pnictogens and related elements . . . . .	S46
S16	Dependence on cluster passivation . . . . .	S47

## S1 Considered clusters

Table S1: Considered series of clusters. Some small blue and black clusters corresponding to  $n = 1$  are identical:  
**rlayer1=olayer1=cluster1**, **rlayer2=olayer2=cluster2**.

Centering	Series ( $n \in \mathbb{N}$ )	List of considered $N$	blue symmetry	black symmetry
atom	$N = 6n(n - 1) + 1$	1, 13, 37, 73, 121, 181	3m	m
bond	$N = 2n(3n - 2)$	2, 16, 42, 80, 130, 192	2/m	2/m
ring	$N = 6n^2$	6, 24, 54, 96, 150	-3m	2/m

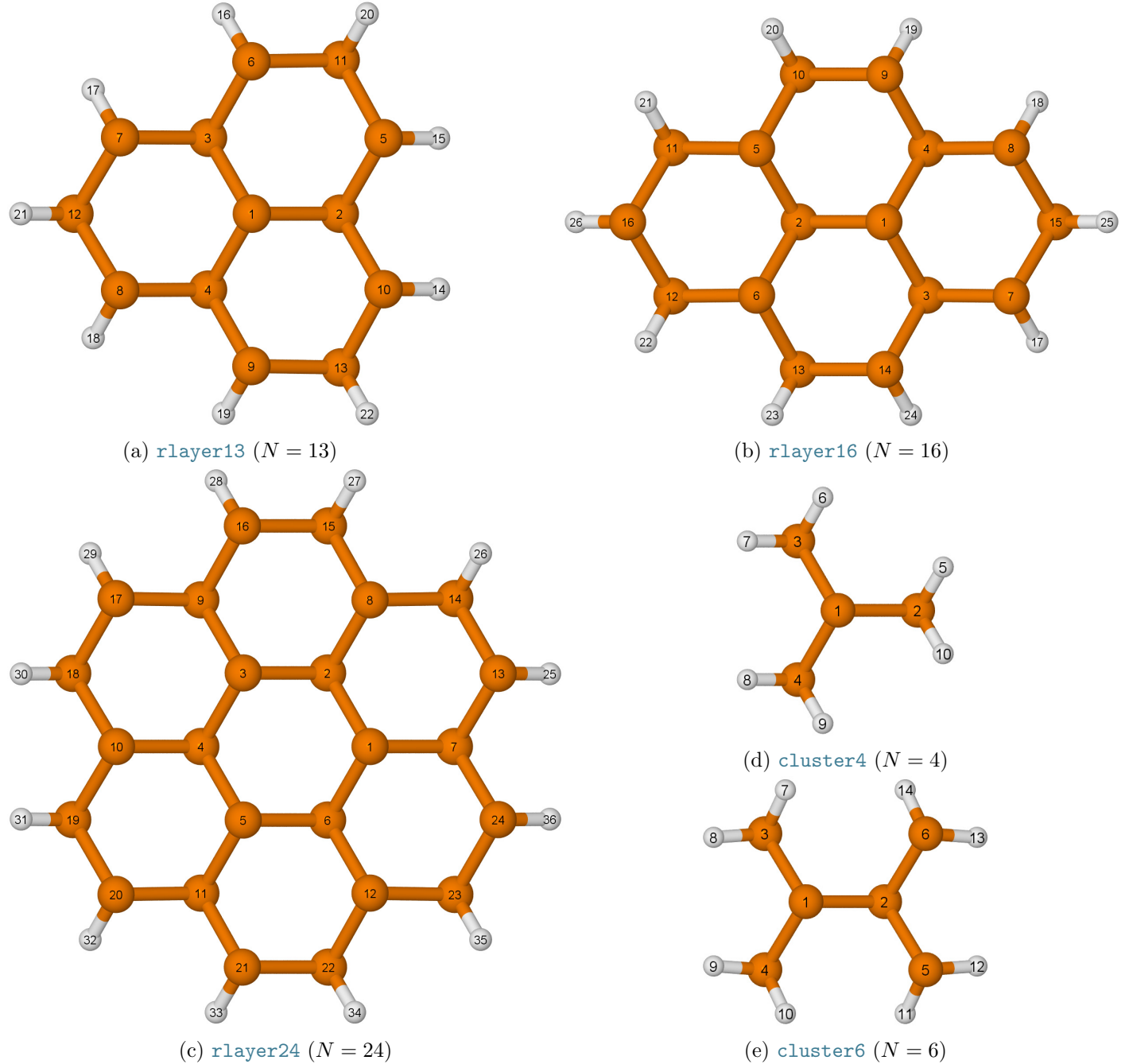
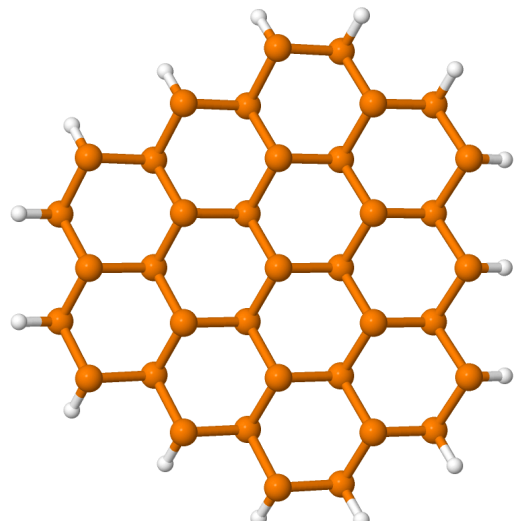
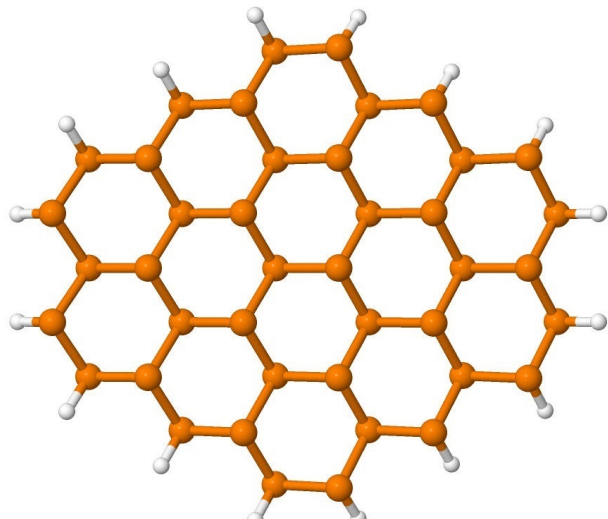


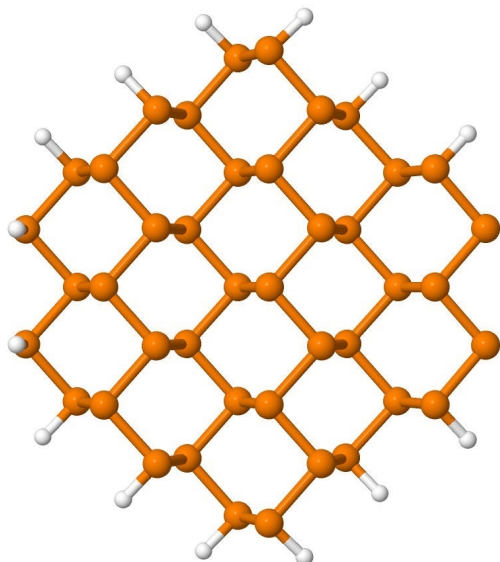
Figure S1: Considered clusters: (a-c) representative serial blue clusters corresponding to  $n = 2$ ; (d-e) small non-serial clusters.



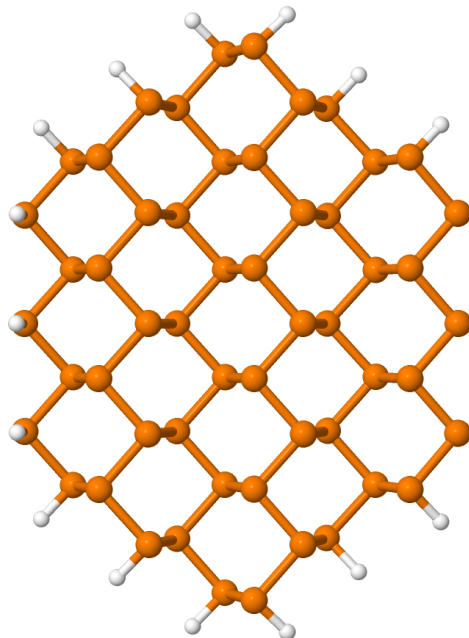
(a) `rlayer37`



(b) `rlayer42`



(c) `olayer42`



(d) `olayer54`

Figure S2: Other examples of serial clusters. Blue and black allotropes are distinguished by prefix ‘r’ and ‘o’ meaning rhombohedral and orthorhombic three-dimensional crystal systems.

## S2 Size convergence of calculations of undistorted clusters

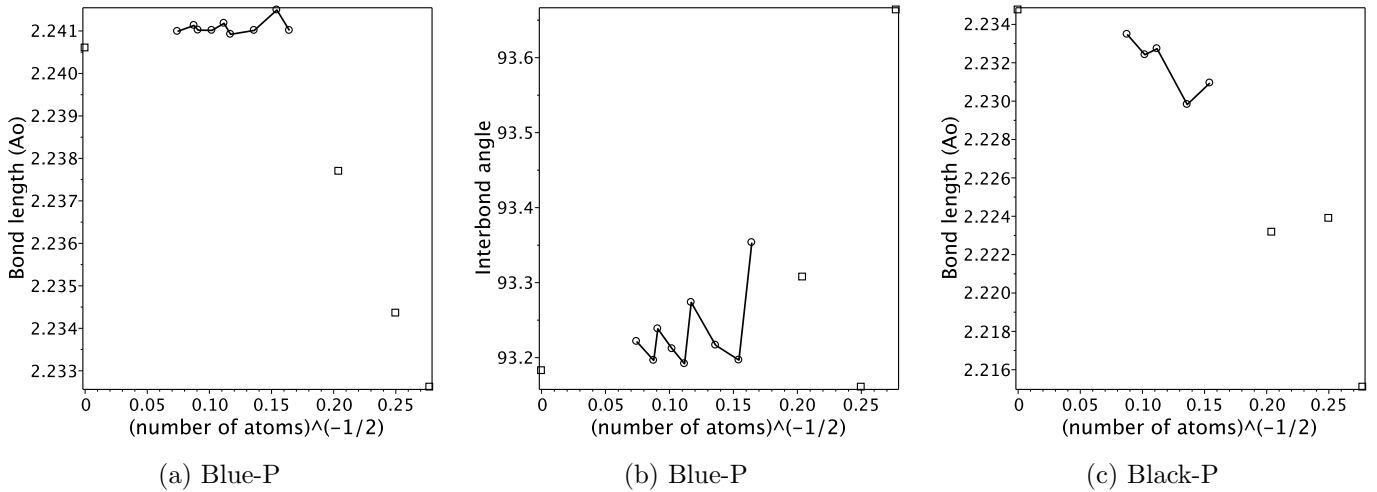


Figure S3: Convergence of local geometry is fast: no extrapolation is needed because a central region of even small clusters have geometry of the infinite cluster. Values at zero are calculated for translationally invariant system.

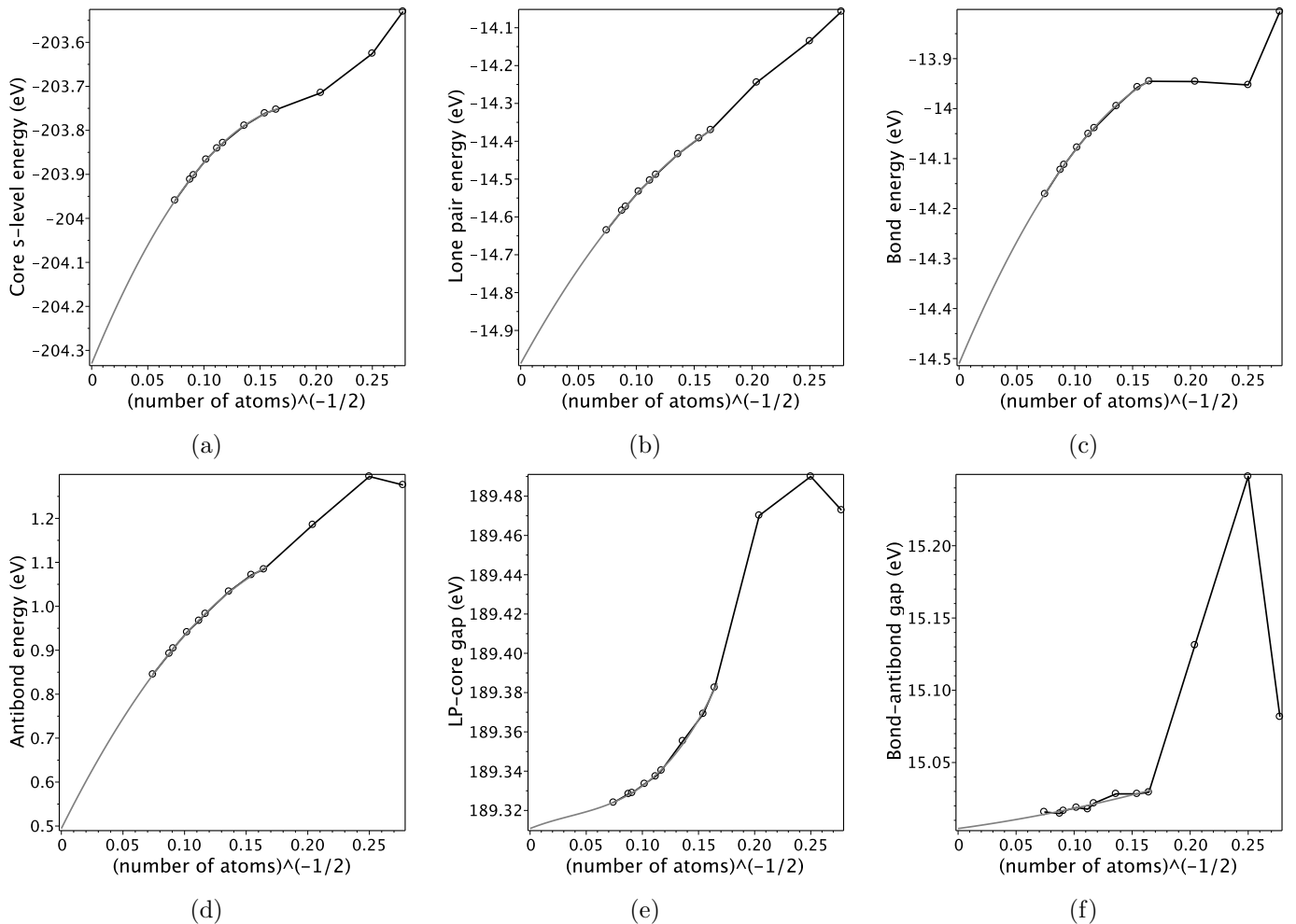


Figure S4: Convergence of NBO energies for blue-P: (a-d) absolute energies converge slowly, (e-f) relative energies converge quickly.

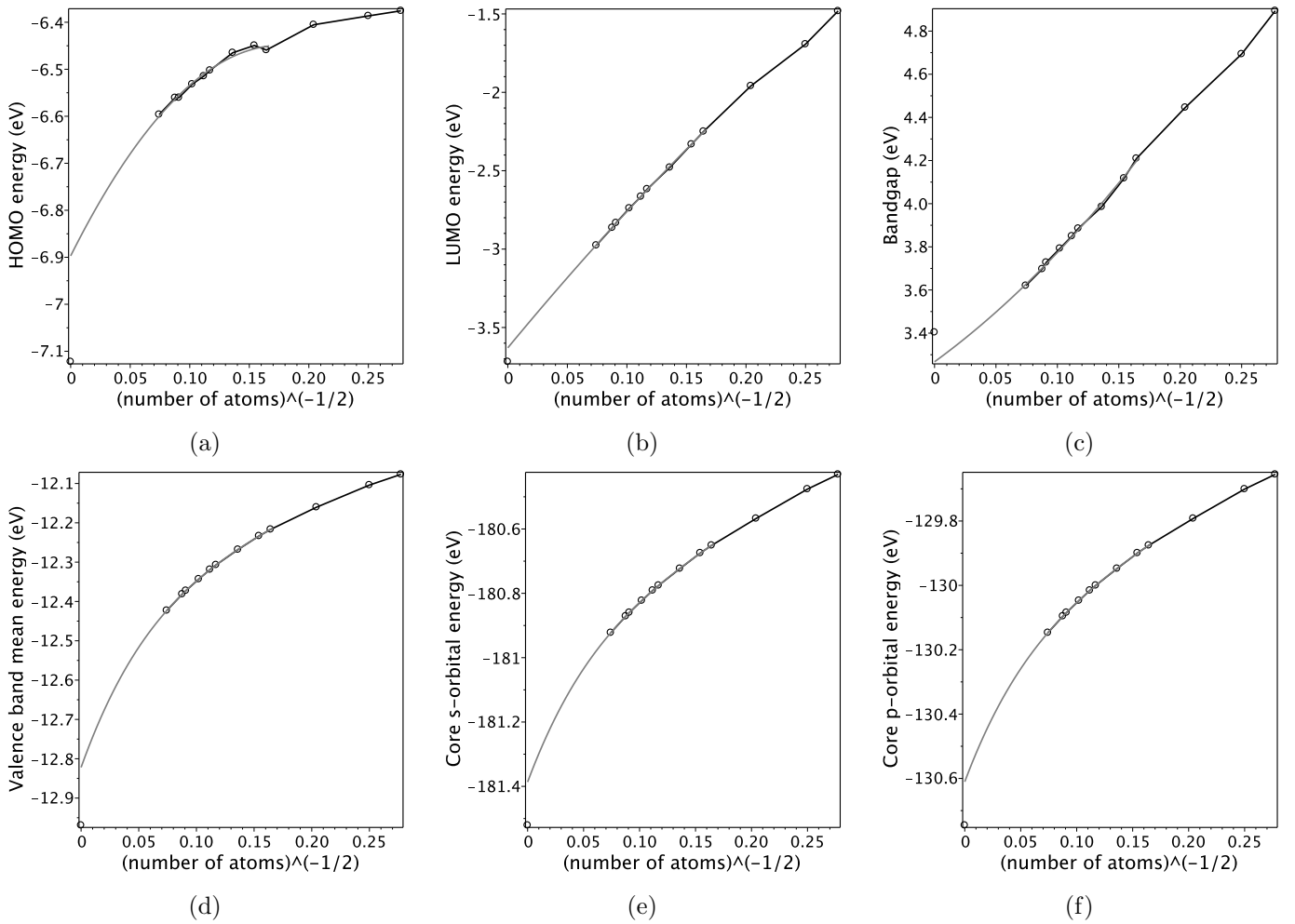
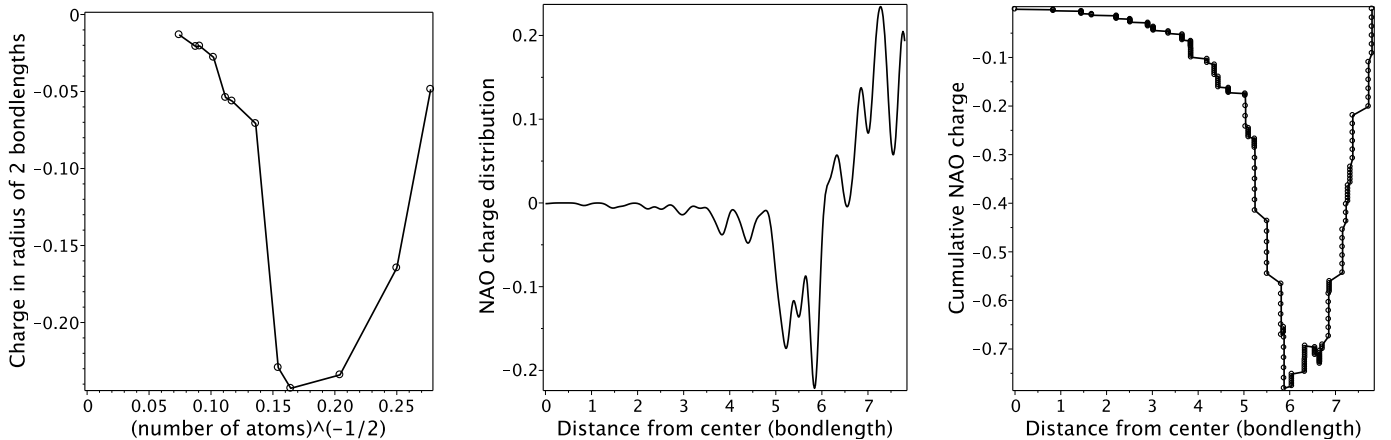


Figure S5: Convergence of MO energies is slow especially for HOMO: larger clusters are required to converge to 0.1 eV precision (see follow-up figures for explanation). For panels (d-f) the size dependence is smoother, so that 4th order polynomial fit (in  $N^{-1/2}$ ) allows to get that precision. Data for blue-P are shown here.



(a) Convergence of the total charge within 2 bondlengths from cluster center (12-14 atoms depending on cluster symmetry).

(b) Radial charge distribution for 181-atom cluster.

(c) Cumulative radial charge distribution for 181-atom cluster.

Figure S6: Natural atomic orbital (NAO) charges for blue-P. The surface layer has the width of 2-4 pnictogens, therefore only for clusters with 50-100 atoms the central region has no artificial extra charge.

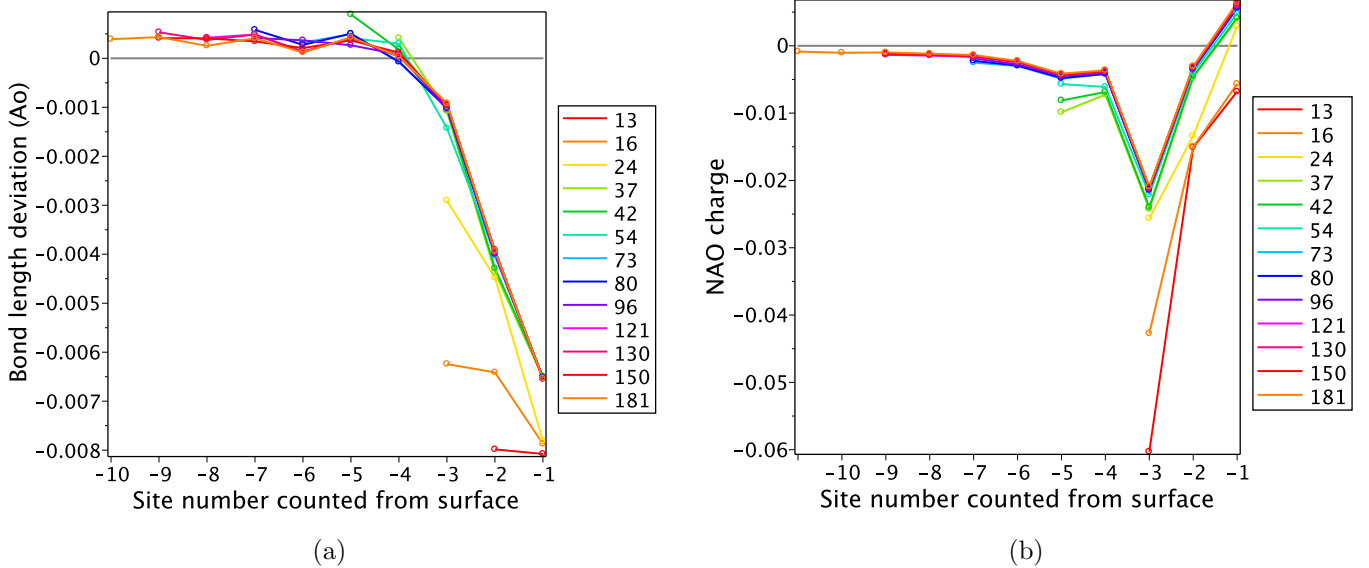


Figure S7: Radial distribution of (a) bond lengths and (b) NAO atomic charges for blue-P.

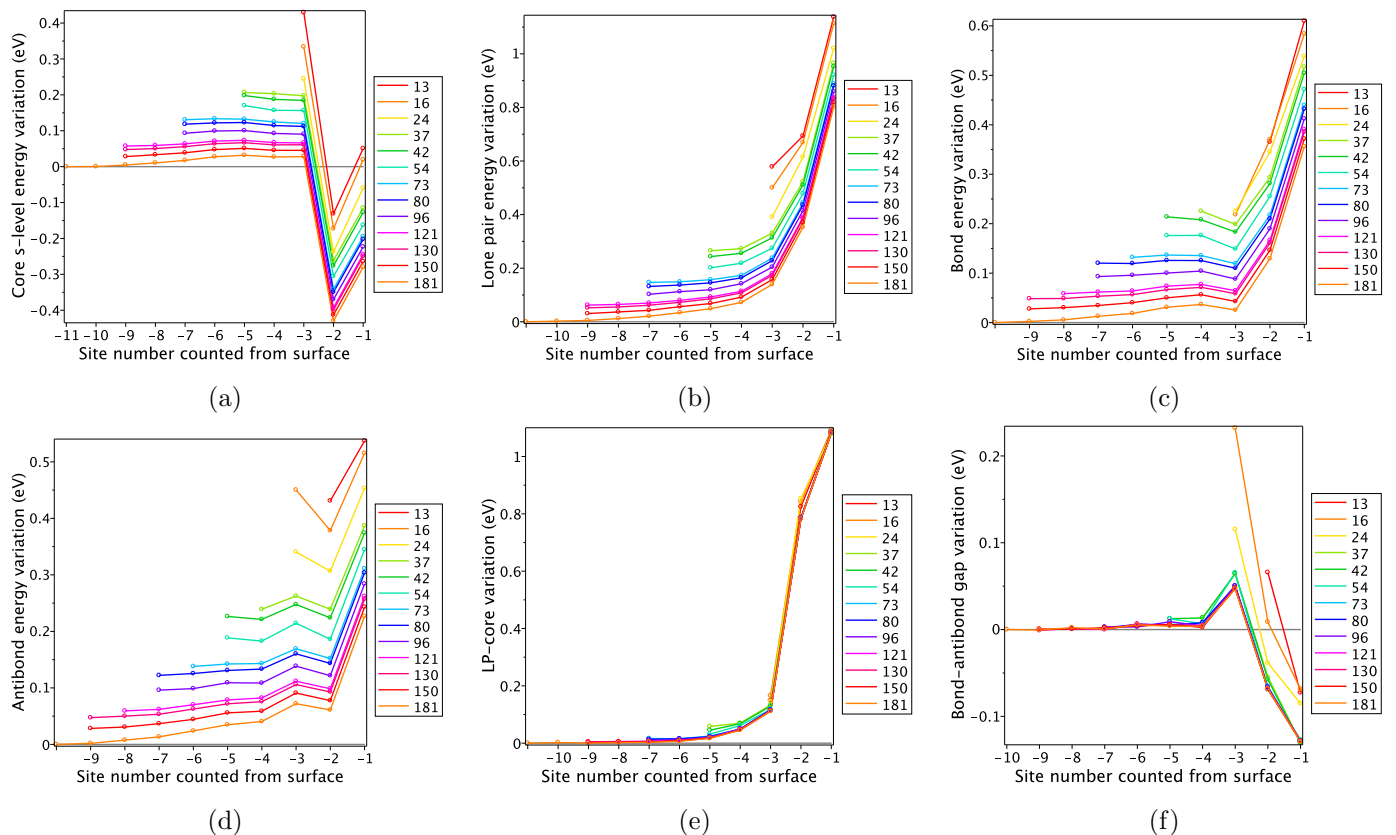


Figure S8: Radial distribution of various NBO energies for blue-P: (a-d) absolute energies converge slow, but (e-f) relative energies converge quickly in the central region.

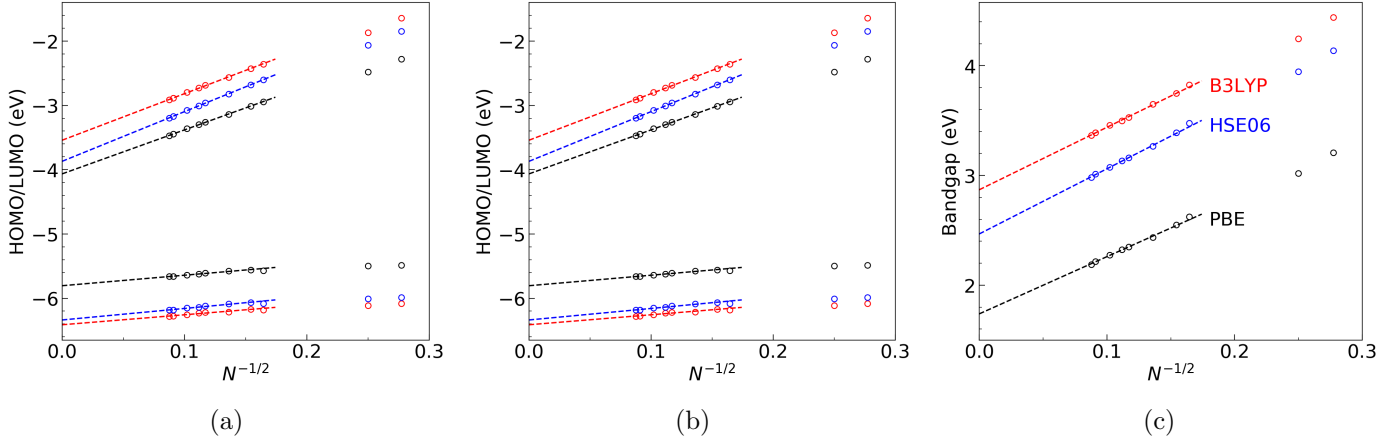


Figure S9: Convergence of cluster calculations for blue-P for other considered density functionals.  $N$  denotes number of pnictogen atoms in a cluster. Dashed lines extrapolate the values to the limit of an infinite-size cluster. Note that at the scale of methods comparison, the above mentioned slow size convergence effects are negligible.

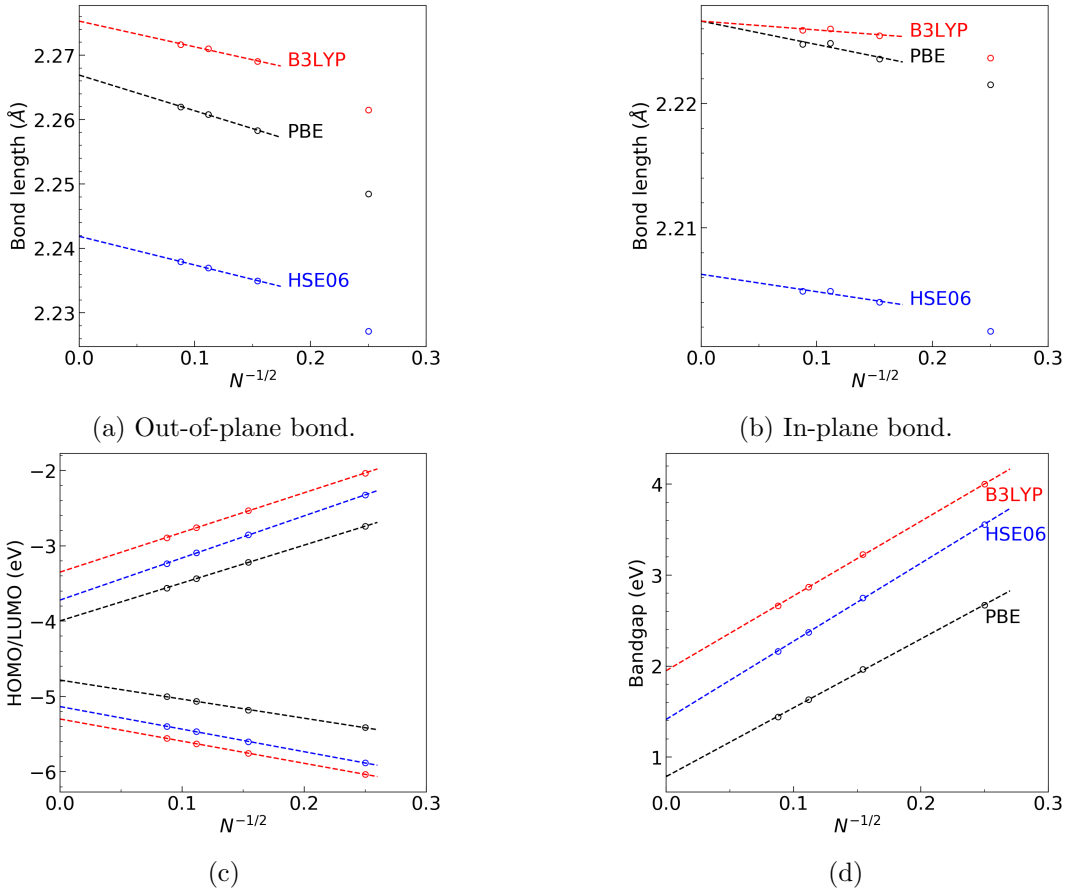


Figure S10: Convergence of cluster calculations for black-P for other considered density functionals.

### S3 Benchmarking basis sets

Basis sets are tested for As clusters using B3LYP functional. Basis set abbreviations: ‘anp’ – Ahlrichs basis sets with  $n$  valence orbitals, ‘cn’ – Dunning basis sets, ‘a’ means diffuse orbitals, ‘p2p’=6-31G\*. Cluster abbreviations: C=cluster, L=rlayer, oL=oLayer, R6 and oR6 are hydrogen-passivated rings in blue and black layers, P/N means cation/anion. Rows are ordered by ‘C6’ column. Evidently, 6-31G\* basis fails for arsenic.

#### Bond length (Angstroms)

basis	C1	C2	C4	C6	C6_P	C6_N	R6	oR6	L13	L13_P	L16	L16_N	oL16
a4p	1.524	2.488	2.496	2.501	2.438	3.121	2.497	2.485	2.501	2.463	2.503	3.215	2.496
p2p	0.019	-0.033	-0.040	-0.049	-0.050	-0.257	-0.043	-0.054	-0.054	-0.050	-0.054	-0.760	-0.088
c4a	-0.001	-0.000	-0.000	-0.000	-0.000	-0.014	-0.000	-0.000	-0.000	-0.000	-0.000	-0.007	-0.000
c4	-0.000	0.000	0.000	0.000	0.000	0.001	0.000	0.000	0.000	0.000	0.000	0.001	0.000
a3p	0.002	-0.000	0.001	0.001	0.000	0.012	0.000	-0.001	0.001	0.001	0.001	0.006	-0.001
c3a	0.001	0.002	0.002	0.002	0.002	-0.010	0.002	0.002	0.002	0.002	0.002	-0.005	0.002
c3	0.001	0.002	0.002	0.003	0.002	0.012	0.002	0.002	0.003	0.003	0.003	0.008	0.003
a2p	0.007	0.004	0.005	0.007	0.007	0.028	0.006	0.005	0.008	0.009	0.008	0.014	0.004
c2a	0.009	0.009	0.010	0.010	0.011	-0.021	0.010	0.009	0.011	0.011	0.011	-0.001	0.006
p3pa	0.007	0.005	0.007	0.010	0.009	-0.017	0.008	0.007	0.010	0.010	0.009	0.000	0.007
p3p	0.007	0.006	0.008	0.010	0.010	-0.007	0.008	0.007	0.010	0.011	0.009	0.007	0.007
c2	0.010	0.009	0.012	0.014	0.013	0.016	0.012	0.010	0.015	0.016	0.014	0.025	0.010

#### Interbond angle (degrees)

basis	C1	C2	C4	C6	C6_P	C6_N	R6	oR6	L13	L13_P	L16	L16_N	oL16
a4p	92.22	91.30	93.56	92.89	101.24	93.43	91.59	96.69	93.50	102.52	93.23	91.57	95.30
p2p	-1.42	-2.01	-1.99	-1.55	-2.95	-2.26	-0.43	-1.60	-3.72	-4.71	-3.85	-2.07	-0.56
a2p	-0.25	-0.14	-0.07	-0.09	-0.24	-0.14	-0.22	-0.41	-0.43	-0.76	-0.43	-0.74	-0.17
c3	-0.08	-0.08	-0.04	-0.06	0.01	-0.06	-0.12	-0.01	-0.10	-0.08	-0.12	-0.22	-0.04
c3a	-0.04	-0.06	-0.05	-0.05	-0.06	0.01	-0.06	-0.02	-0.04	-0.02	-0.05	0.06	-0.05
a3p	-0.19	-0.16	-0.10	-0.01	-0.03	-0.16	-0.14	-0.04	-0.20	-0.19	-0.21	-0.32	-0.04
c4a	0.01	-0.00	-0.00	0.01	-0.01	0.04	-0.00	0.01	0.02	0.03	0.01	0.09	0.02
p3p	-0.51	-0.41	0.06	0.01	0.01	-0.07	-0.19	-0.03	-0.16	-0.52	-0.19	-0.44	-0.02
c4	-0.01	-0.01	0.01	0.01	-0.00	0.03	-0.02	0.04	0.01	-0.01	0.00	-0.00	0.01
p3pa	-0.45	-0.36	0.07	0.02	-0.11	0.02	-0.15	-0.02	-0.07	-0.50	-0.08	-0.14	-0.04
c2a	-0.14	-0.07	-0.05	0.04	-0.30	0.03	-0.12	-0.31	-0.16	-0.45	-0.14	-0.22	-0.23
c2	-0.31	-0.20	0.06	0.10	-0.04	-0.24	-0.29	-0.30	-0.31	-0.74	-0.32	-0.71	-0.13

#### Binding energy wrt C1 and C2 (eV/pnictogen)

basis	C1	C2	C4	C6	C6_P	C6_N	R6	oR6	L13	L13_P	L16	L16_N	oL16
a4p	0.000	0.000	0.008	0.012	-1.213	0.169	0.007	0.005	0.027	-0.512	0.032	0.118	0.015
c2	0.000	0.000	-0.005	-0.006	0.002	-0.051	-0.006	-0.008	-0.009	-0.005	-0.010	-0.020	-0.009
a2p	0.000	0.000	-0.002	-0.002	0.003	-0.046	-0.002	-0.004	-0.003	0.000	-0.003	-0.014	-0.003
p3p	0.000	0.000	-0.000	-0.001	-0.006	-0.009	-0.002	-0.002	-0.001	-0.005	-0.001	-0.000	-0.001
c3	0.000	0.000	-0.001	-0.001	-0.001	-0.006	-0.001	-0.001	-0.001	-0.001	-0.001	-0.002	-0.001
c4	0.000	0.000	-0.000	-0.000	0.001	-0.000	-0.000	0.000	-0.000	0.000	-0.000	-0.000	0.000
c2a	0.000	0.000	-0.000	0.000	-0.002	0.003	-0.000	-0.001	-0.000	-0.001	-0.000	0.000	0.001
c3a	0.000	0.000	-0.000	0.000	0.000	0.006	-0.000	-0.001	-0.000	-0.001	-0.000	0.001	-0.000
c4a	0.000	0.000	0.000	0.000	0.001	0.005	-0.000	0.000	0.000	0.000	0.000	0.001	0.000
a3p	0.000	0.000	-0.000	0.000	0.003	-0.022	-0.000	-0.000	0.000	0.002	0.001	-0.004	0.001
p3pa	0.000	0.000	0.002	0.002	-0.004	0.008	0.000	-0.000	0.003	-0.001	0.003	0.006	0.004
p2p	0.000	0.000	0.066	0.113	0.093	0.008	0.090	0.095	0.169	0.156	0.187	0.143	0.265

HOMO-LUMO gap (eV)														
basis	C1	C2	C4	C6	C6_P	C6_N	R6	oR6	L13	L13_P	L16	L16_N	oL16	
a4p	7.758	5.676	4.963	4.627	4.517	2.935	4.819	4.886	4.122	3.955	3.962	1.996	3.686	
c2a	-0.636	-0.101	-0.083	-0.045	-0.019	-0.431	-0.065	-0.057	-0.047	-0.013	-0.039	-0.101	-0.023	
c3a	-0.639	-0.091	-0.069	-0.042	-0.020	-0.451	-0.053	-0.038	-0.034	-0.021	-0.028	-0.069	-0.023	
c4a	-0.645	-0.084	-0.064	-0.039	-0.012	-0.498	-0.048	-0.031	-0.031	-0.016	-0.025	-0.060	-0.020	
p3pa	-0.484	-0.058	-0.047	-0.029	0.001	-0.444	-0.031	-0.030	-0.033	0.012	-0.017	-0.075	-0.019	
c4	0.106	-0.007	-0.009	-0.005	-0.008	-0.006	-0.004	-0.001	-0.007	-0.011	-0.009	-0.002	-0.004	
c3	0.182	0.059	0.049	0.027	-0.006	0.149	0.033	0.026	0.022	-0.002	0.014	0.036	0.014	
p3p	0.213	0.104	0.080	0.046	0.007	0.120	0.049	0.038	0.026	0.021	0.025	0.032	0.026	
a3p	0.268	0.150	0.127	0.076	0.041	0.238	0.084	0.076	0.063	0.029	0.055	0.099	0.056	
c2	0.349	0.216	0.206	0.142	0.033	0.301	0.136	0.097	0.093	0.062	0.087	0.116	0.089	
a2p	0.372	0.289	0.307	0.204	0.126	0.430	0.181	0.144	0.158	0.131	0.152	0.170	0.128	
p2p	0.465	0.428	0.496	0.416	0.656	0.025	0.193	0.096	0.452	0.566	0.485	-1.295	-0.210	

## S4 Benchmarking density functionals against CCSD

Table S2: Benchmarking neutral phosphorus clusters. See Section S3 for notations.

d1 - Bond length (Ao)								
method	C1	C2	C4	C6	C6_P	C6_N	R6	oR6
<hr/>								
CCSD	1.416	2.241	2.240	2.243	2.166	2.759	2.244	2.231
<hr/>								
WB97X	-0.002	-0.027	-0.025	-0.023	-0.021	-0.024	-0.025	-0.023
MP2	-0.005	-0.009	-0.011	-0.014	-0.026	-0.143	-0.010	-0.013
PBE0	0.004	-0.013	-0.012	-0.009	0.002	-0.078	-0.013	-0.014
HSE06	0.004	-0.011	-0.010	-0.007	0.005	-0.070	-0.010	-0.012
CAM-B3LYP	-0.002	-0.011	-0.009	-0.005	-0.002	0.039	-0.010	-0.008
APF	0.004	-0.010	-0.008	-0.005	0.007	-0.056	-0.009	-0.010
PBE	0.016	0.010	0.012	0.015	0.032	-0.078	0.011	0.009
B3LYP	0.003	0.013	0.016	0.022	0.030	0.107	0.015	0.015
PBE0-D3	NaN	-0.014	NaN	NaN	NaN	NaN	-0.015	-0.017
<hr/>								
a1 - Interbond angle (deg)								
method	C1	C2	C4	C6	C6_P	C6_N	R6	oR6
<hr/>								
CCSD	93.85	92.85	94.15	93.55	103.46	95.78	93.23	98.70
<hr/>								
MP2	-0.11	-0.27	-1.85	-1.78	-0.31	-1.63	-0.49	-0.88
PBE	-1.52	-1.63	-1.00	-1.20	-1.10	-1.64	-1.17	-0.21
PBE0	-0.76	-0.87	-0.53	-0.69	-0.39	-0.72	-0.67	0.23
HSE06	-0.70	-0.90	-0.47	-0.62	-0.49	-0.70	-0.71	0.16
APF	-0.75	-0.85	-0.36	-0.62	-0.44	-0.71	-0.67	0.25
B3LYP	-0.48	-0.55	0.56	0.20	-0.60	-0.12	-0.51	0.53
CAM-B3LYP	-0.19	-0.27	0.65	0.45	0.13	0.43	-0.21	0.81
WB97X	-0.19	-0.28	0.31	0.55	0.87	0.77	-0.17	0.79
PBE0-D3	NaN	-0.86	NaN	NaN	NaN	NaN	-0.67	0.04
<hr/>								
Eb - Binding energy wrt [cluster1,chain2] (eV)								
method	C1	C2	C4	C6	C6_P	C6_N	R6	oR6
<hr/>								
CCSD	0.000	0.000	0.037	0.057	-1.199	0.125	0.050	0.076
<hr/>								
B3LYP	0.000	0.000	-0.025	-0.043	-0.011	0.020	-0.040	-0.042
CAM-B3LYP	0.000	0.000	-0.023	-0.039	-0.026	0.007	-0.039	-0.034
APF	0.000	0.000	-0.016	-0.029	-0.003	0.023	-0.027	-0.027
PBE0	0.000	0.000	-0.013	-0.024	0.002	0.023	-0.026	-0.025
HSE06	0.000	0.000	-0.013	-0.024	0.005	0.026	-0.026	-0.026
WB97X	0.000	0.000	-0.013	-0.021	-0.026	0.013	-0.033	-0.024
PBE	0.000	0.000	-0.009	-0.019	0.030	0.038	-0.022	-0.029
MP2	0.000	0.000	0.040	0.064	0.041	0.059	0.059	0.054
<hr/>								
f1 - Lowest vibrational frequency (icm)					f2 - Second lowest vibrational frequency (icm)			
method	C1	C2			method	C1	C2	
<hr/>								
CCSD	1044.1	79.1			CCSD	1167.1	450.0	
<hr/>								
WB97X	-25.3	8.2			WB97X	-11.3	22.1	
HSE06	-40.2	12.9			HSE06	-32.8	-0.9	
CAM-B3LYP	-17.8	-1.9			CAM-B3LYP	-12.1	1.6	
B3LYP	-22.6	1.2			B3LYP	-25.5	-25.4	
PBE	-67.4	11.6			PBE	-71.3	-25.3	
PBE0	-40.7	3.1			PBE0	-32.7	2.0	
MP2	-8.3	6.5			MP2	9.0	7.5	
APF	-39.2	4.4			APF	-33.0	-2.0	

Table S3: Benchmarking charged phosphorus clusters.

IP - Vertical ionization potential (eV)				EA - Vertical electron affinity (eV)			
method	C1	C2	C6	method	C1	C2	C6
CCSD	10.392	9.045	7.923	CCSD	-3.243	-1.885	-0.953
PBE	0.149	-0.072	-0.322	WB97X	0.091	-0.504	0.034
B3LYP	0.185	0.010	-0.242	CAM-B3LYP	0.363	-0.245	0.261
HSE06	0.091	-0.027	-0.174	MP2	-0.026	-0.010	0.364
APF	0.121	-0.004	-0.163	PBE0	0.457	0.298	0.521
PBEO	0.096	-0.020	-0.155	APF	0.480	0.327	0.553
CAM-B3LYP	0.148	0.038	-0.093	HSE06	0.465	0.316	0.558
WB97X	0.114	0.057	0.049	B3LYP	0.463	0.381	0.580
MP2	-0.036	0.098	0.237	PBE	0.600	0.432	0.795
dP - Cation contracted bond length (Ao)				dN - Anion broken bond length (Ao)			
method	C6	method	C6	method	C6	method	C6
CCSD	2.166	CCSD	2.759	MP2	-0.143	PBE0	-0.078
MP2	-0.026	PBE	-0.078	PBE	-0.078	HSE06	-0.070
WB97X	-0.021	HSE06	-0.070	APF	-0.056	APF	-0.056
CAM-B3LYP	-0.002	WB97X	-0.024	WB97X	-0.024	CAM-B3LYP	0.039
PBEO	0.002	CAM-B3LYP	0.039	B3LYP	0.107	B3LYP	0.107
HSE06	0.005						
APF	0.007						
B3LYP	0.030						
PBE	0.032						
aP - Cation interbond angle at contracted bond (deg)				dN - Anion interbond angle at broken bond (deg)			
method	C6	method	C6	method	C6	method	C6
CCSD	103.46	CCSD	95.78	MP2	-1.64	PBE	-1.64
PBE	-1.10	PBE0	-0.72	PBE0	-1.63	APF	-0.72
B3LYP	-0.60	HSE06	-0.70	APF	-0.71	HSE06	-0.70
HSE06	-0.49	B3LYP	-0.12	B3LYP	-0.12	CAM-B3LYP	0.43
APF	-0.44	CAM-B3LYP	0.43	WB97X	0.77	WB97X	0.77
PBEO	-0.39						
MP2	-0.31						
CAM-B3LYP	0.13						
WB97X	0.87						

Table S4: Differential quantities are more sensitive to density functional. Here the first subtable contains energy difference between hydrogen-passivated rings of blue- and black-P (a negative value means that black-P ring has lower energy). The bond ‘d1’ is out-of-plane bond, ‘d2’ is in-plane bond, ‘a1’ is the angle between ‘d2’ bonds, ‘a2’ is the angle between ‘d1’ and ‘d2’ bonds.

dE – Conformational energy difference per atom (eV)

method	oR6
<hr/>	
CCSD	-0.0134
<hr/>	
WB97X	-0.0044
CAM-B3LYP	-0.0026
PBE0-D3	-0.0017
PBE0	-0.0005
HSE06	-0.0003
APF	-0.0001
B3LYP	0.0012
MP2	0.0022
PBE	0.0033

d21 – Bond length difference d1-d2 (Å)

method	oR6
<hr/>	
CCSD	0.0119
<hr/>	
MP2	-0.0020
PBE0-D3	-0.0003
HSE06	0.0008
PBE0	0.0009
PBE	0.0010
APF	0.0014
WB97X	0.0028
CAM-B3LYP	0.0036
B3LYP	0.0049

a12 – Interbond angle difference a2-a1 (deg)

method	oR6
<hr/>	
CCSD	1.56
<hr/>	
PBE0-D3	-0.49
PBE0	-0.30
WB97X	-0.20
MP2	-0.18
APF	-0.18
HSE06	-0.10
CAM-B3LYP	-0.05
PBE	0.17
B3LYP	0.45

PRE – Hole polaron relaxation energy (eV)

method	C6
<hr/>	
CCSD	0.389
<hr/>	
B3LYP	-0.047
PBE	-0.029
CAM-B3LYP	-0.014
APF	-0.007
HSE06	-0.004
PBE0	0.001
WB97X	0.017
MP2	0.101

NRE – Electron polaron relaxation energy (eV)

method	C6
<hr/>	
CCSD	1.360
<hr/>	
PBE	-0.450
MP2	-0.392
HSE06	-0.260
APF	-0.242
PBE0	-0.237
B3LYP	-0.203
CAM-B3LYP	0.014
WB97X	0.167

## S5 Benchmarking density functionals by Koopman's theorem

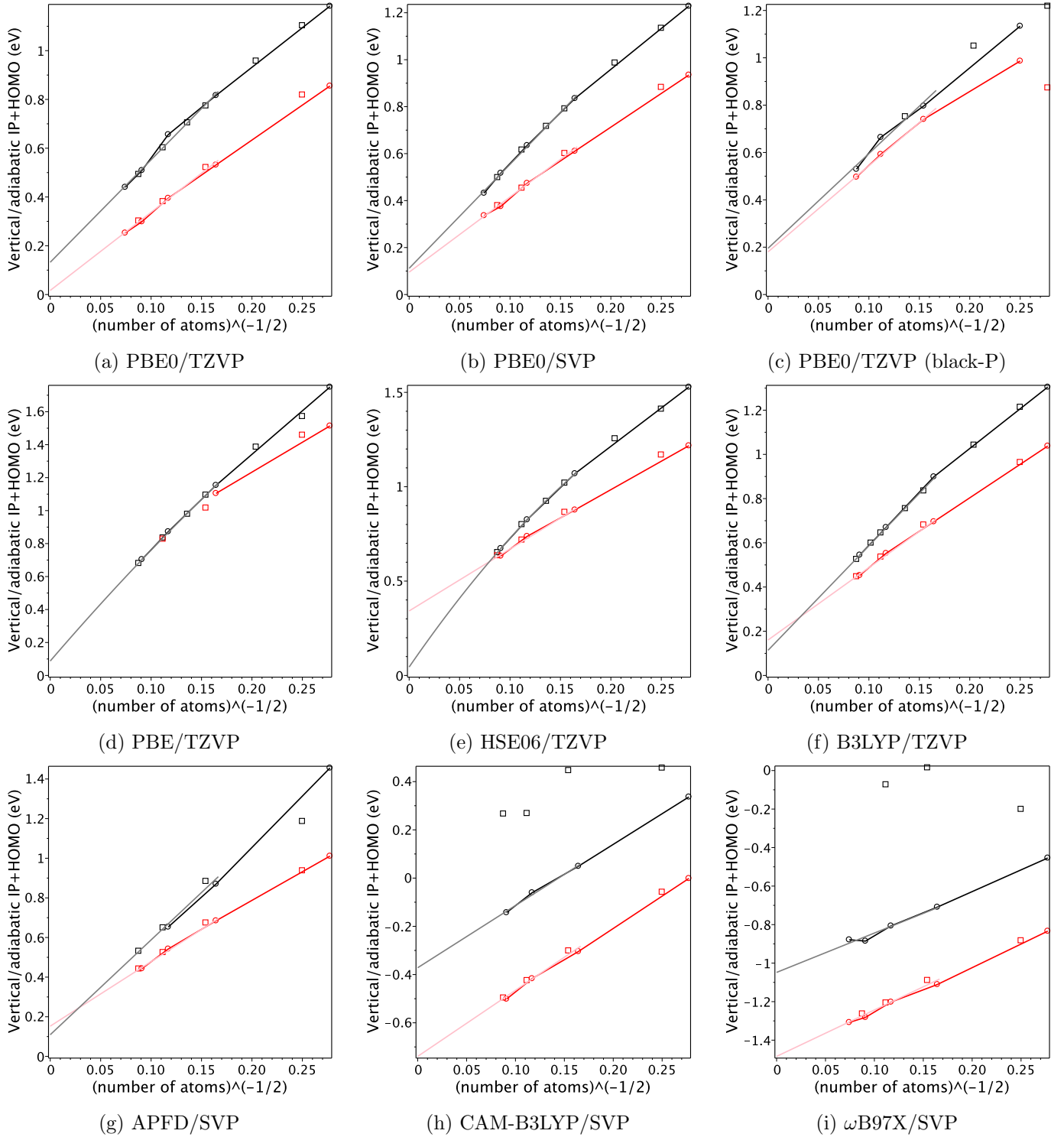


Figure S11: Sum of the vertical (black dots) or adiabatic (red dots) IP and HOMO energies for all considered density functionals for blue phosphorene clusters except for panel (c).

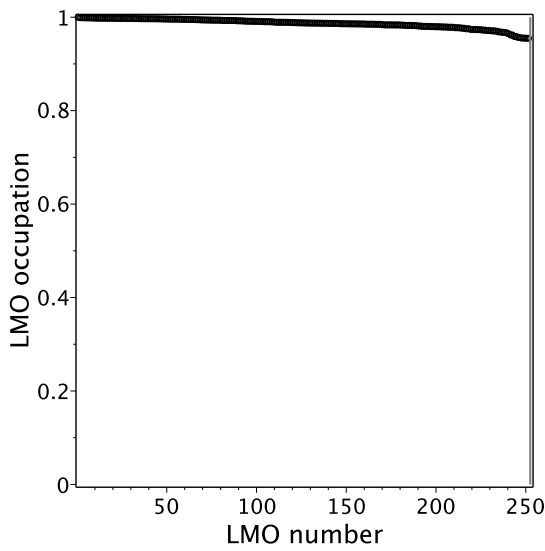
## S6 Main parameters of blue- and black-P monolayers

Table S5: Main parameters of blue- and black-P monolayers. Data are grouped by basis set: a3p=def2-TZVP, a2p=def2-SVP, paw400=PAW method with 400 eV cutoff. Density functionals are ordered by the band gap. Black-P data are marked by asterisk “\*”, blue-P data have no asterisk. NBO energies are calculated for 96-atom clusters: energies of LP orbitals are absolute, those of bonding orbitals are relative to the LP. In case of CAM-B3LYP and  $\omega$ B97 functionals with def2-TZVP basis, the wave-function is not converging for black-P at the default for Gaussian 16 precision.

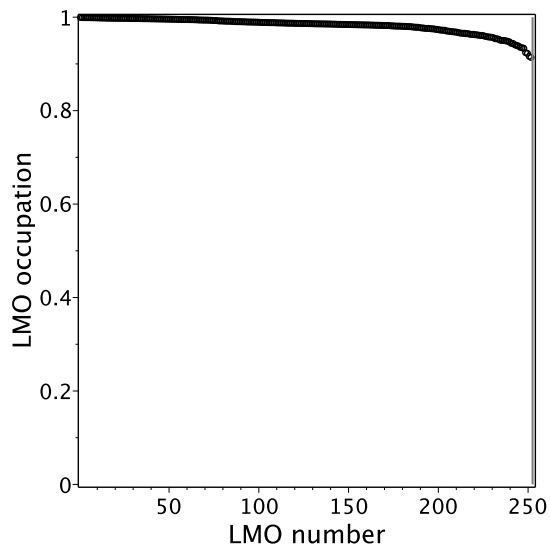
Method	dE meV	bondlengths Å		angles deg		gap eV	HOMO eV	LUMO eV	LP eV	bonding eV	orbitals eV
<b>---</b> paw400 <b>---</b>											
PBE		2.261		92.9		1.93	-4.29	-2.36			
	-1.6	2.258	2.221	96.0	104.1	0.91	-2.84	-1.93			*
PBE0		2.234		93.3		3.39	-5.19	-1.80			
	-7.1	2.229	2.197	96.5	104.1	2.21	-3.50	-1.29			*
<b>---</b> a3p <b>---</b>											
PBE		2.265		92.8		1.94	-6.17	-4.23	-13.48	1.22	
	-4.5	2.263	2.224	95.9	104.1	0.92	-5.05	-4.12	-12.20	-0.32	-0.81 *
HSE06		2.243		93.3		2.70	-6.75	-4.04	-14.19	0.54	
	-11.3	2.239	2.204	96.5	104.3	1.63	-5.48	-3.86	-12.77	-1.23	-1.72 *
B3LYP		2.271		94.1		3.10	-6.79	-3.69	-14.33	1.00	
	-2.4	2.272	2.226	96.8	105.4	2.16	-5.65	-3.49	-12.98	-0.58	-1.18 *
APF		2.244		93.3		3.28	-7.05	-3.77	-14.46	0.54	
	-8.7	2.238	2.205	96.4	104.3	2.19	-5.77	-3.58	-13.02	-1.27	-1.74 *
PBE0		2.241		93.2		3.40	-7.12	-3.72	-14.53	0.45	
	-9.6	2.234	2.202	96.4	104.2	2.28	-5.81	-3.53	-13.08	-1.40	-1.85 *
CAM-B3LYP		2.245		94.3		5.44	-8.15	-2.72	-15.57	0.14	
									-14.07	-1.74	-2.25 *
WB97X		2.230		94.2		7.21	-9.23	-2.02	-16.41	-0.45	
									-14.80	-2.47	-2.95 *
<b>---</b> a2p <b>---</b>											
PBE		2.291		92.4		2.10	-6.29	-4.19	-13.91	2.08	
	2.4	2.289	2.251	95.8	102.7	0.83	-5.18	-4.34	-12.77	0.59	0.14 *
HSE06		2.268		92.8		2.89	-6.90	-4.01	-14.73	1.43	
	-3.9	2.263	2.228	96.3	103.1	1.54	-5.65	-4.11	-13.44	-0.34	-0.82 *
B3LYP		2.294		93.6		3.26	-6.83	-3.57	-14.75	1.86	
	10.6	2.294	2.250	96.5	104.2	2.13	-5.75	-3.63	-13.54	0.32	-0.23 *
APF		2.269		92.8		3.46	-7.22	-3.76	-15.02	1.43	
	-0.5	2.264	2.229	96.3	103.1	2.09	-5.95	-3.86	-13.71	-0.37	-0.83 *
PBE0		2.266		92.7		3.58	-7.30	-3.71	-15.10	1.35	
	-2.6	2.260	2.226	96.3	103.0	2.18	-5.99	-3.81	-13.77	-0.50	-0.95 *
CAM-B3LYP		2.267		93.8		5.62	-8.20	-2.58	-16.08	1.00	
	2.0	2.263	2.227	96.9	104.1	4.32	-6.88	-2.56	-14.70	-0.84	-1.33 *
WB97X		2.251		93.8		7.41	-9.32	-1.91	-16.95	0.31	
	-11.8	2.246	2.210	97.3	104.2	5.94	-7.84	-1.89	-15.45	-1.70	-2.19 *

Table S6: Tight-binding parameters of the valence band of blue- and black-P monolayers (in meV) derived from the Fock matrix of 96-atom clusters using NBO orbitals to project MOs onto LMOs. Here sites are numbered by the chemical distance, LP=lone pair, BD=bonding orbital (see Fig.3d), prime denotes in-plane bonds in black-P, r/o denotes blue/black allotrope. Site labels ‘p’ and ‘o’ have the following meaning: ‘p’ denotes sites which are closer to a chain of bonds along vectors  $\mathbf{a}'$ ,  $\mathbf{b}$ ,  $\mathbf{b}'$  in Fig.1 (path of the strongest connectivity), whereas ‘o’ means opposite sites in 6-membered rings. Only sites closer than 4th neighbor and with couplings stronger than 50 meV are listed comprehensively.

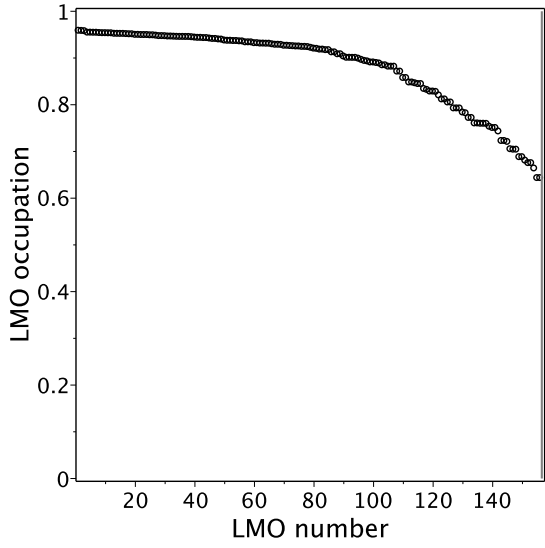
site	LP	r	o	site	BD	r	o	site	BD'	o
0		-11770	-11090	0		-12793	-12895	0		-13360
1	BD	-2505	-2497	1	LP	-2505	-2497	1	LP	-2453
1	BD'		-2453		1	BD	-1438	1	BD'	-1645
					1	BD'		1	BD	-1325
1	LP	515	504							
			-115							
2	BD	-335	591	2	LP	-335	591	2	LP	-277
2	BD'		-277							-270
			-270		2	BD	565	2	BD'	521
										467
										-177
					2	BD'	-266	2	BD	-213
2	LP	-116	135							
			-115							
3p	LP	-147	-473							
			174							
			-59							
3o	LP	41	98							
				3p	BD	62	<20	3p	BD'	-133
				3o	BD	-175	-114	3o	BD'	-138
				3p	BD'	-142	131	3p	BD	131
				3o	BD'	61	52	3o	BD	52
3p	BD	147	-120	3p	LP	147	-120	3p	LP	-183
3o	BD	39	70	3o	LP	39	70			100
3p	BD'		-183							
			100							
3o	BD'		64					3o	LP	64
----- selective -----										
4p	BD'		133					4p	LP	133
4p	BD	-24	-64	4p	LP	-24	-64	4p	BD'	92
4o	BD	-51	-48	4o	LP	-51	-48			
				4p	BD		99			
4p	LP	-39	-58							



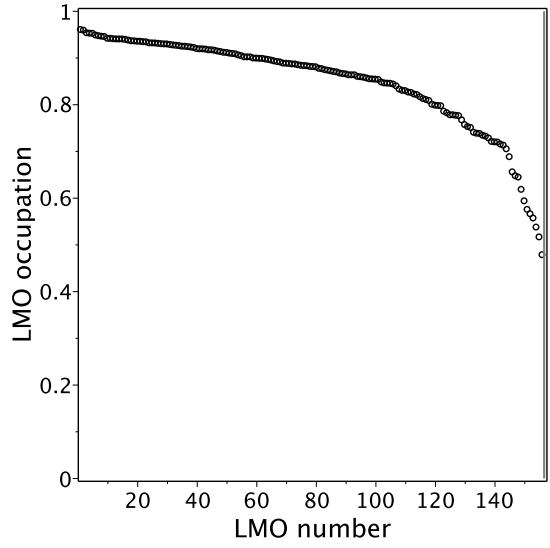
(a) Blue-P hole LMO “occupations”.



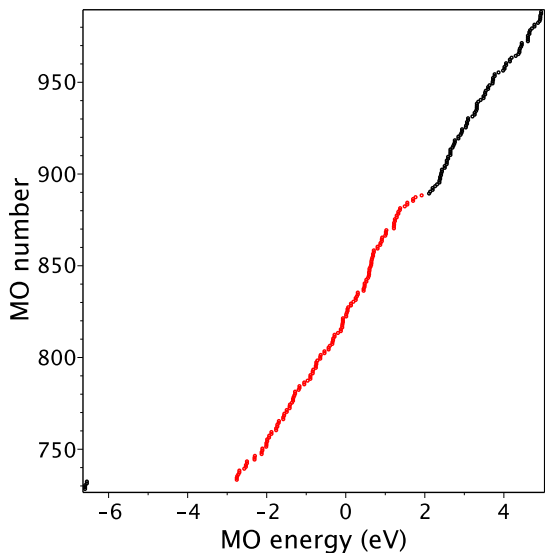
(b) Black-P hole LMO “occupations”.



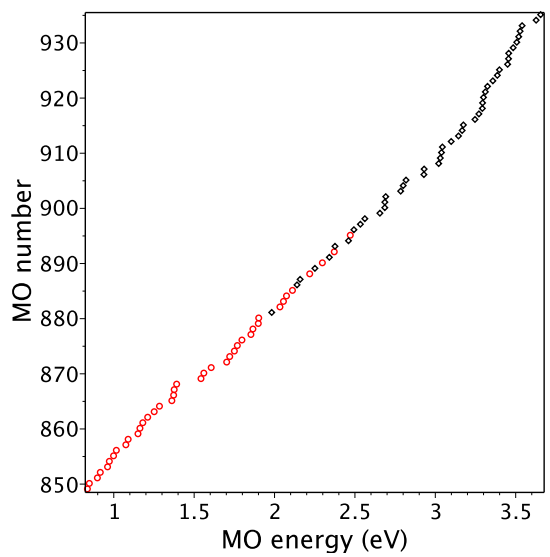
(c) Blue-P electron LMO “occupations”.



(d) Black-P electron LMO “occupations”.



(e) Blue-P MOs used to generate electron LMOs (shown in red).



(f) Black-P MOs used to generate electron LMOs (for clarity only boundary region is shown).

Figure S12: Technical details of LMOs. Here “occupations” are singular eigenvalues of the scalar product of selected MOs and NBOs. The shown figures are for 96-atom clusters.

## S7 Electronic structure of monolayers

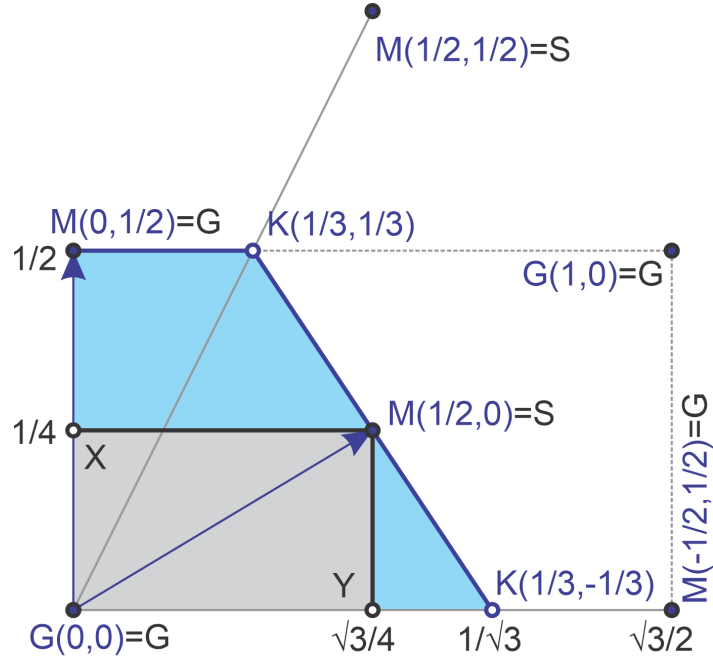


Figure S13: Mapping between k-vectors of rhombohedral (blue-colored) and orthorhombic (black-colored) lattices. Cartesian coordinates are given in fractions of the translation k-vector of the rhombohedral lattice. Lattice coordinates of k-vectors of the rhombohedral lattice are written in blue color. The first quarters of Brillouin zones are shaded with the corresponding color.

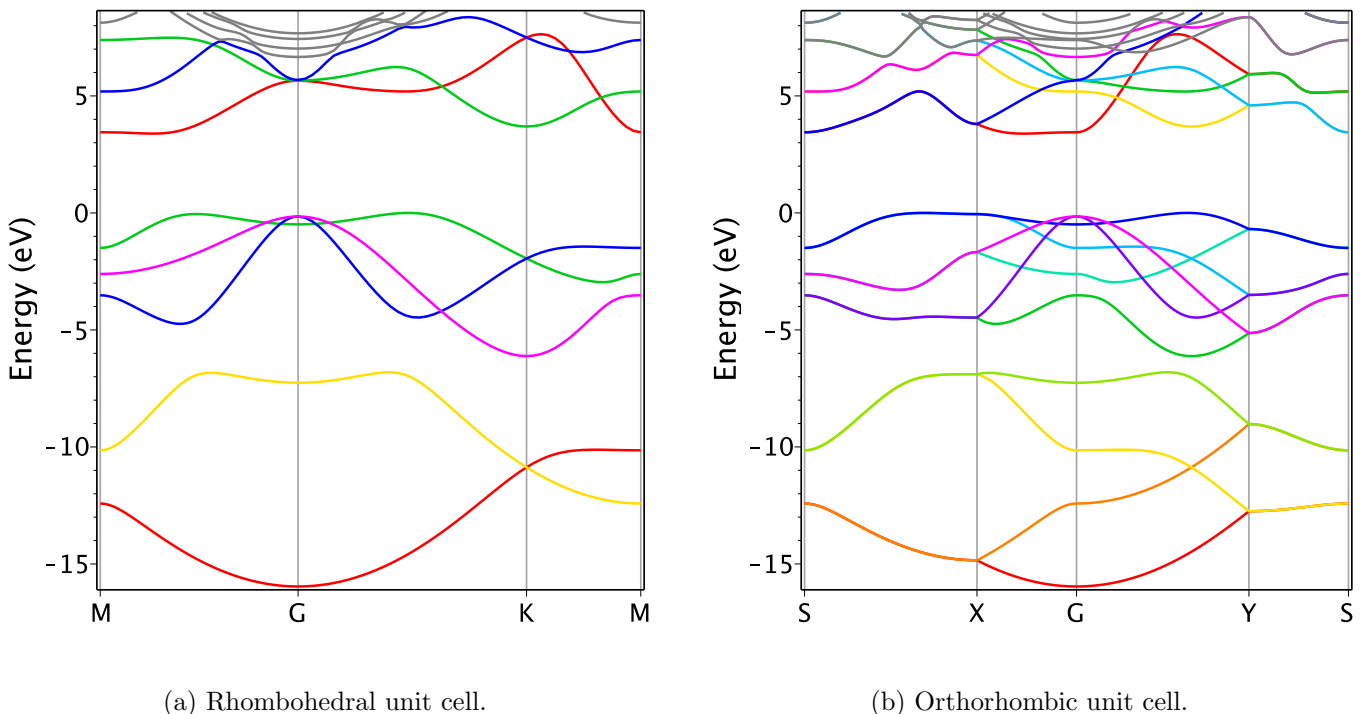
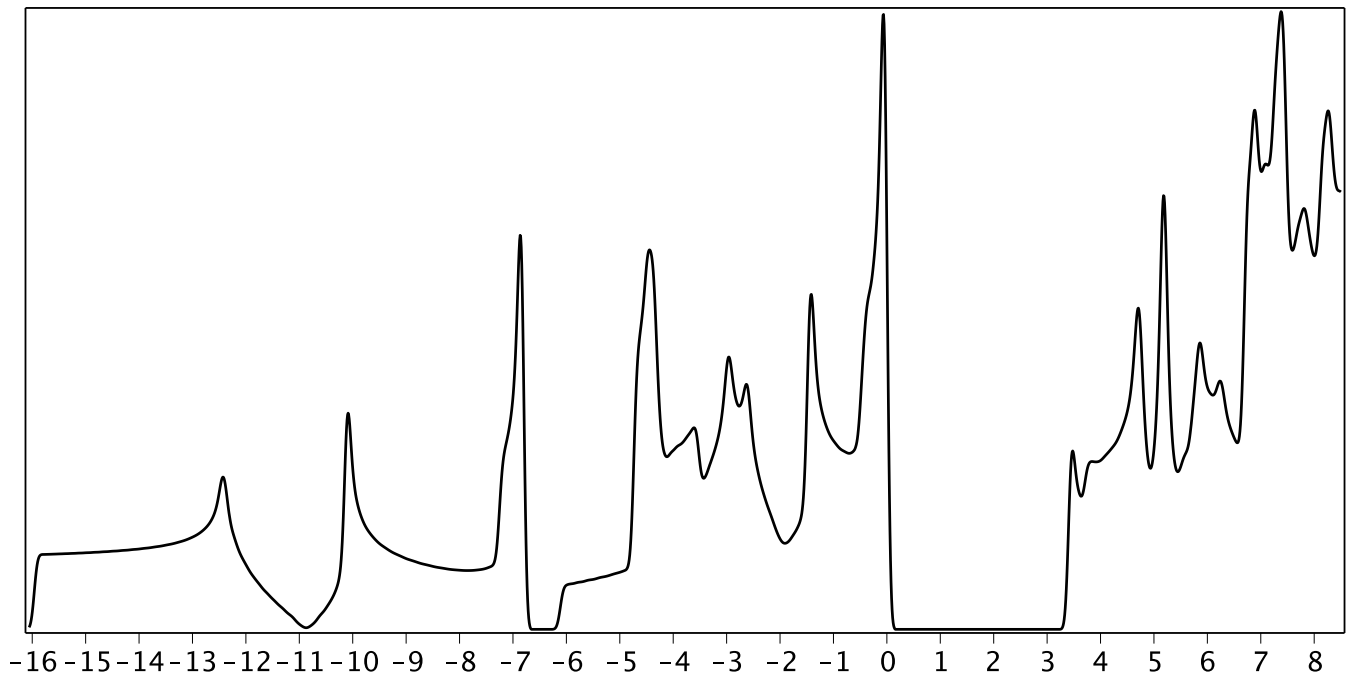
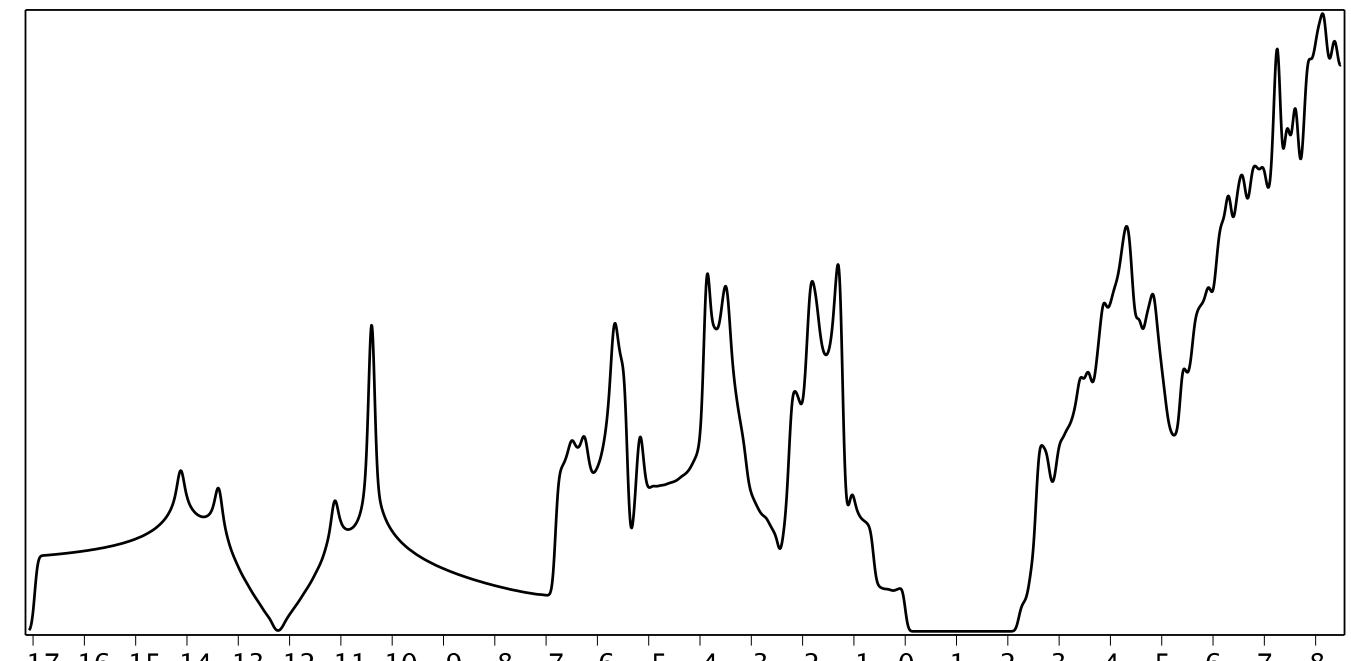


Figure S14: Comparison of band structure of blue-P in rhombohedral and orthorhombic unit cells (PBE0/PAW400).

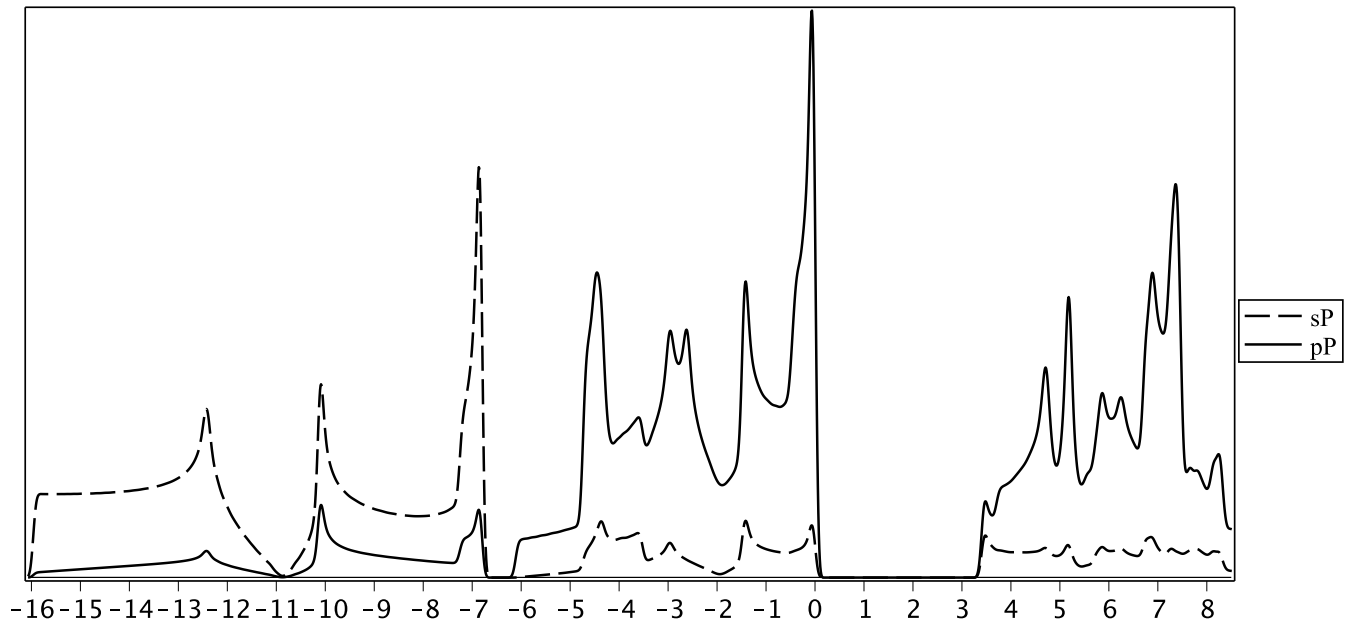


(a) Blue-P.

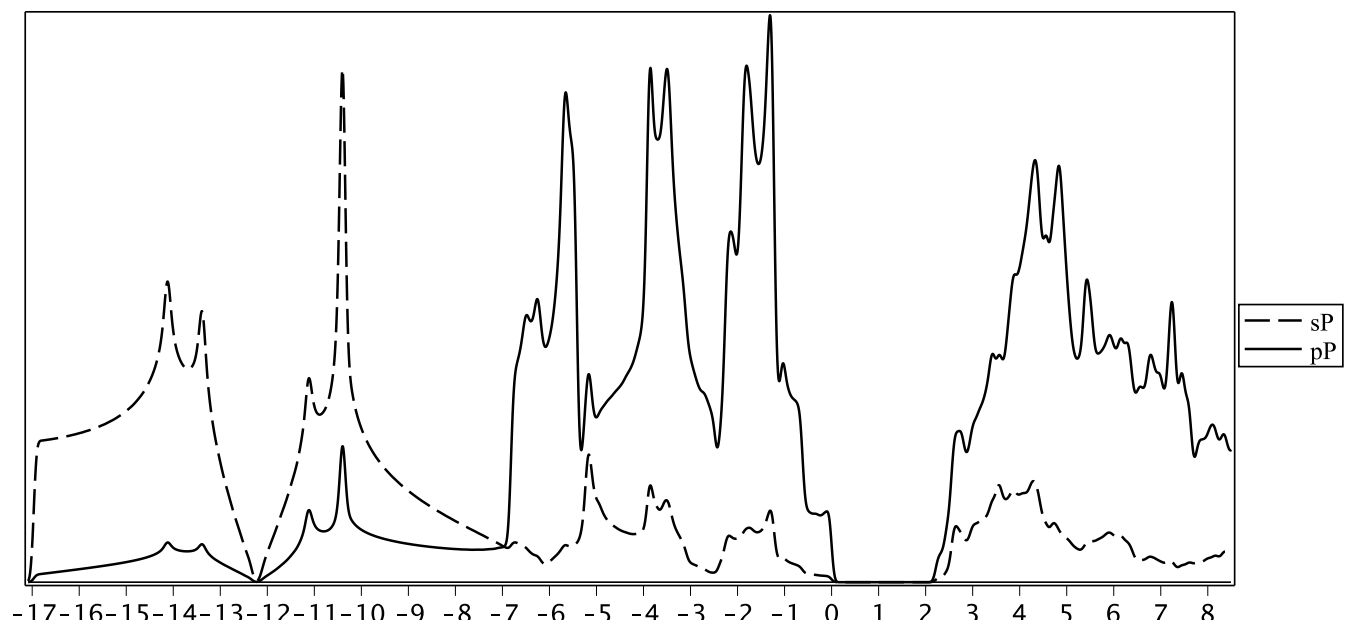


(b) Black-P.

Figure S15: Density of states: blue-P vs black-P (PBE0).

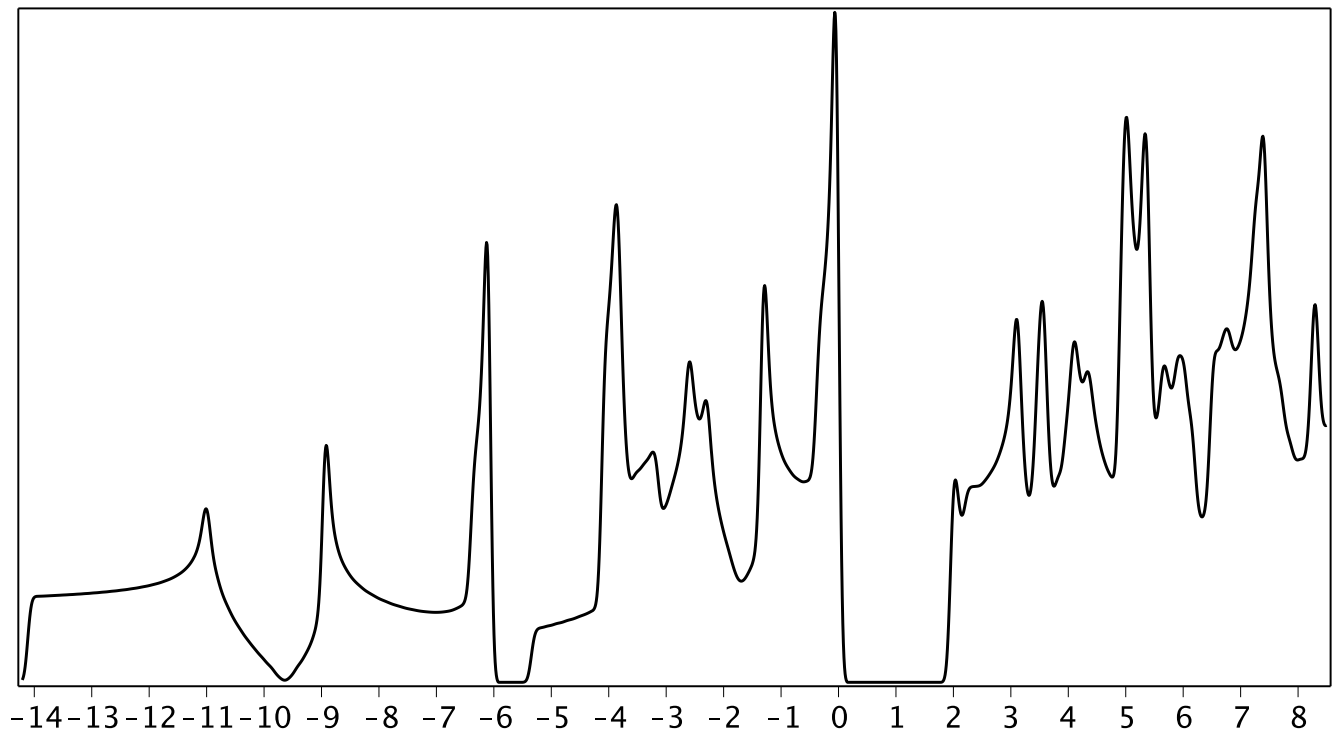


(a) Blue-P.

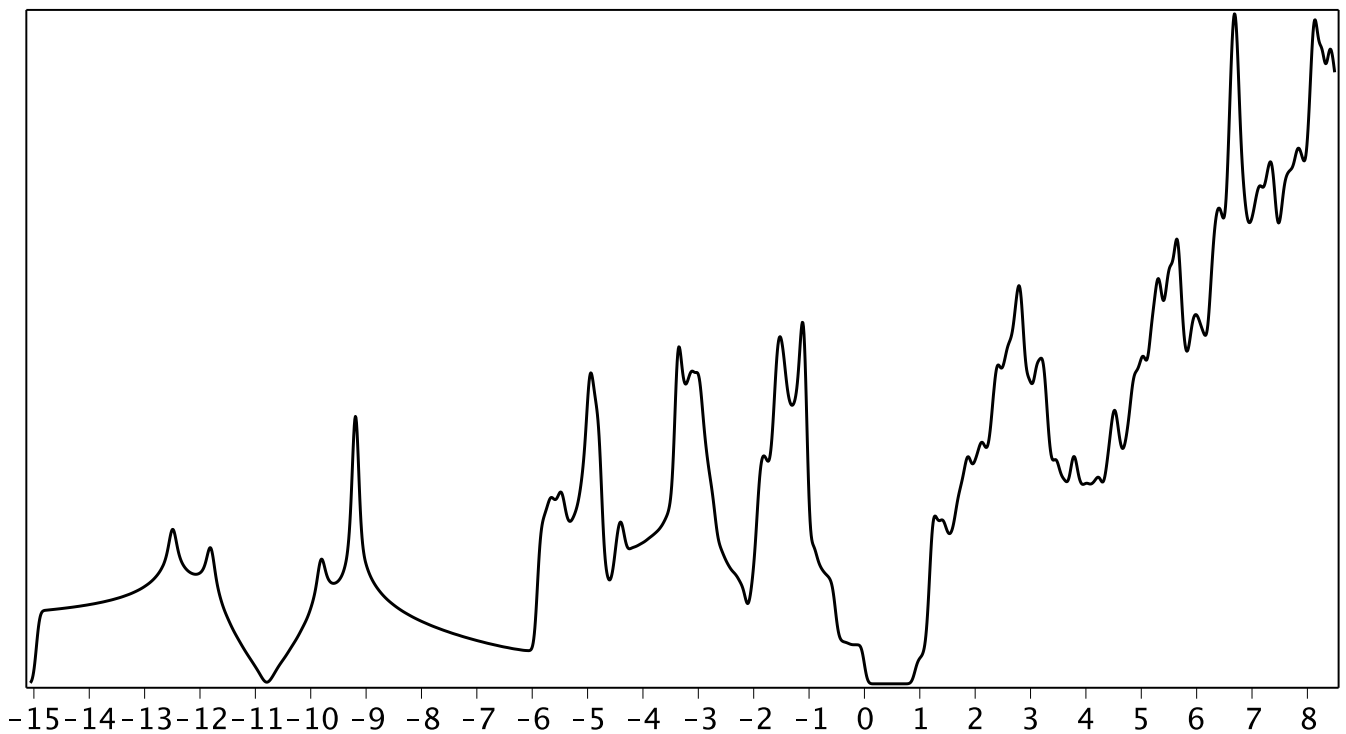


(b) Black-P.

Figure S16: Partial density of states: blue-P vs black-P (PBE0).

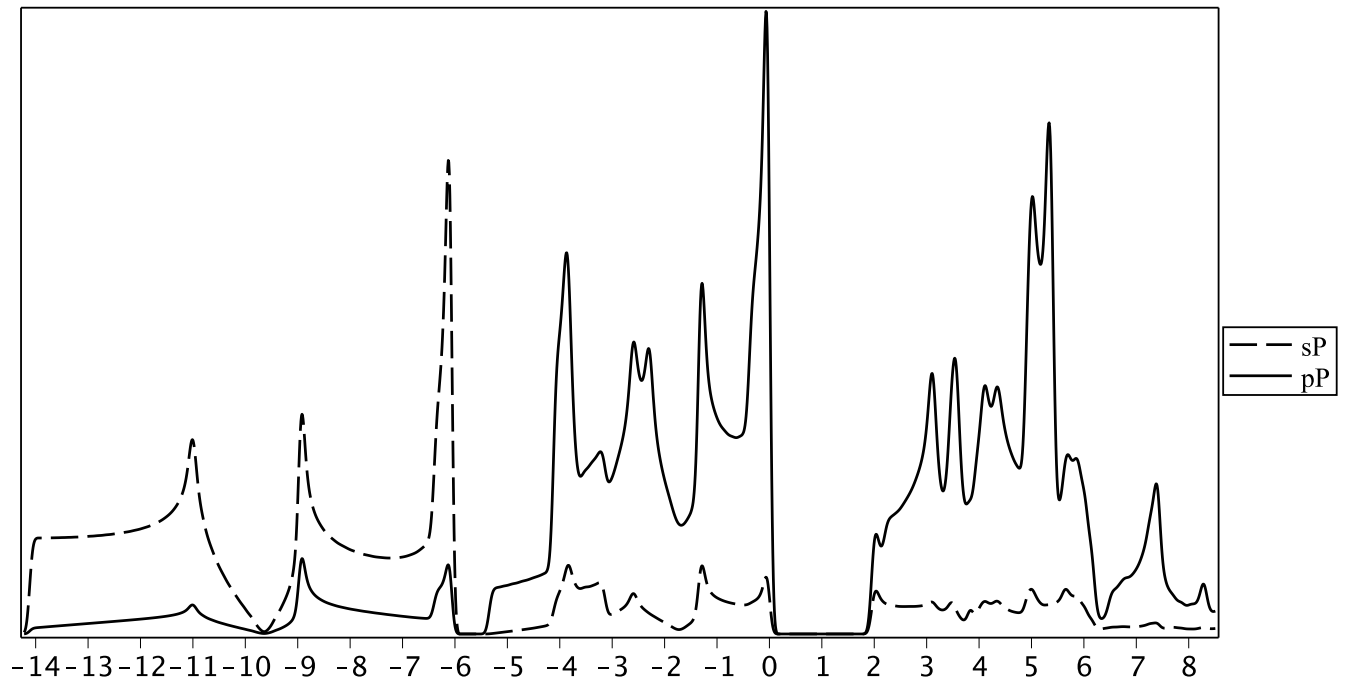


(a) Blue-P.

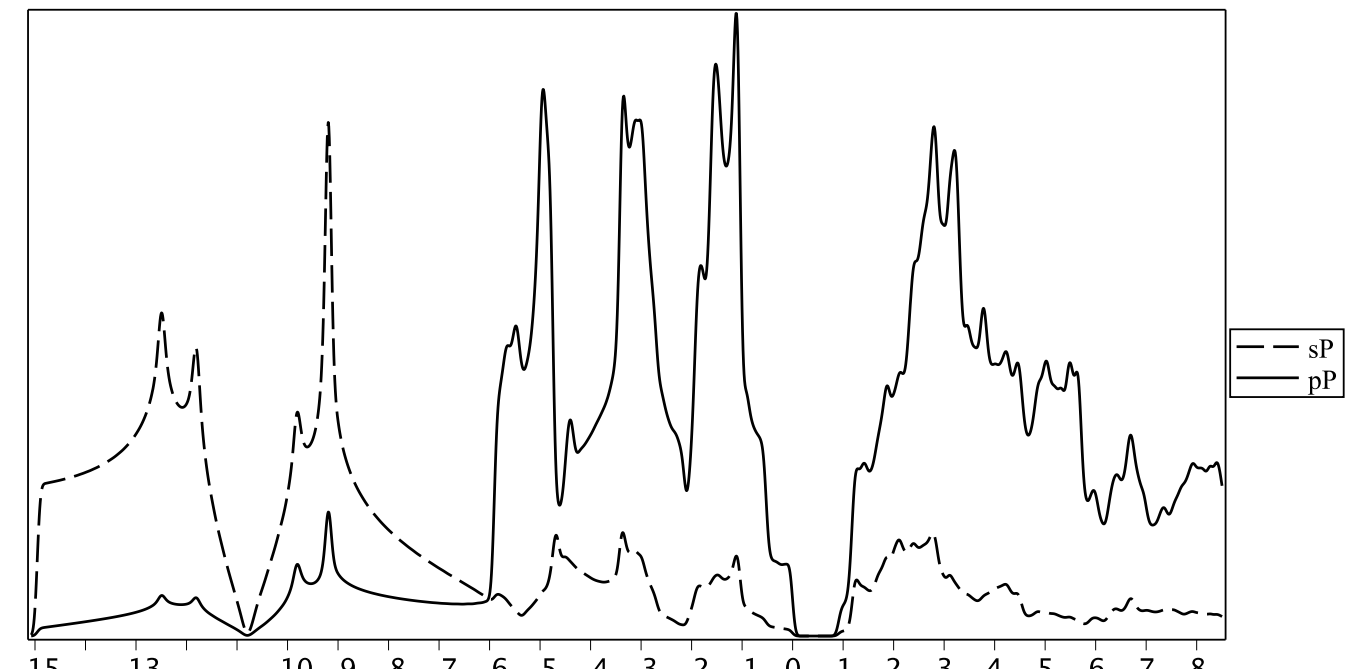


(b) Black-P.

Figure S17: Density of states: blue-P vs black-P (PBE).

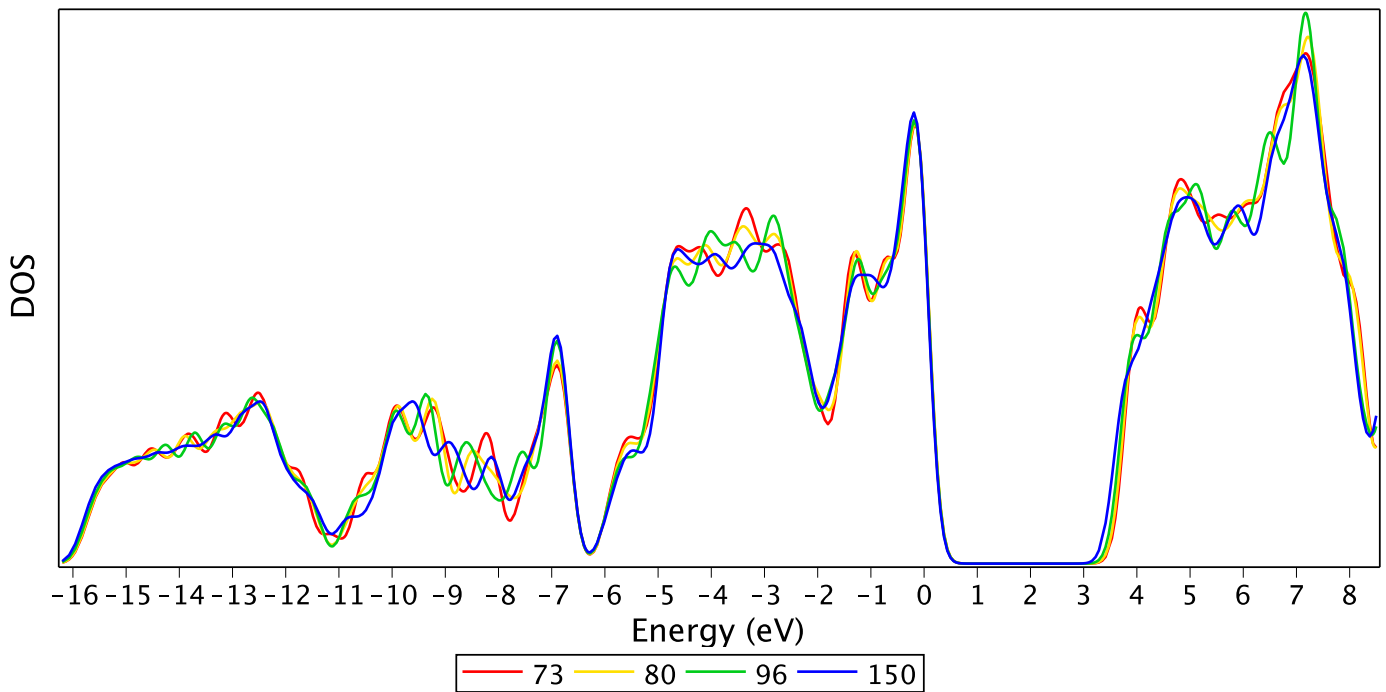


(a) Blue-P.

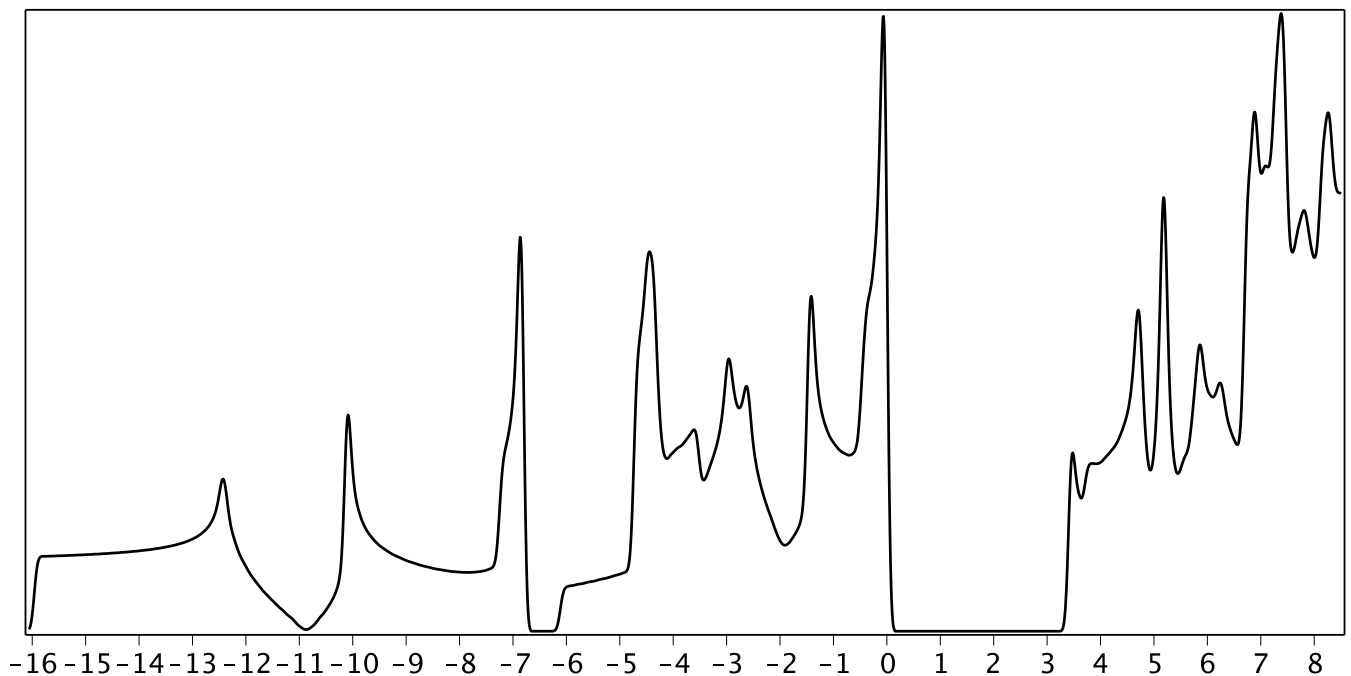


(b) Black-P.

Figure S18: Partial density of states: blue-P vs black-P (PBE).



(a) Clusters in TZVP basis.



(b) Monolayer in PAW400 basis.

Figure S19: Comparison of DOS of blue-P calculated with PBE0 using cluster approach and plane waves.

## S8 Polaron wave-function and lattice deformation

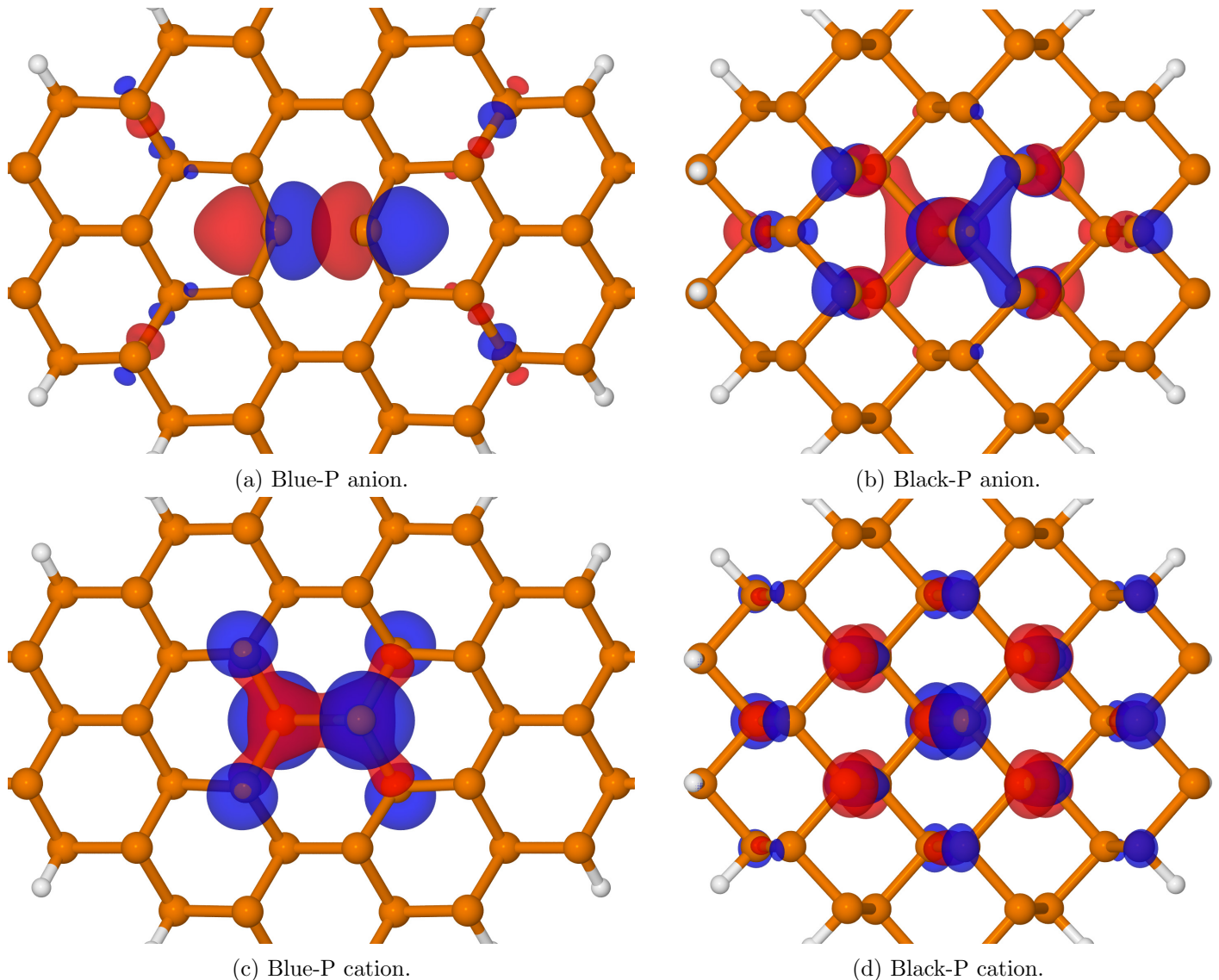


Figure S20: Natural orbitals of relaxed anions (a,b) and cations (c,d) of hydrogen-passivated 42-atom cluster for blue-P (a,c) and black-P (b,d). In all figures of the current work, the wave-function isovalue is typically 0.05 for LMO and 0.03 for MO. In case of comparison, all figures are plotted with the same isovalue.

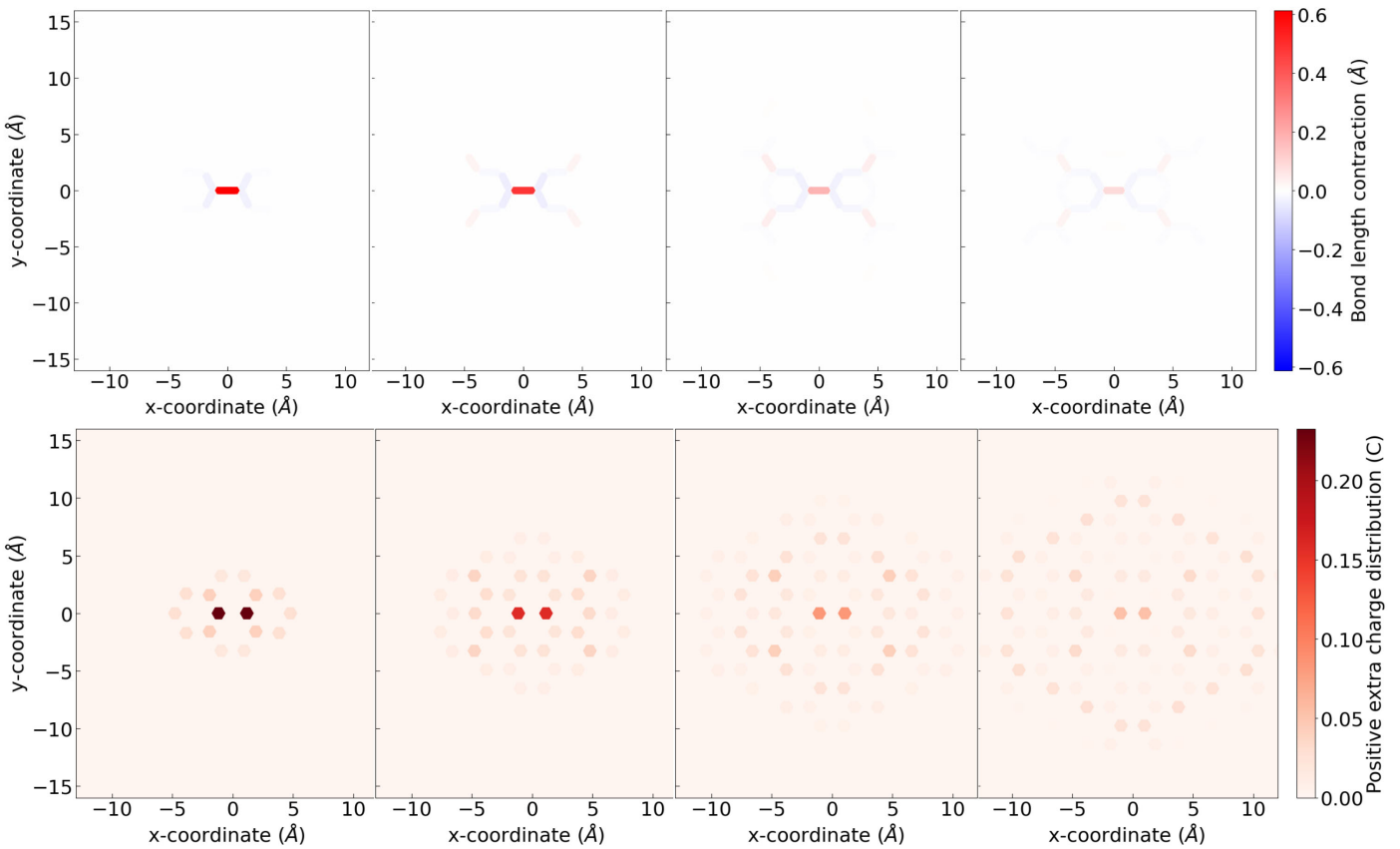


Figure S21: Blue-P bond elongation and negative extra charge distribution profiles for an electron polaron as the number of P atoms in a cluster increases.

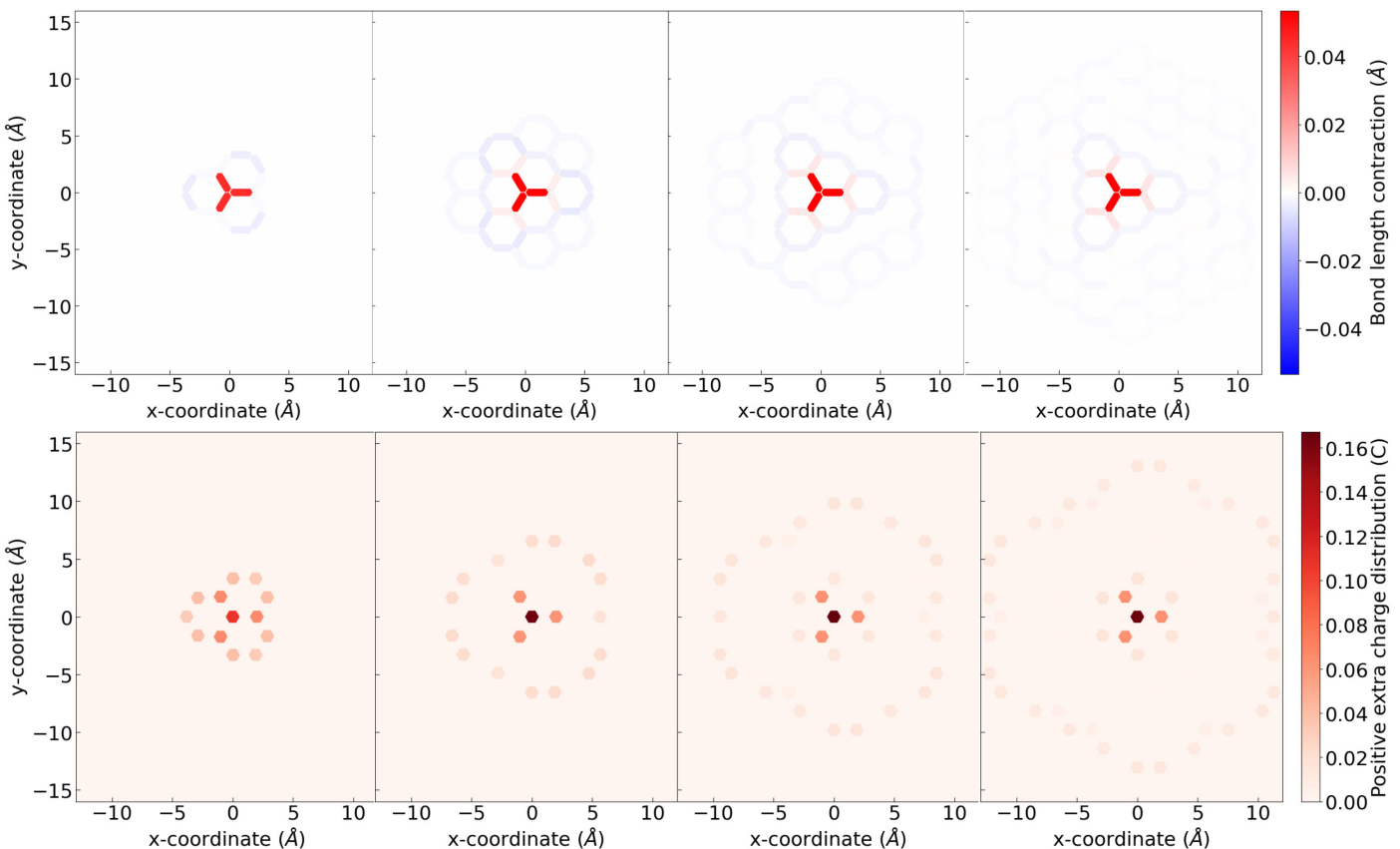


Figure S22: Blue-P bond contraction and positive extra charge distribution profiles for a hole polaron as the number of P atoms in a cluster increases.

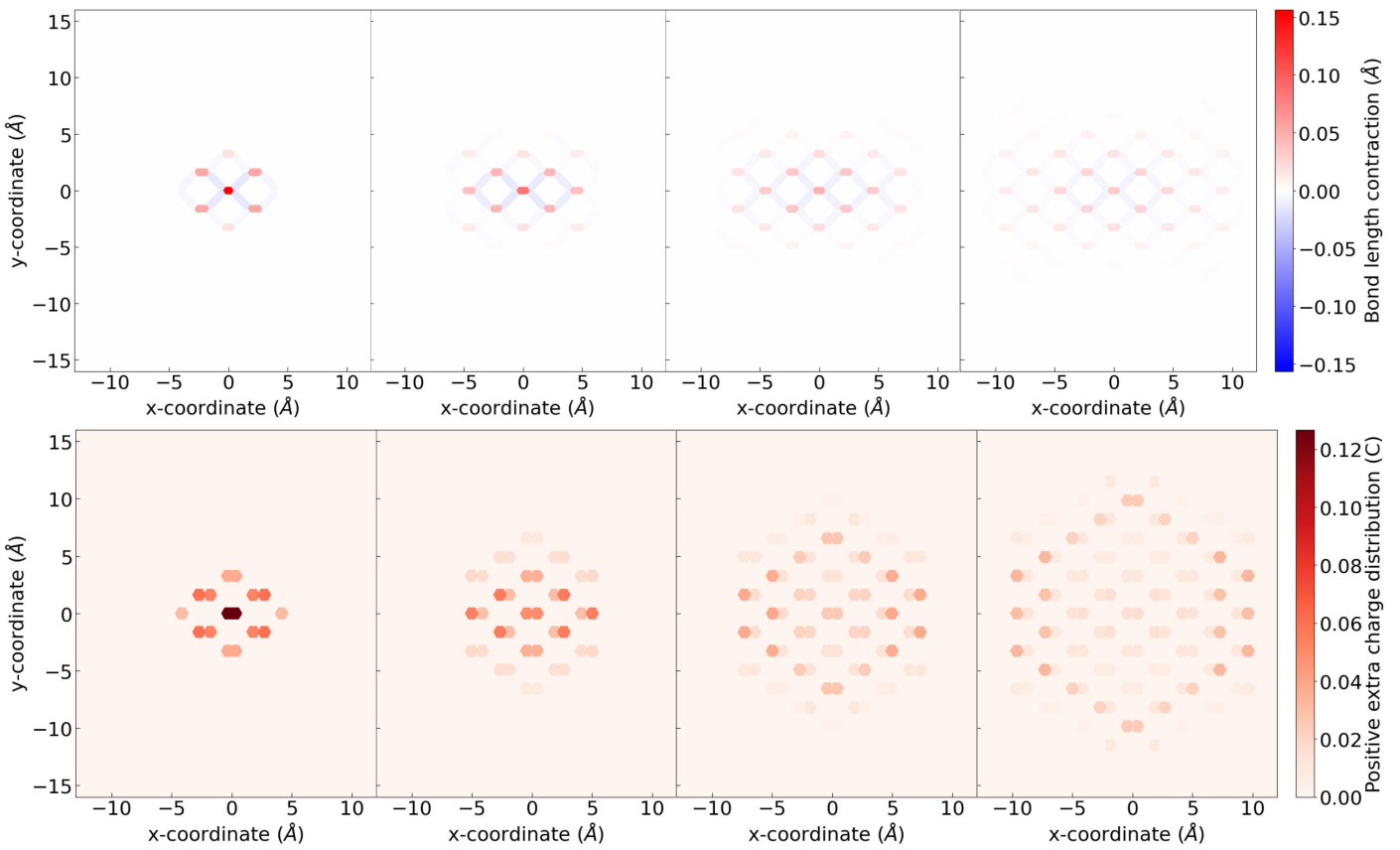


Figure S23: Black-P bond elongation and negative extra charge distribution profiles for an electron polaron as the number of P atoms in a cluster increases.

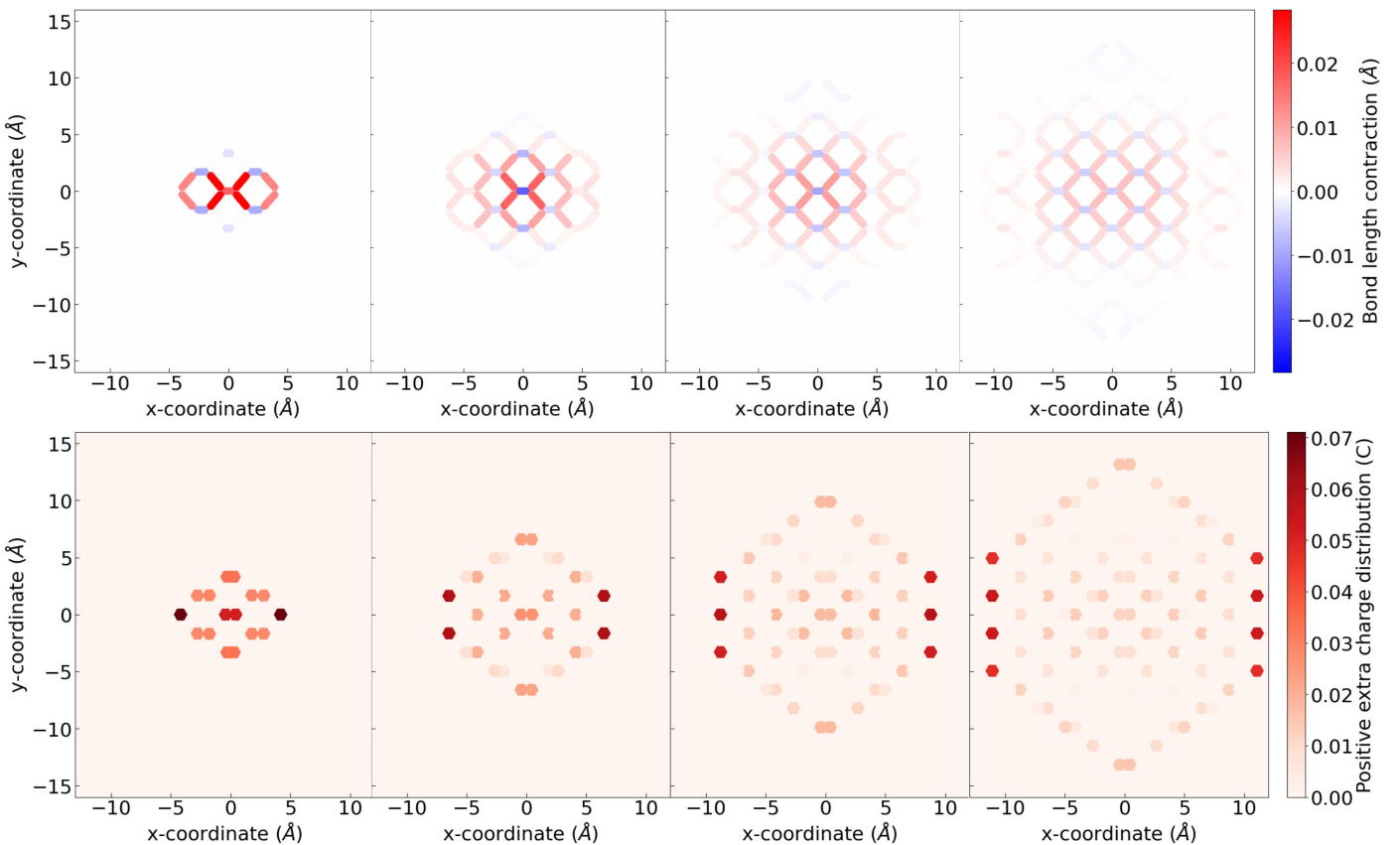
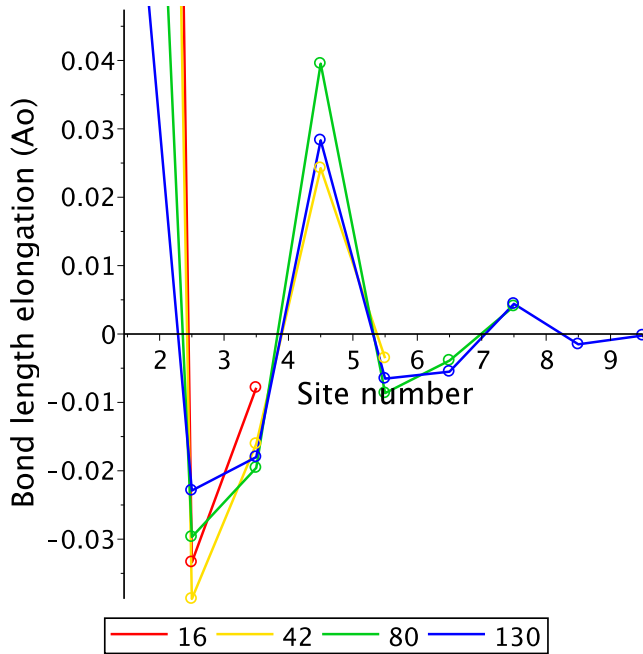
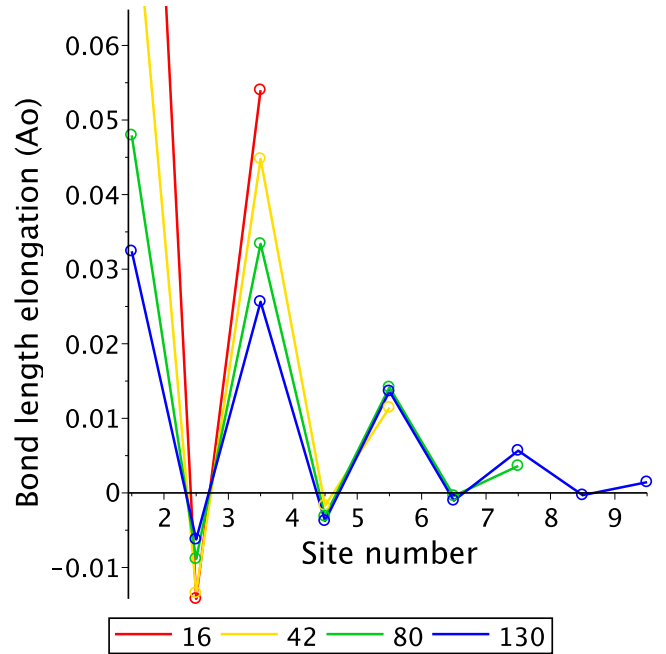


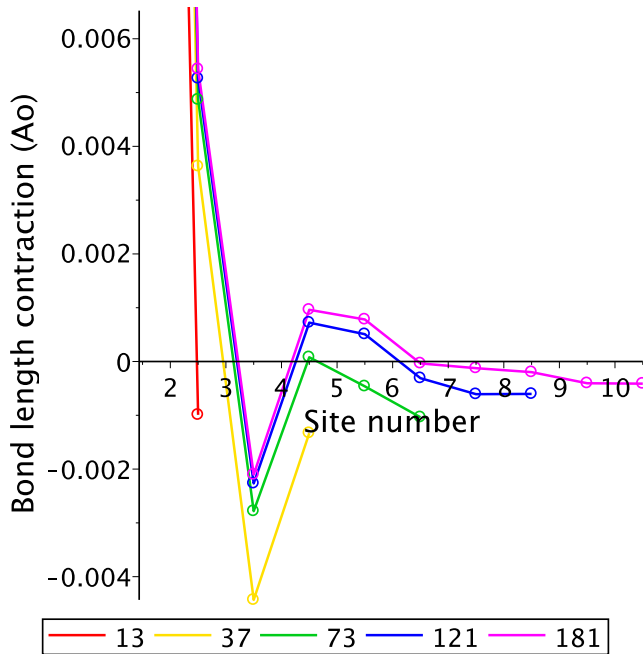
Figure S24: Black-P bond contraction and positive extra charge distribution profiles for a hole polaron as the number of P atoms in a cluster increases.



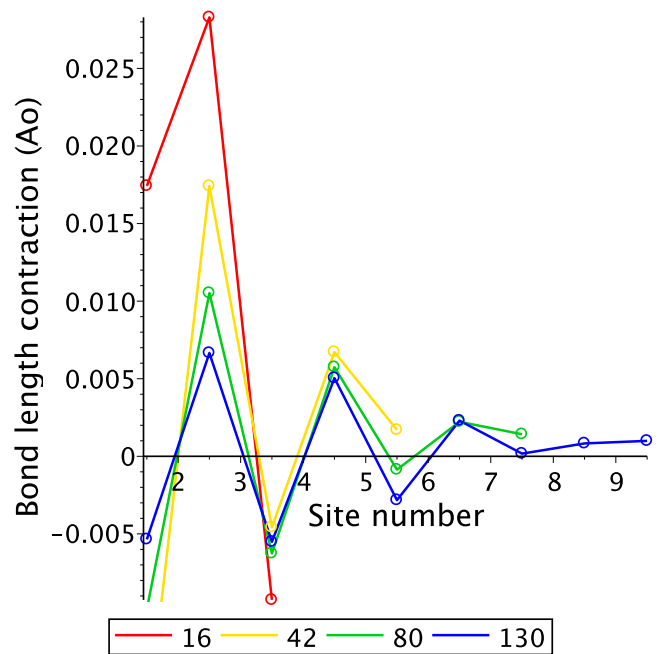
(a) Blue-P anion.



(b) Black-P anion.

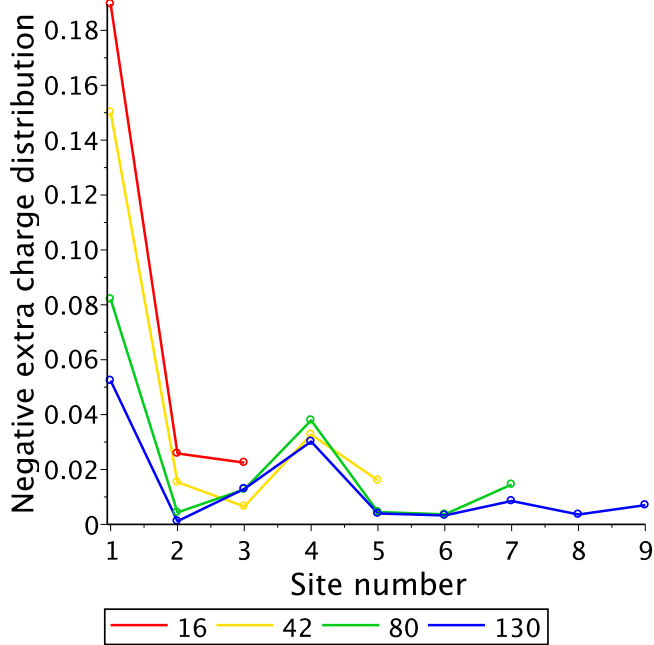


(c) Blue-P cation.

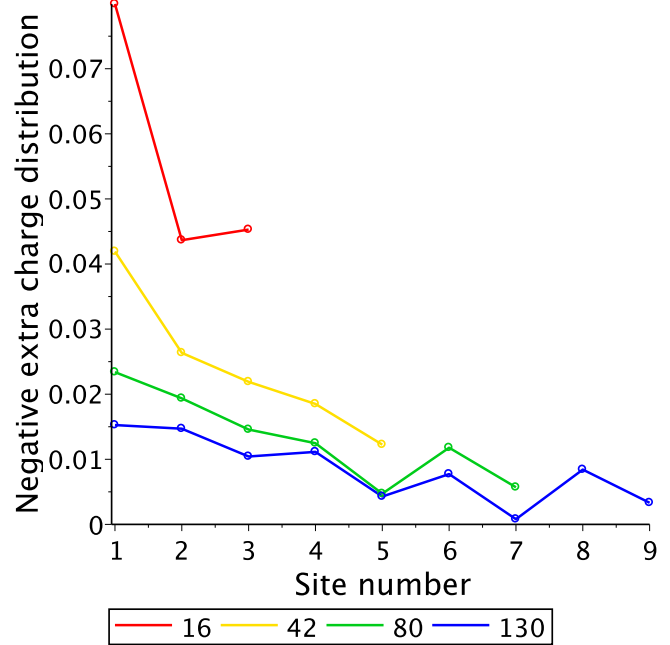


(d) Black-P cation.

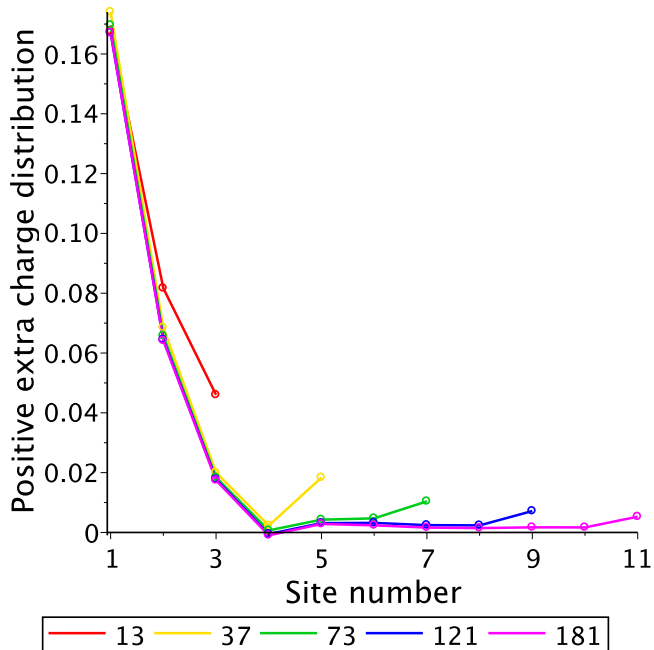
Figure S25: Bond length change profiles along a linear path for anions and cations of hydrogen-passivated clusters of various sizes (the size is given in the legends). The change is given with respect to the neutral cluster. The path goes from the center to the edge along  $\mathbf{a}'$  or symmetry-equivalent translation vectors, e.g., atoms {3, 2, 1, 7, 24} in Fig. S1c.



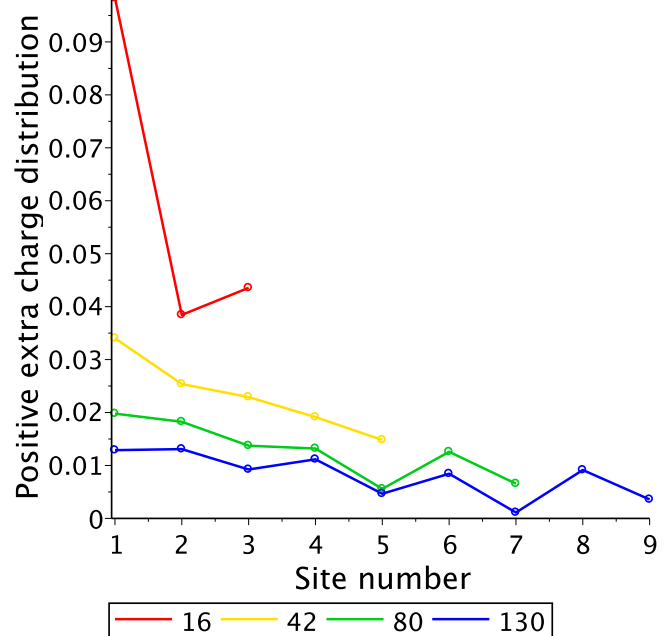
(a) Blue-P anion.



(b) Black-P anion.



(c) Blue-P cation.



(d) Black-P cation.

Figure S26: Extra charge distribution profiles along a linear path for anions and cations of hydrogen-passivated clusters of various sizes, see details in the previous figure. NBO atomic charges are used here.

## S9 Size convergence studies of hole polaron in blue-P

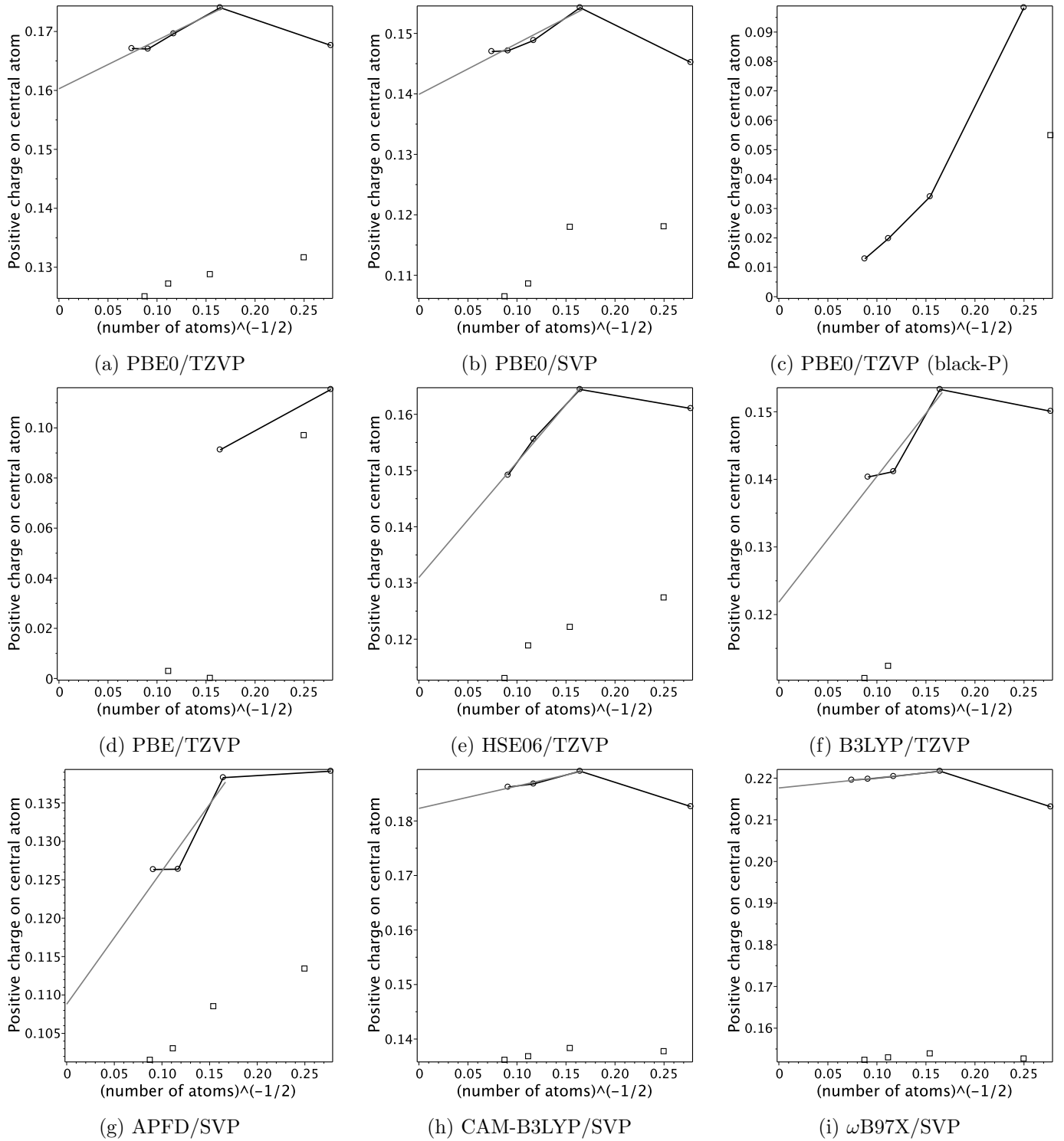


Figure S27: Hole polaron extra charge on central atom for all considered density functionals for blue phosphorene clusters except for panel (c).

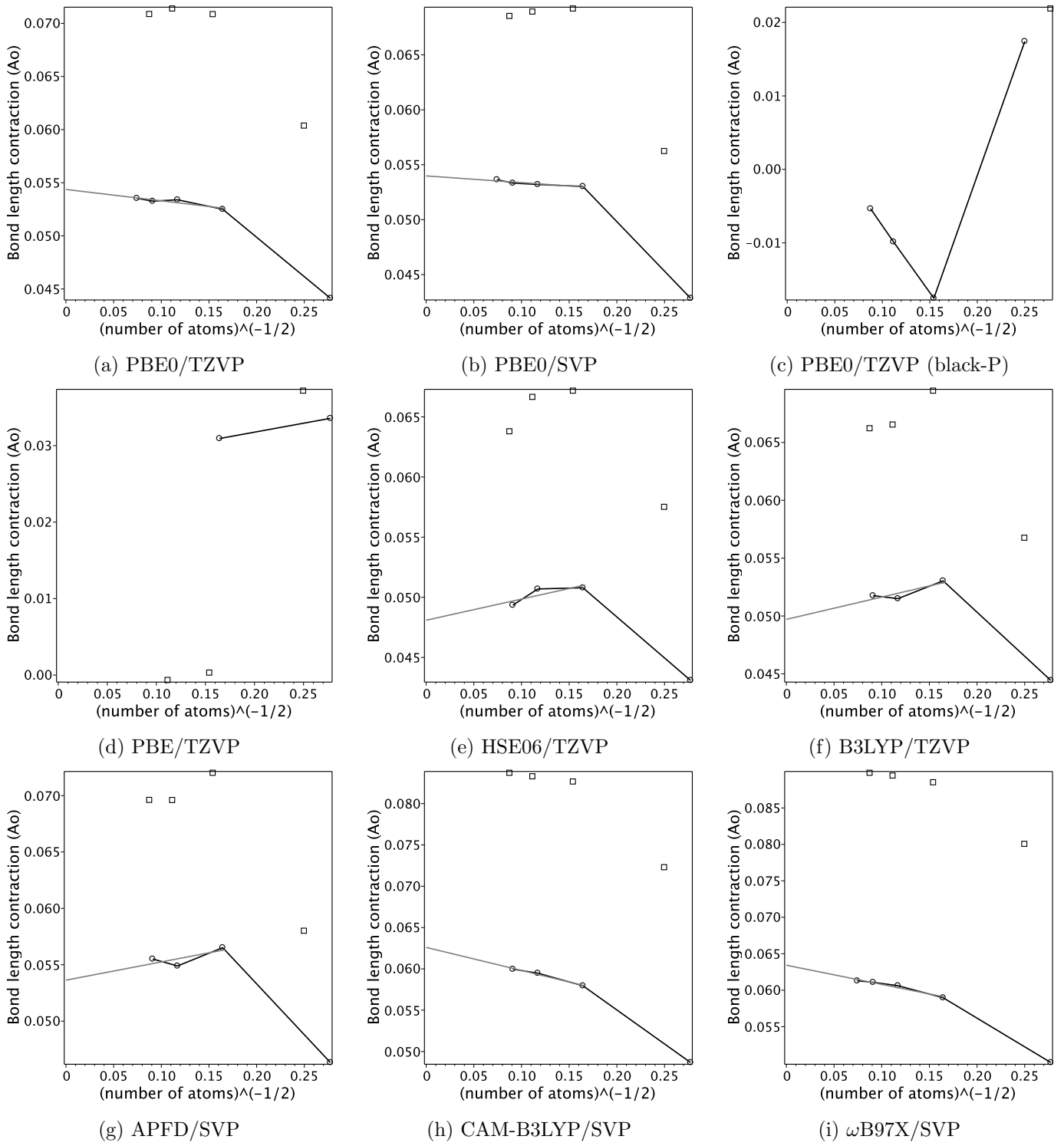


Figure S28: Hole polaron central bond length contraction for all considered density functionals for blue phosphorene clusters except for panel (c).

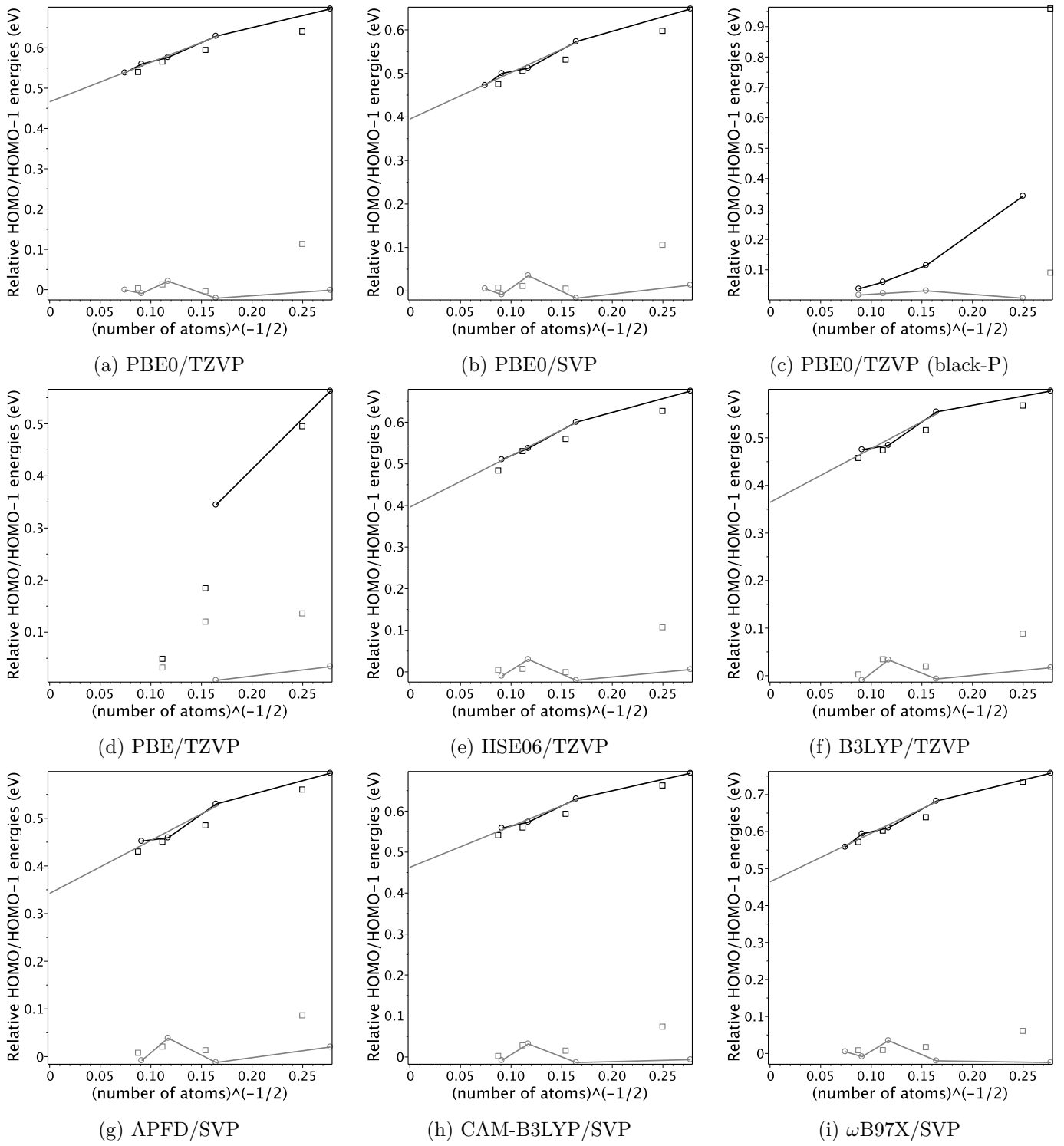


Figure S29: Hole polaron localized electronic level for all considered density functionals for blue phosphorene clusters except for panel (c).

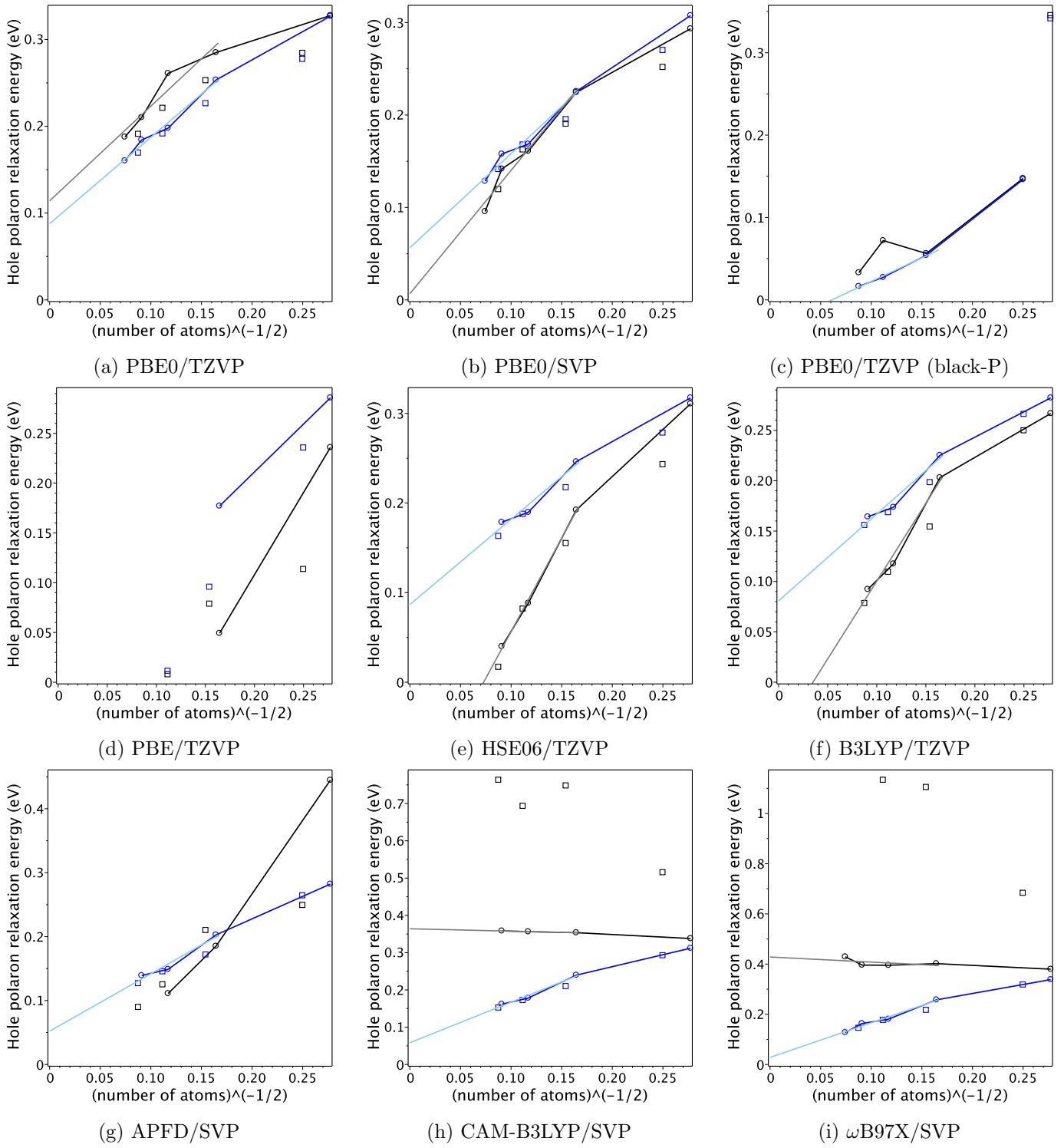


Figure S30: Hole polaron relaxation energy calculated by Eq. 1 (black colored) and with approximation given by Eq. 2 (blue colored) for all considered density functionals for blue phosphorene clusters except for panel (c).

Table S7: Extrapolated parameters of the hole polaron in blue-P. Here  $\Delta q$  is the extra charge on central atom,  $\Delta d$  is the central bond length contraction (there are three such bonds),  $\varepsilon^{\text{polaron}}$  is the polaron electronic level above the valence band edge,  $E^{\text{polaron}}$  is the polaron energy calculated with the use of Eq. 2, and  $\Delta\text{IP}^{\text{v/a}} = \text{IP}^{\text{v/a}} + \varepsilon_{\text{HOMO}}$  where  $\text{IP}^{\text{v/a}}$  is vertical/adiabatic ionization potential and HOMO is taken for relaxed neutral cluster.

Method	$\Delta q$ e	$\Delta d$ Å	$\varepsilon^{\text{polaron}}$ meV	$E^{\text{polaron}}$ meV	$\Delta\text{IP}^{\text{v}}$ meV	$\Delta\text{IP}^{\text{a}}$ meV
PBE/TZVP					88	
APFD/SVP	0.109	0.0536	342	52	109	153
B3LYP/TZVP	0.122	0.0497	364	81	114	160
HSE06/TZVP	0.131	0.0481	396	87	45	342
PBE0/SVP	0.140	0.0540	395	56	112	95
PBE0/TZVP	0.160	0.0544	466	88	132	20
CAM-B3LYP/SVP	0.182	0.0626	463	58	-372	-739
WB97X/SVP	0.218	0.0634	464	28	-1048	-1484

## S10 Potential energy surfaces

**Computational methodology.** In this work we use electron-phonon couplings defined through single-site Holstein Hamiltonian (independent boson model, displaced harmonic oscillator):

$$H = \varepsilon n + \sum_{\alpha} \hbar \omega_{\alpha} \left( b_{\alpha}^{\dagger} b_{\alpha} + \frac{1}{2} \right) + \sum_{\alpha} \hbar \omega_{\alpha} g_{\alpha} \left( b_{\alpha}^{\dagger} + b_{\alpha} \right) n, \quad (\text{S1})$$

where  $n = c^{\dagger}c$ ,  $c_i^{\dagger}$  is an electronic quasiparticle creation operator and  $b_{\alpha}^{\dagger}$  is phonon (vibrational normal mode) creation operator. Only a single electronic level  $\varepsilon$  is considered – it is the polaron level. A vibrational mode with frequency  $\omega_{\alpha}$  is coupled to the electronic level via dimensionless coupling constant  $g_{\alpha}$ , so that  $S_{\alpha} = g_{\alpha}^2$  is the corresponding Huang–Rhys factor. The polaron relaxation energy is given by

$$\Delta E_{\text{harmonic}}^{\text{charged}} = \sum_{\alpha} S_{\alpha} \hbar \omega_{\alpha} \equiv \sum_{\alpha} \lambda_{\alpha} = \frac{1}{\sqrt{2\pi\sigma^2}} \int \lambda(\omega) d\omega, \quad (\text{S2})$$

where the function

$$\lambda(\omega) = \sum_{\alpha} \lambda_{\alpha} e^{-\left(\frac{\omega-\omega_{\alpha}}{\sigma}\right)^2} \quad (\text{S3})$$

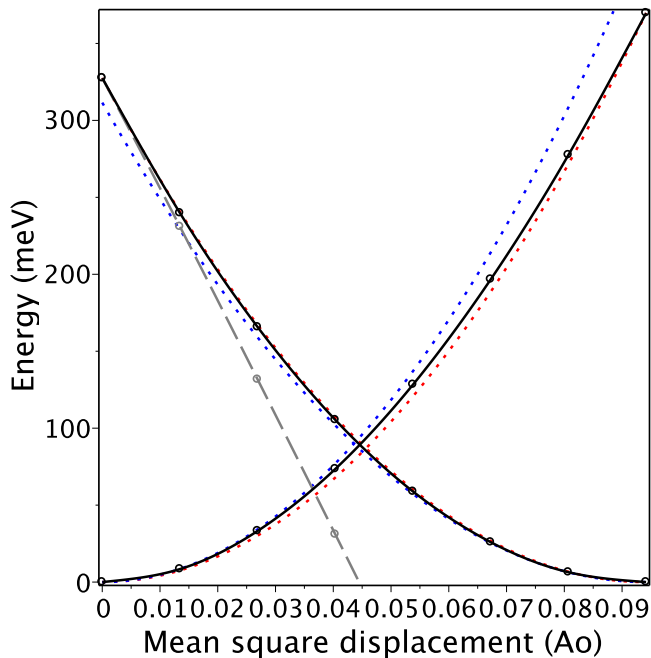
is plotted in Fig. 4c and  $\sigma$  is the line broadening parameter. The classical version of the above Hamiltonian is given by

$$\varepsilon n + \frac{1}{2} \sum_{\alpha} \hbar \omega_{\alpha} \left( \omega_{\alpha}^{-2} \dot{\xi}_{\alpha}^2 + \xi_{\alpha}^2 \right) + \sqrt{2} \sum_{\alpha} \hbar \omega_{\alpha} g_{\alpha} \xi_{\alpha} n, \quad (\text{S4})$$

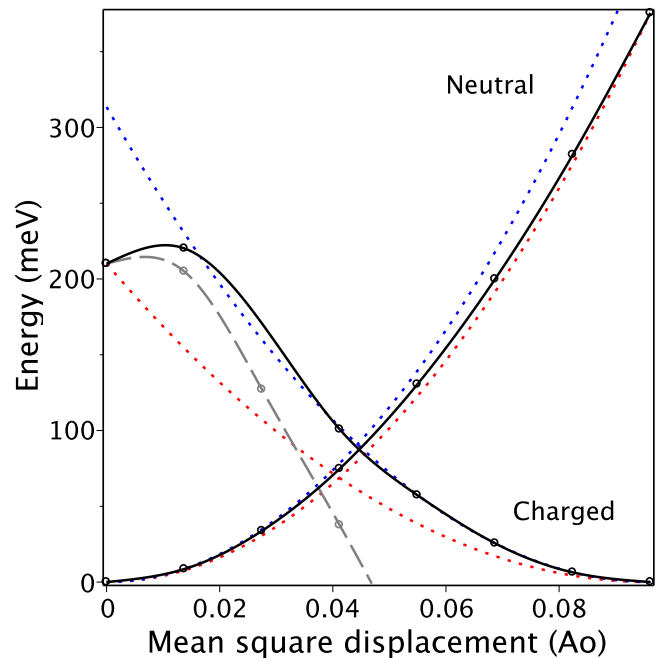
where  $\xi_{\alpha}$  is the dimensionless vibrational coordinate. From this formula it is easy to obtain the relation between electron-phonon couplings and equilibrium displacements:

$$\xi_{\alpha}^{(0)} = -\sqrt{2} g_{\alpha}. \quad (\text{S5})$$

In this way the couplings are computed from equilibrium geometries of the neutral and charged states using vibrational modes of the charged state.

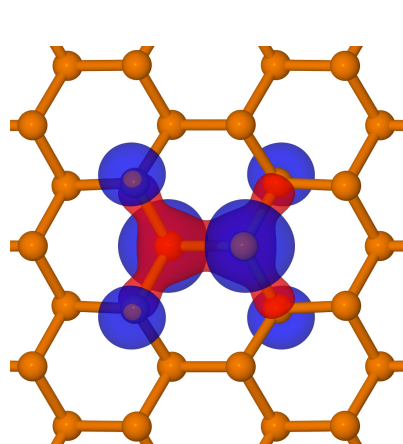


(a)

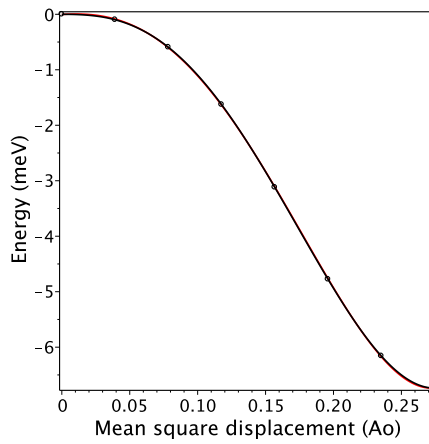


(b)

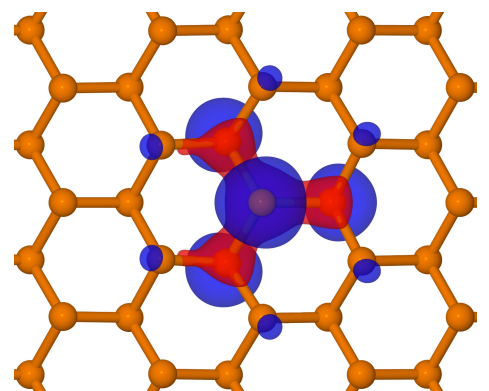
Figure S31: Displacement potential energy surface for the blue-P cluster with (a) 13 and (b) 121 atoms. As the system size grows, there is a substantial deviation from the displaced harmonic oscillator: the asymmetry becomes larger and a qualitatively different state appears at zero displacement. Nevertheless the charged PES remains locally harmonic justifying use of linearized empirical Hamiltonians.



(a)

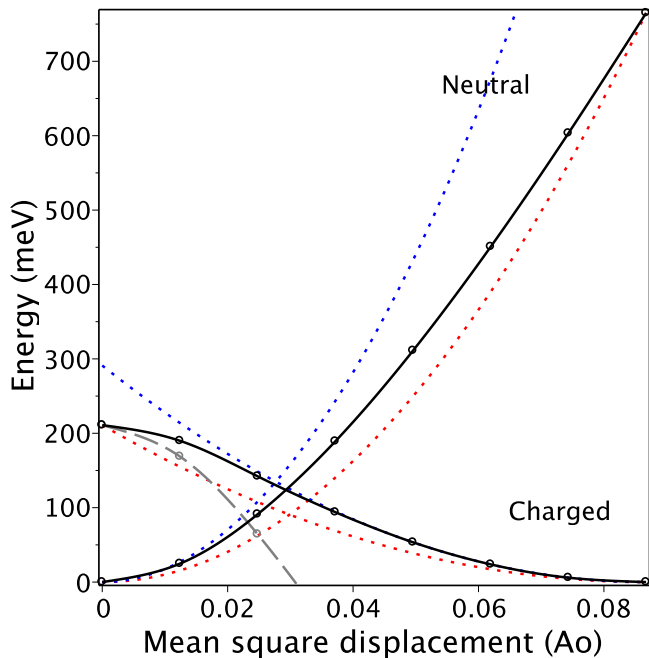


(b)

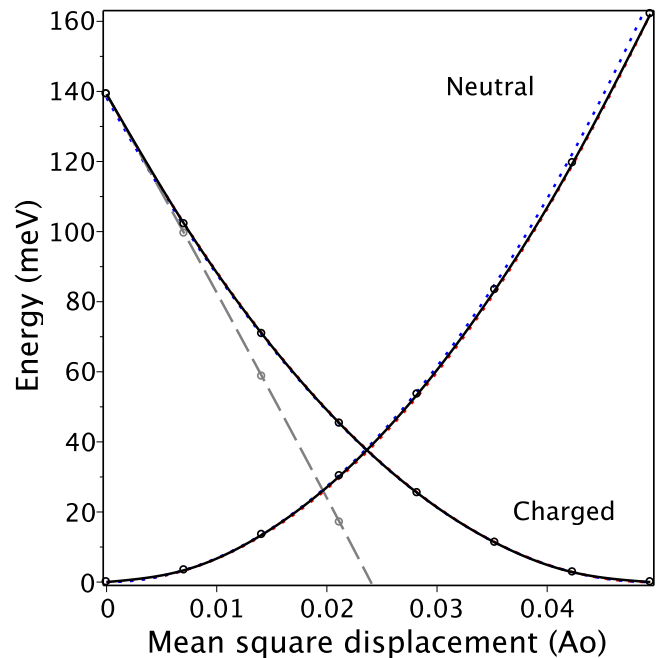


(c)

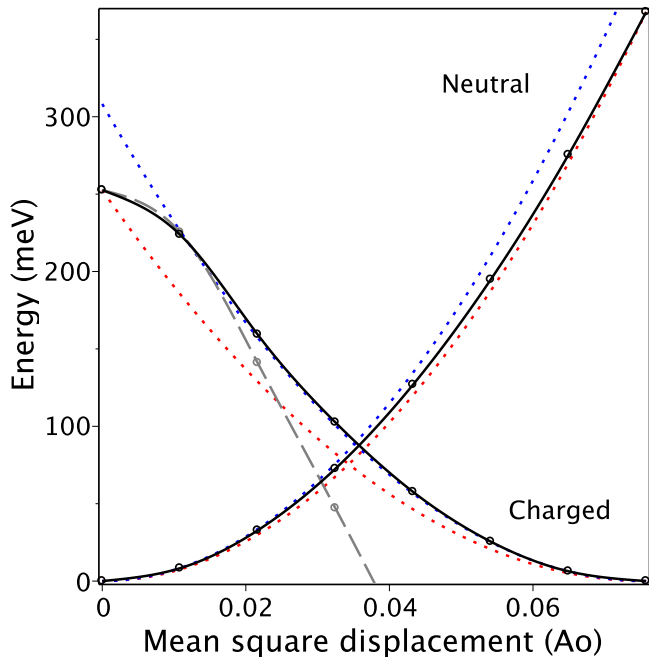
Figure S32: Adiabatic potential energy surface for polaron motion in blue-P: (a) polaron wave-function at saddle point between two minima; (b) linear PES scan between the saddle point and the minimum; (c) polaron wave-function at the minimum.



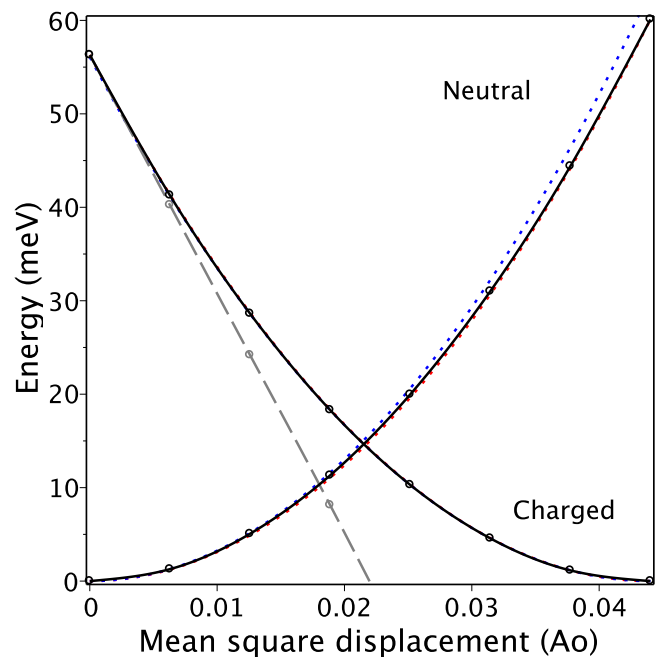
(a) Blue-P anion.



(b) Black-P anion.

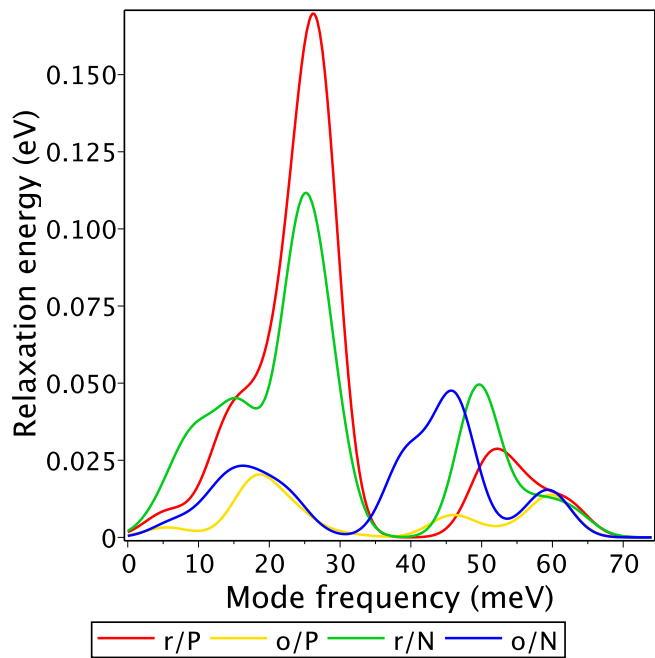


(c) Blue-P cation.

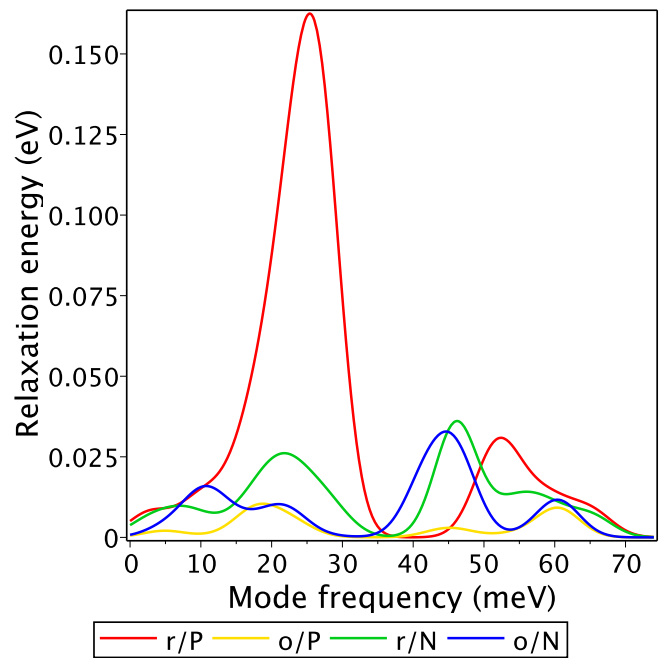


(d) Black-P cation.

Figure S33: Displacement potential energy surface for 42-atom clusters of the two allotropes and the two possible charges.

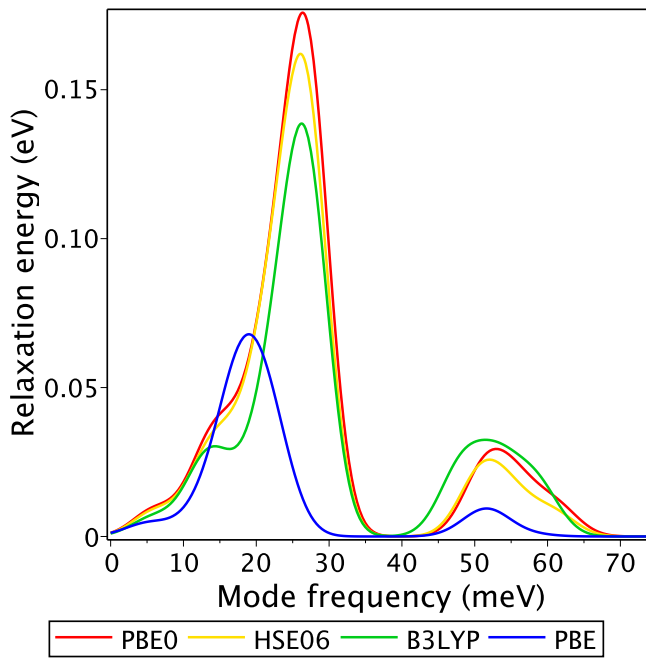


(a) 42-atom clusters.

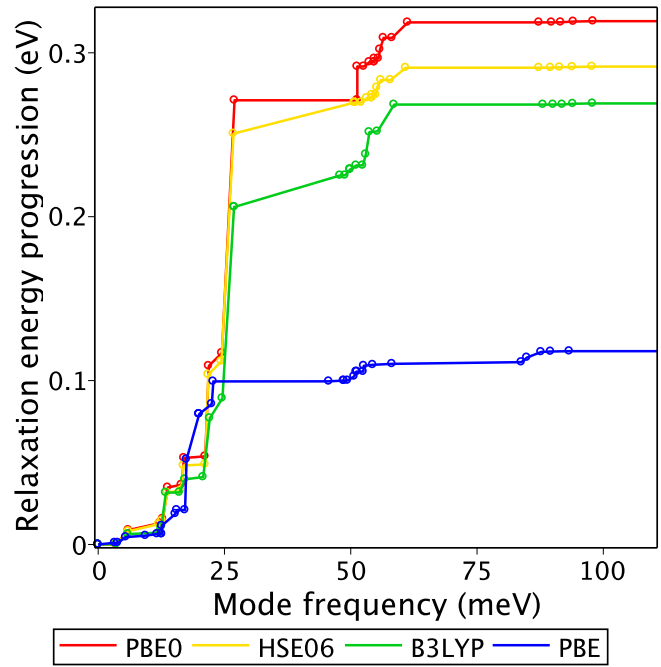


(b) 80-atom clusters.

Figure S34: Spectral decomposition of the polaron harmonic relaxation energy  $\Delta E_{\text{harmonic}}^{\text{charged}}$  for two cluster sizes of blue ('r') and black ('o') phosphorus cation ('P') and anion ('N').

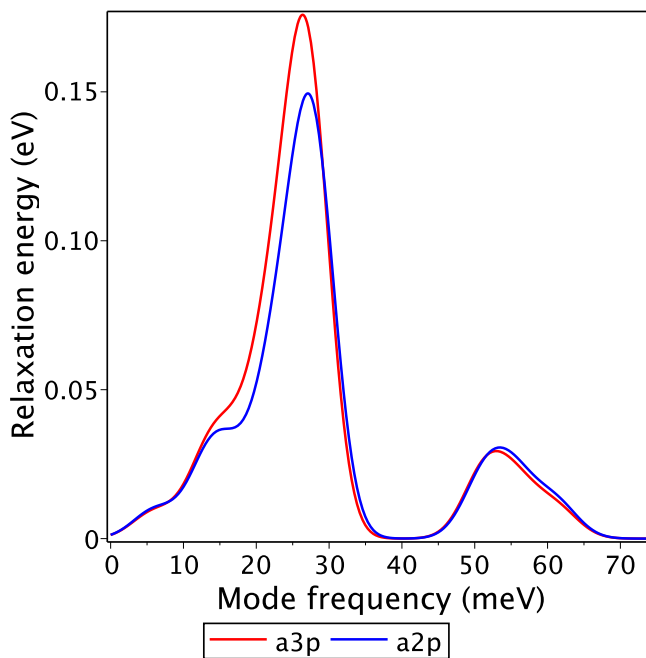


(a)

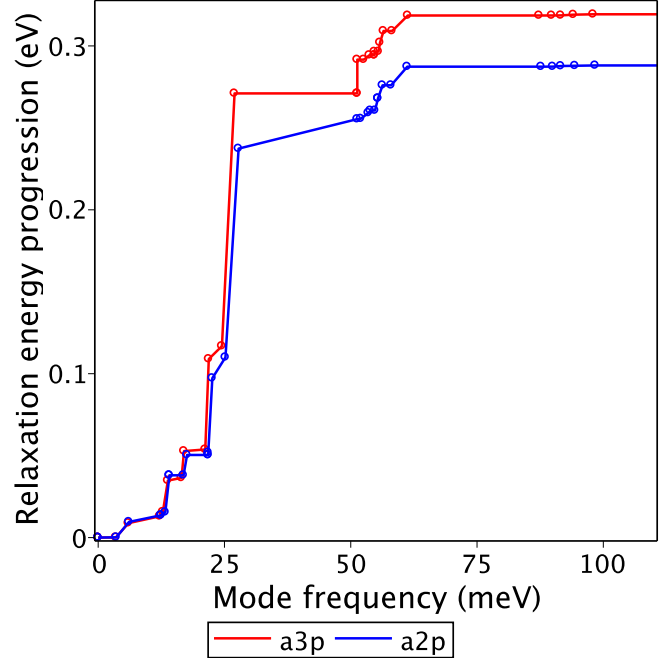


(b)

Figure S35: Dependence of electron-phonon couplings on density functional for 37-atom blue-phosphorene cation.



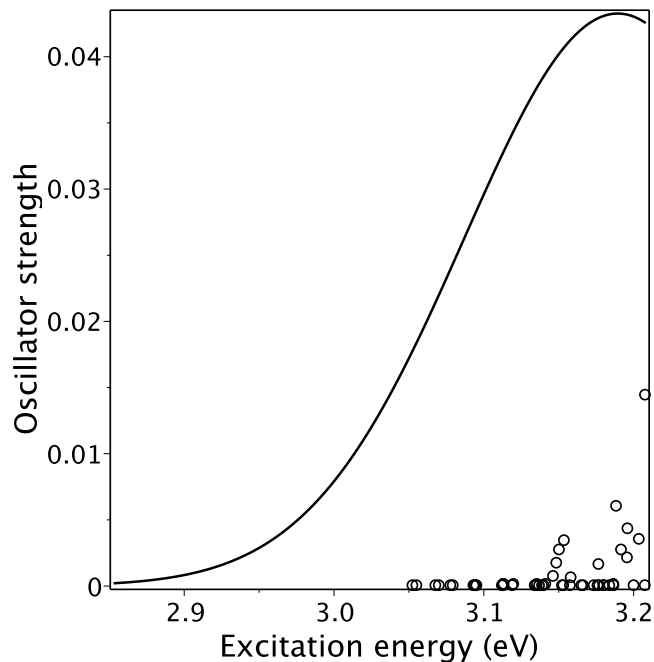
(a)



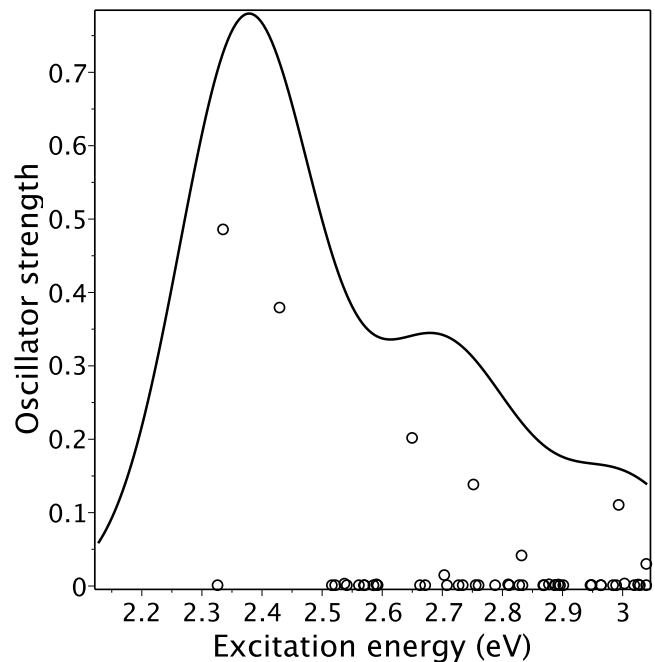
(b)

Figure S36: Dependence of electron-phonon couplings on basis set for 37-atom blue-phosphorene cation. Here 'a3p'=TZVP, 'a2p'=SVP, and the density functional is PBE0.

## S11 Excited states

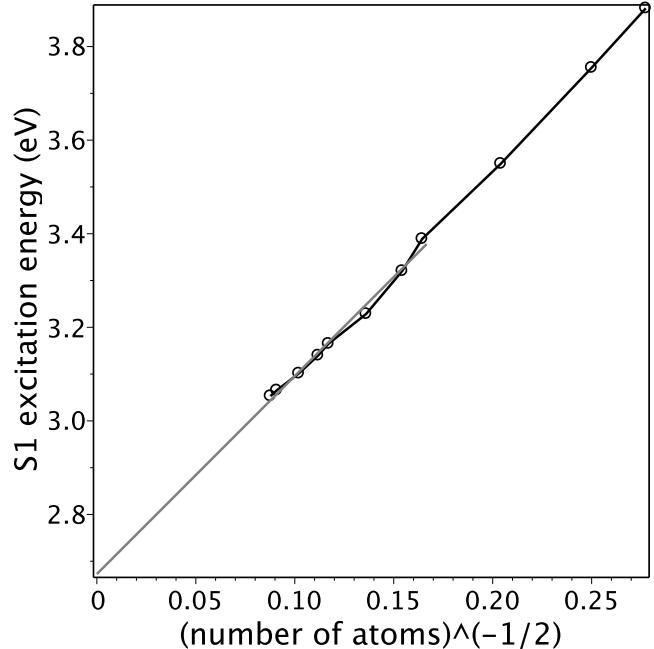


(a) Blue-P.

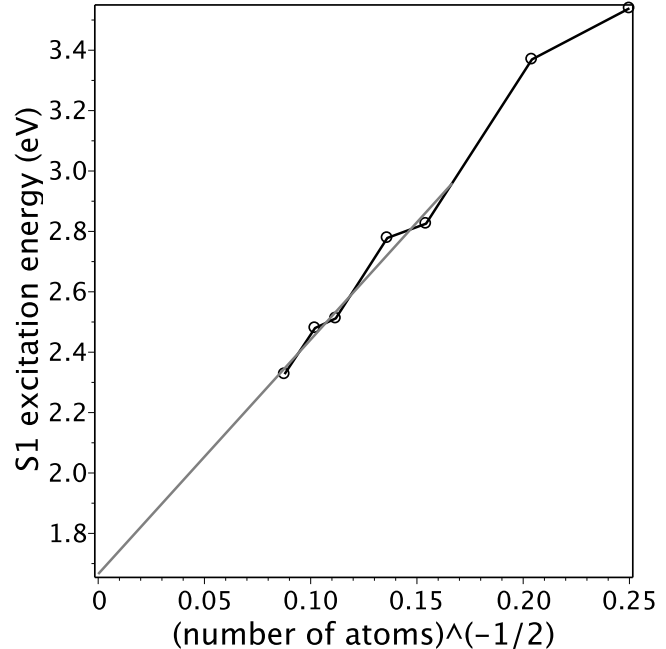


(b) Black-P.

Figure S37: Gaussian-broadened (0.1 eV) oscillator strengths for 50 excited singlets of 130-atom clusters calculated by TDDFT (PBE0/TZVP).



(a) Blue-P.



(b) Black-P.

Figure S38: Size convergence of the lowest excited singlet energy (TDDFT, PBE0/TZVP).

## S12 Triplet exciton

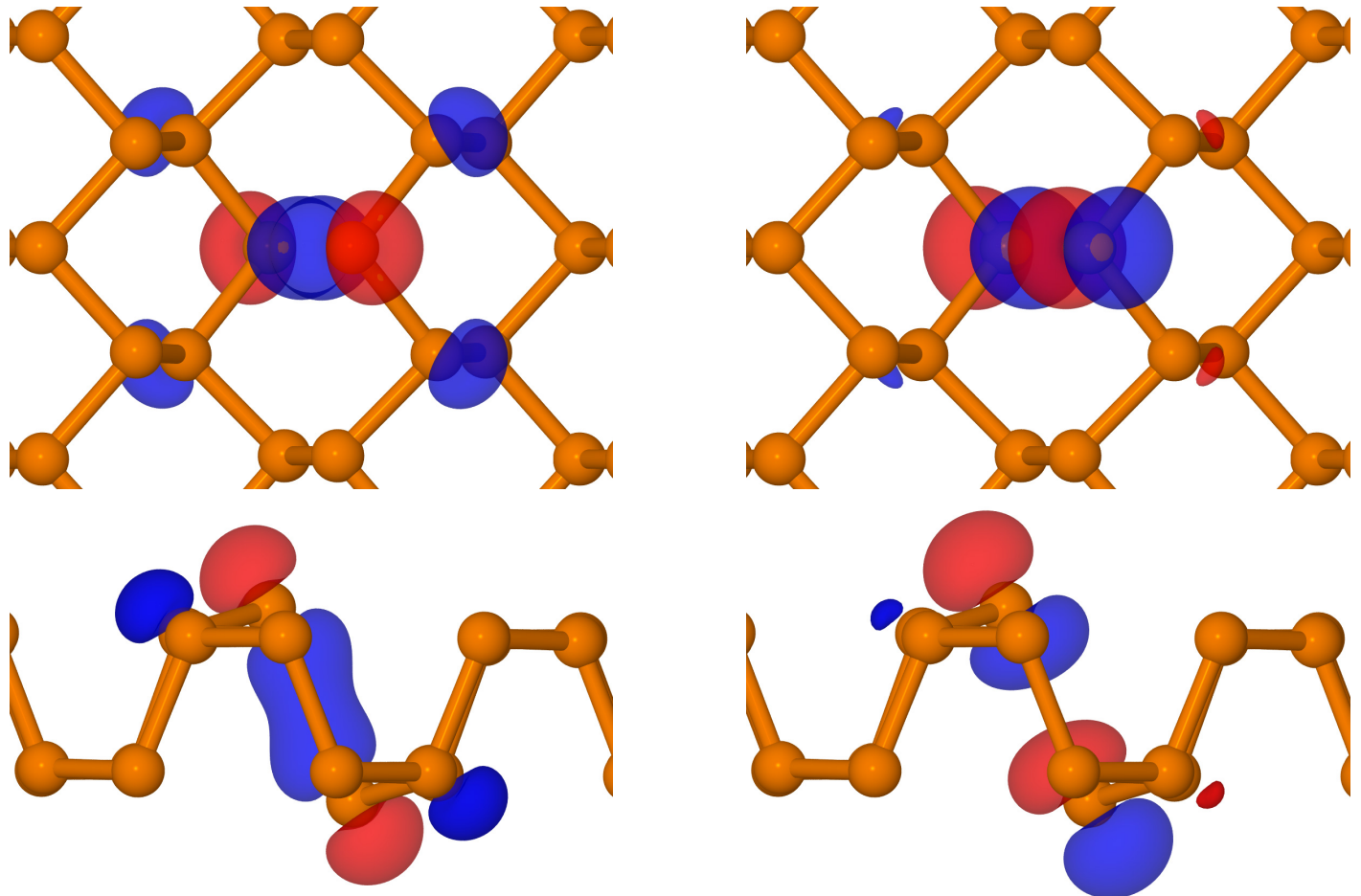


Figure S39: Unpaired natural orbitals of the triplet exciton in black-P.

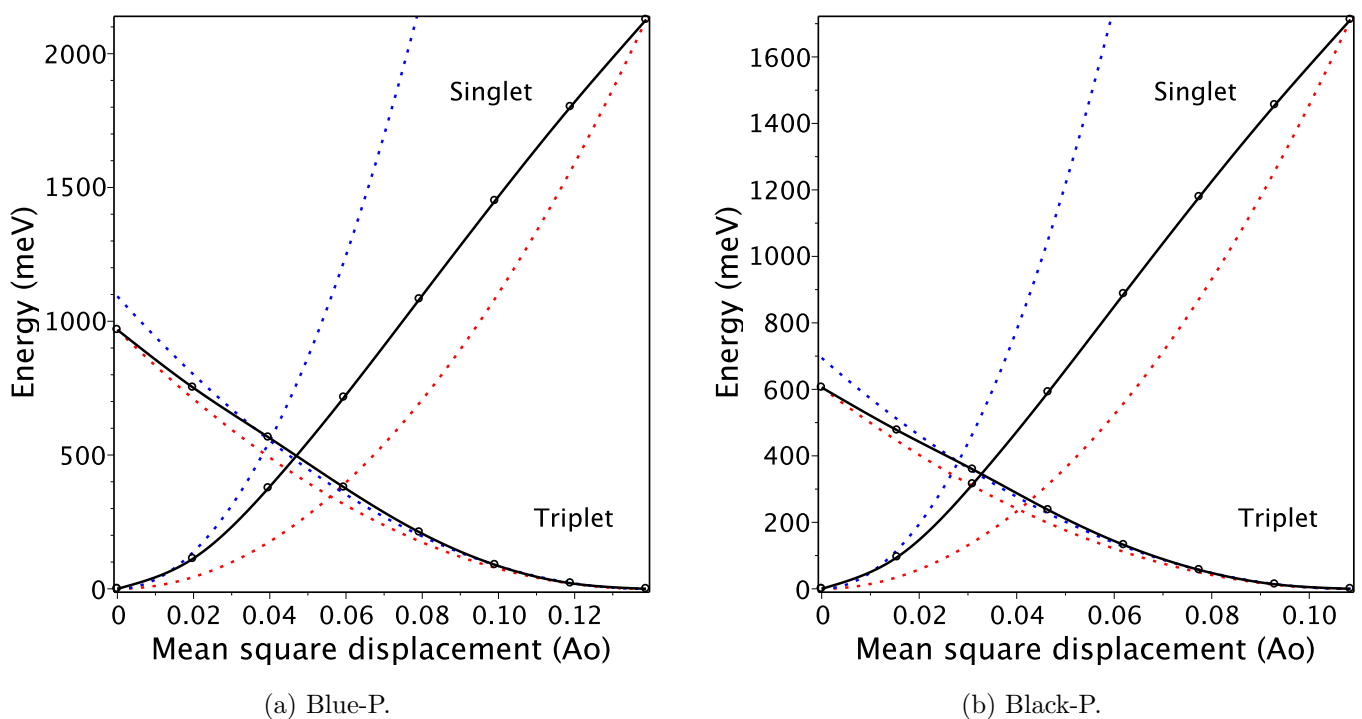


Figure S40: Displacement potential energy surface for triplet exciton for 42-atom clusters of the two allotropes.

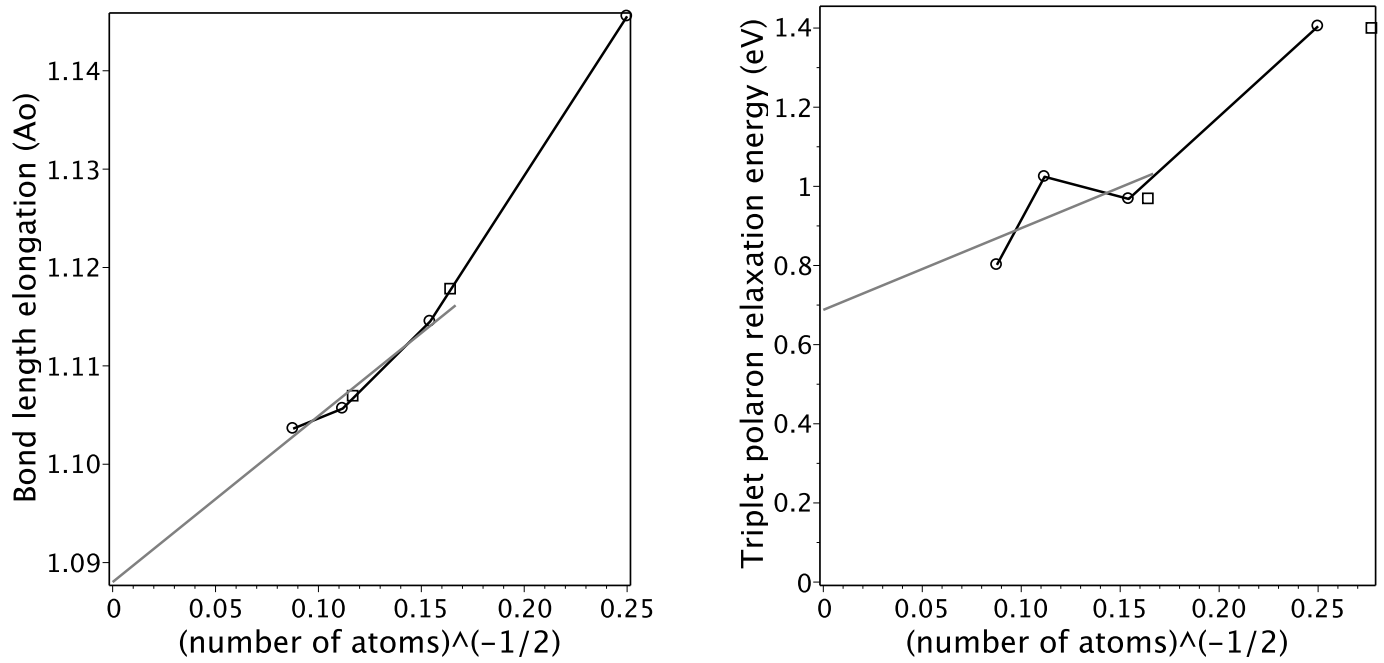


Figure S41: Cluster size convergence of the localized triplet exciton parameters in blue-P.

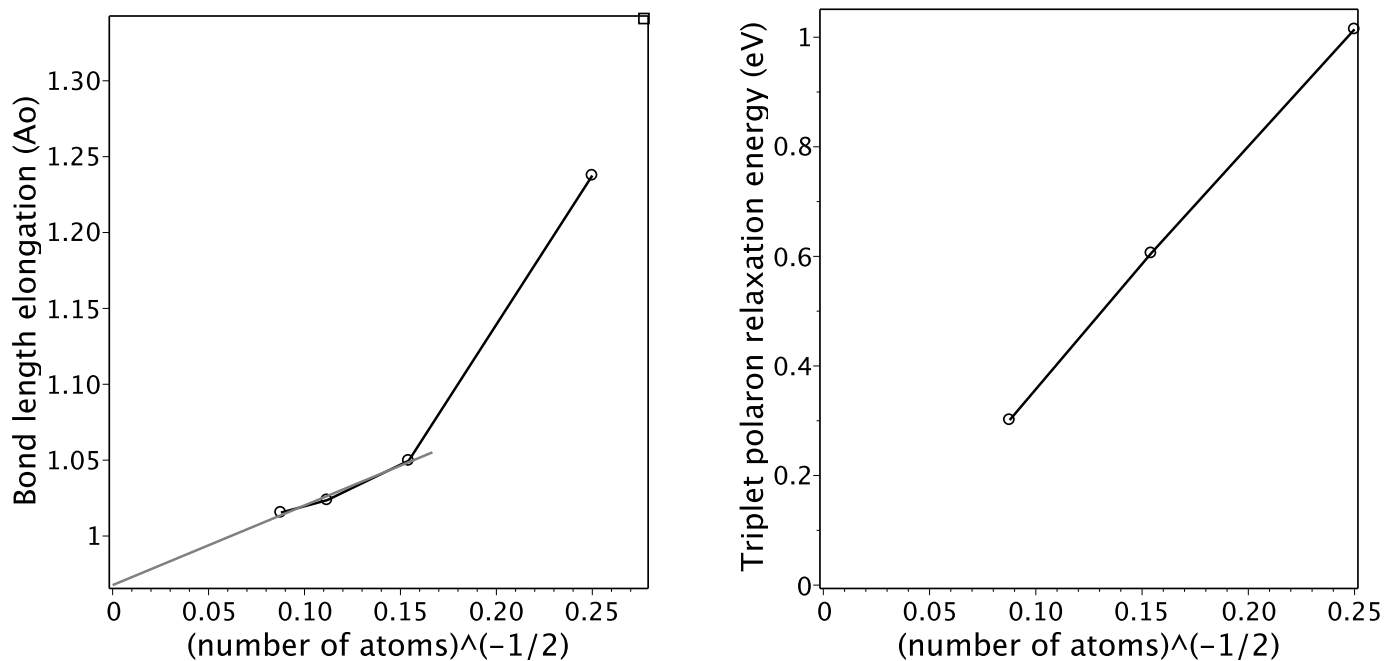


Figure S42: Cluster size convergence of the localized triplet exciton parameters in black-P.

## S13 Results for arsenic

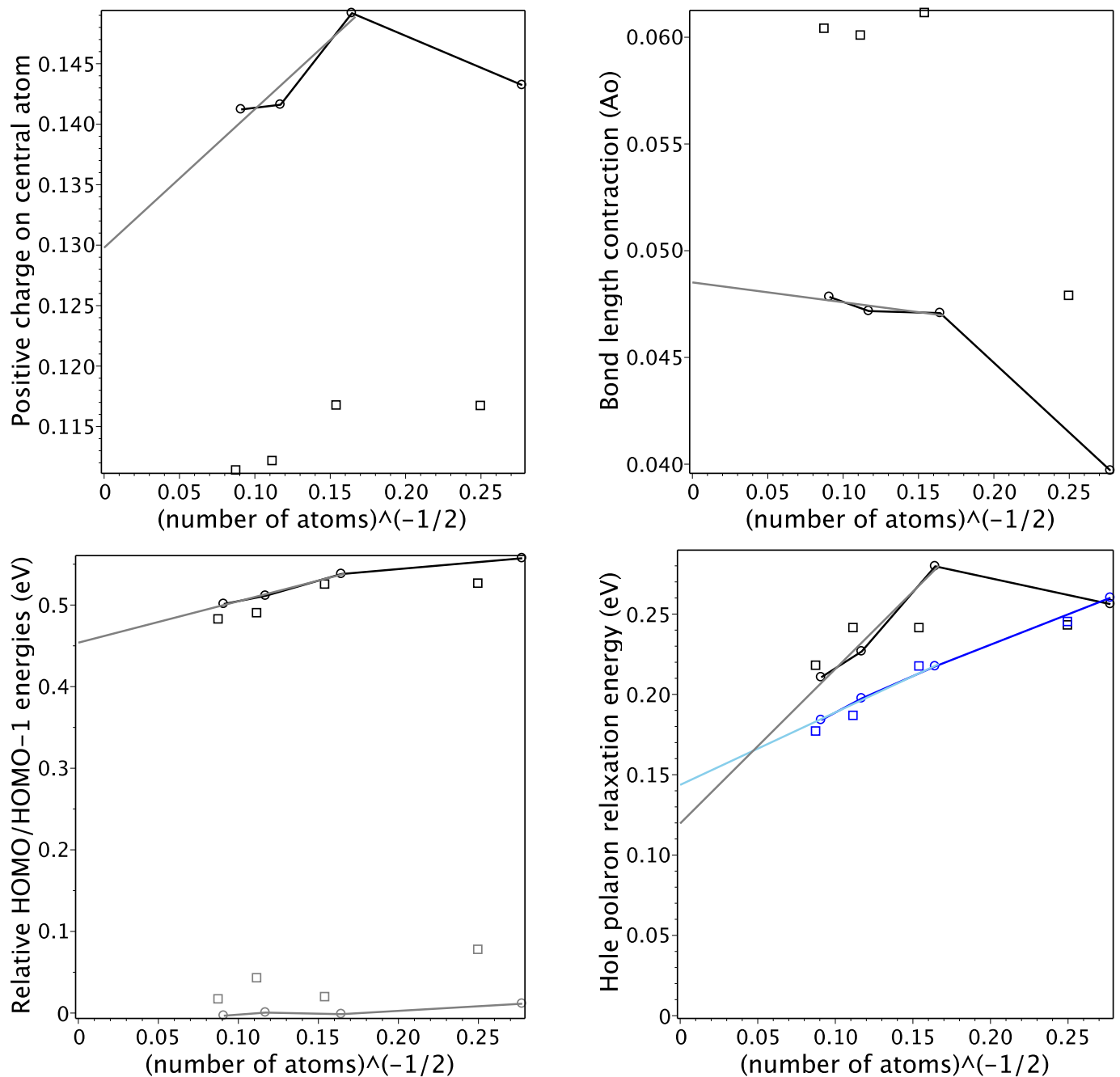


Figure S43: Cluster size convergence of the hole polaron parameters in blue-As (see Fig. 3 for explanation).

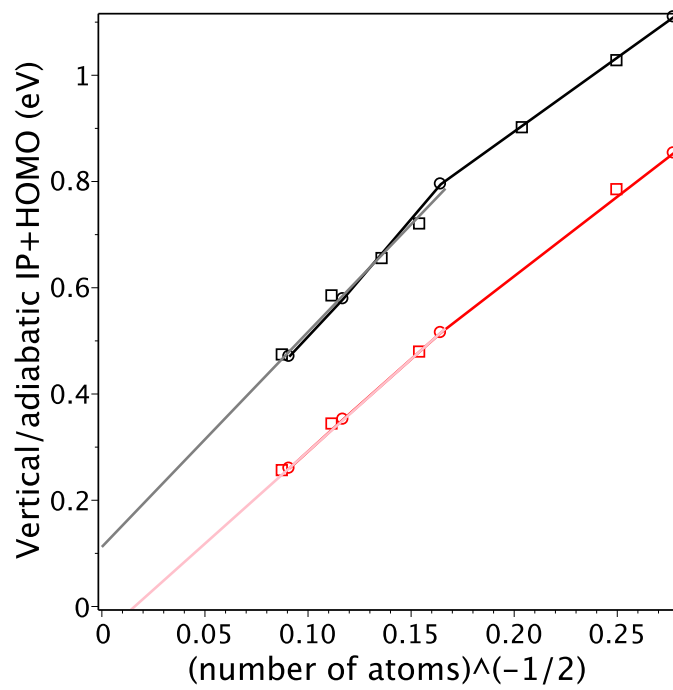


Figure S44: IP+HOMO for blue-As.

Table S8: Main parameters of blue- and black-As monolayers. See Table S5 for notations.

Method	dE meV	bondlengths Å		angles deg		gap eV	HOMO eV	LUMO eV	LP eV	bonding eV	orbitals eV
<hr/> --- paw400 ---											
PBE		2.509		92.0		1.60	-3.54	-1.93			
	37.2	2.496	2.511	94.5	100.6	0.81	-2.56	-1.76		*	
<hr/> --- a3p ---											
PBE		2.506		92.0		1.71	-5.48	-3.76			
	30.0	2.493	2.500	94.5	101.0	0.94	-4.76	-3.82		*	
HSE06		2.479		92.3		2.40	-6.02	-3.63	-17.28	5.00	
	26.9	2.468	2.468	94.7	101.6	1.55	-5.19	-3.64	-16.30	3.60	3.62 *
B3LYP		2.511		93.2		2.93	-6.23	-3.30	-17.47	5.55	
	38.8	2.507	2.493	95.0	103.1	2.09	-5.42	-3.33	-16.56	4.39	4.27 *
PBE0		2.473		92.3		3.02	-6.34	-3.32	-17.55	4.79	
	29.0	2.461	2.461	94.6	101.7	2.21	-5.52	-3.31	-16.52	3.31	3.35 *
<hr/> --- a2p ---											
PBE		2.512		91.8		1.79	-5.53	-3.75			
	27.8	2.501	2.509	94.7	100.5	0.93	-4.78	-3.85		*	
HSE06		2.486		92.2		2.47	-6.11	-3.63			
	26.2	2.476	2.477	94.7	101.2	1.57	-5.28	-3.70		*	
B3LYP		2.518		92.9		2.99	-6.24	-3.25	-17.04	5.54	
	39.0	2.513	2.502	94.9	102.6	2.12	-5.44	-3.32	-16.27	4.52	4.42 *
PBE0		2.481		92.1		3.11	-6.44	-3.34	-17.27	4.86	
	29.0	2.469	2.470	94.6	101.3	2.23	-5.63	-3.40	-16.38	3.52	3.53 *
WB97X		2.466		93.0		6.67	-8.32	-1.64			

## S14 Results for antimony

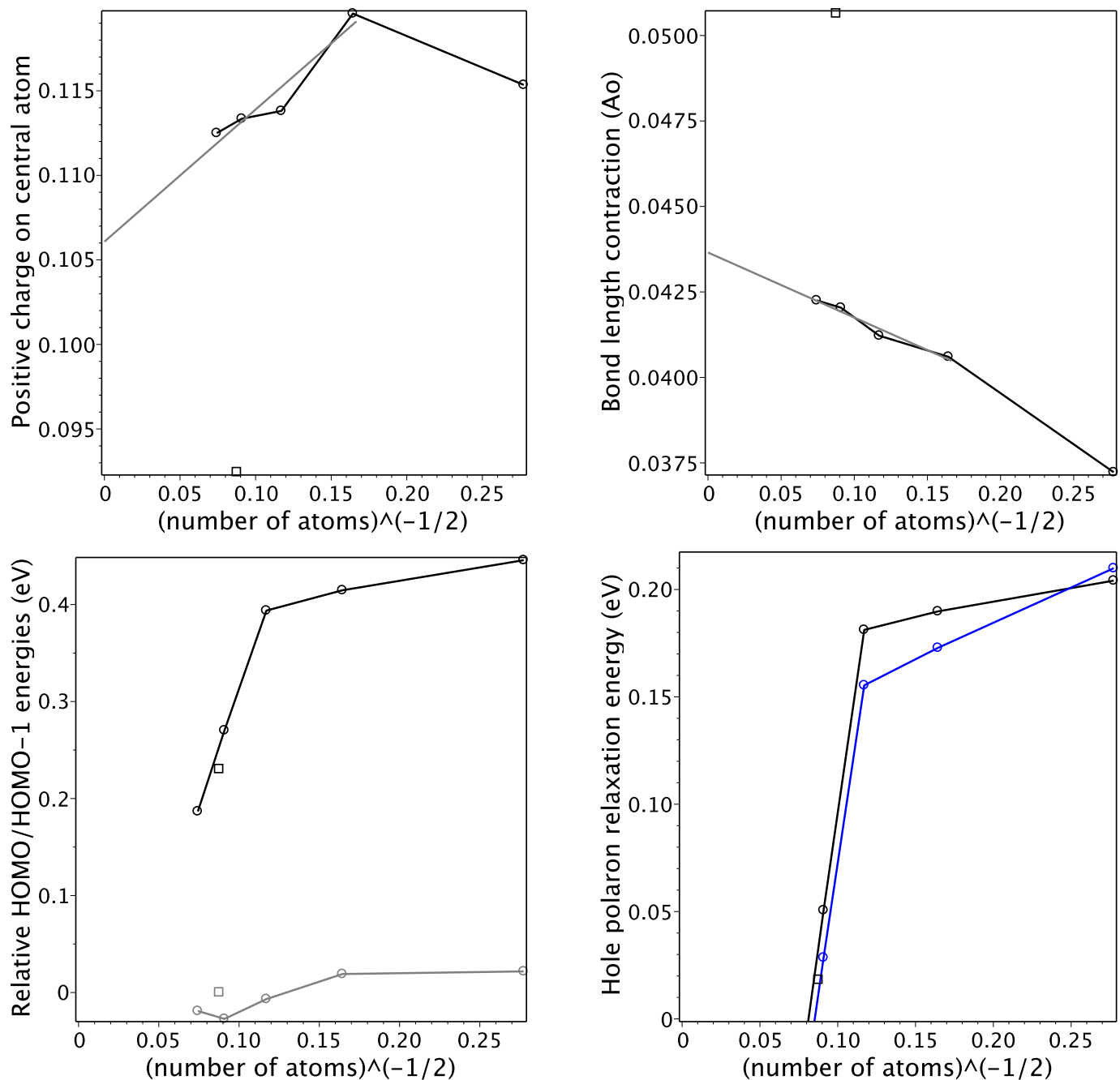


Figure S45: Cluster size convergence of the hole polaron parameters in blue-Sb (SVP basis, no spin-orbit coupling, see Fig. 3 for explanation).

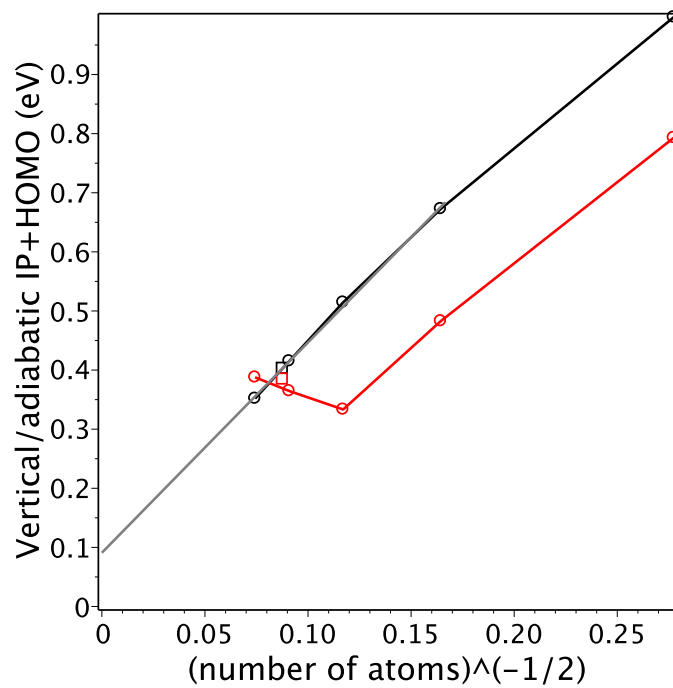


Figure S46: IP+HOMO for blue-Sb (SVP basis).

## S15 Atomic data for pnictogens and related elements

Table S9: Atomic data for pnictogens, their cations and isoelectronic elements from NIST Atomic Spectra Database (DOI:10.18434/T4W30F). Shown here are level energies in eV relative to the ground state except for “spin-orbit” parameter. The latter is defined as the fine structure splitting between the listed level  ${}^{2S+1}L_J$  and level  ${}^{2S+1}L_{J-1}$ . The “exchange” parameter involves energy difference between levels with the same electronic configuration but different spins, which is proportional to the exchange integral between  $p$ -orbitals. The rest of columns characterize relative energies of one-electron orbitals belonging to different shells and subshells:  $s \rightarrow p$  is between valence orbitals and  $p \rightarrow s, p, d$  is between the valence and the next shell. In all these cases the lowest energy excitation is listed; if its symmetry is different from the one indicated in the heading row, the symmetry is listed right to the energy. Multiconfigurational states are combined (the top last column). For heavy elements (Bi and Pb) jj-coupling scheme is used and thus level re-interpretation in LS-coupling is not always obvious.

$s^2p^3$ elements, ground state is ${}^4S_{3/2}^o$					
	spin-orbit ${}^2D_{5/2}^o$	exchange ${}^2D_{3/2}^o$	$p \rightarrow s$ ${}^4P_{1/2}$	$p \rightarrow p$ ${}^2S_{1/2}^o$	$s \rightarrow p, p \rightarrow d, s$ ${}^4P_{5/2}$
N	.001	2.38	10.33	11.60	10.92
P	.002	1.41	6.94	7.96	7.38
As	.040	1.31	6.29	7.46	6.86
Sb	.17	1.06	5.36	6.41	6.63
Bi	.50	1.42	4.04	5.10	5.44
$s^2p^2$ elements and ions, ground state is ${}^3P_0$					
	spin-orbit ${}^3P_1$	exchange ${}^1D_2$	$s \rightarrow p$ ${}^5S_2^o$	$p \rightarrow s$ ${}^3P_0^o$	$p \rightarrow p$ ${}^1P_1$
C	.002	1.26	4.18	7.48	8.54
Si	.010	0.78	4.13	4.92	5.86
Ge	.069	0.88	5.20	4.64	5.70
Sn	.21	1.07	4.91	4.29	5.25
Pb	.97	2.66	—	4.33	5.32
$N^+$	.006	1.90	5.80	18.46	20.41
$P^+$	.020	1.10	5.67	10.74	12.60
$As^+$	.13	1.25	6.80	9.76	11.82
$Sb^+$	.38	1.59	6.41	8.57	10.39
$Bi^+$	1.65	4.21	9.44	8.57	10.45
					—
					9.81
					—

## S16 Dependence on cluster passivation

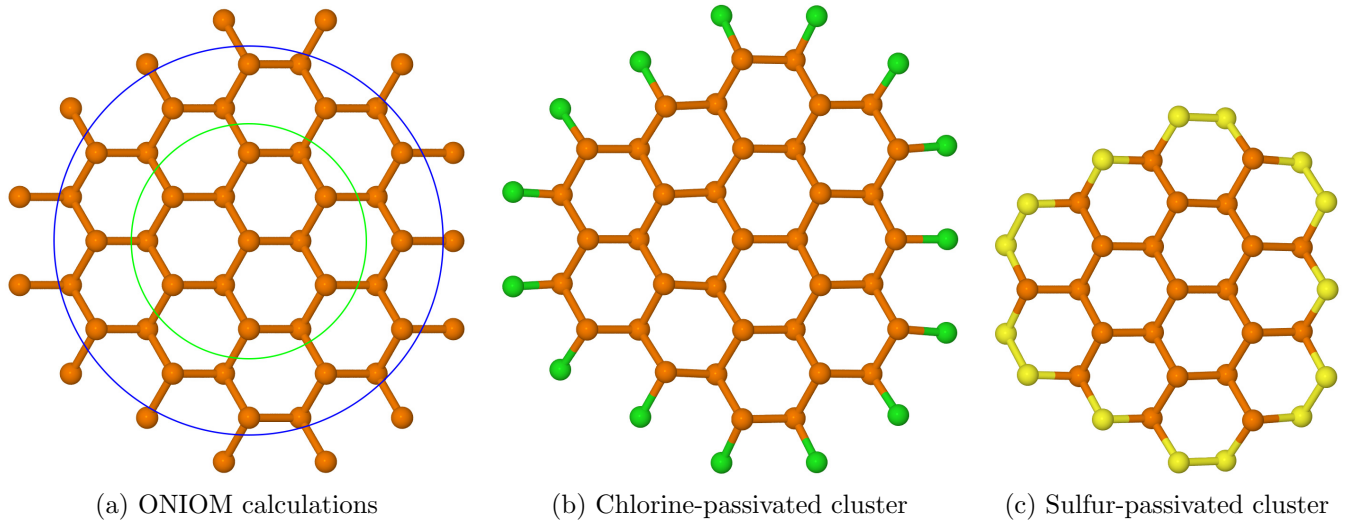


Figure S47: Other passivations considered. The ONIOM calculations are performed with the standard settings of Gaussian 16 program; the molecular mechanics layer includes atoms beyond the blue circle; positions of atoms beyond the green circle are fixed in the infinite monolayer geometry. Note that the interior of sulfur-passivated clusters is compressed because S-S and S-P bonds are shorter than P-P bonds.

Table S10: Dependence of hole polaron relaxation energy on cluster passivation for blue-P. “Charge” is the NAO charge of the central atom. For the largest considered Cl-passivated cluster the wave-function of the undistorted cation has not been converged.

Passivation	Cluster size				Charge
	37	73	121	181	
H	224	161	142	96	-0.0014
ONIOM	232	168	151	105	-0.0015
Cl	257	206	150	—	+0.0007
S	79	92	104	116	+0.0206

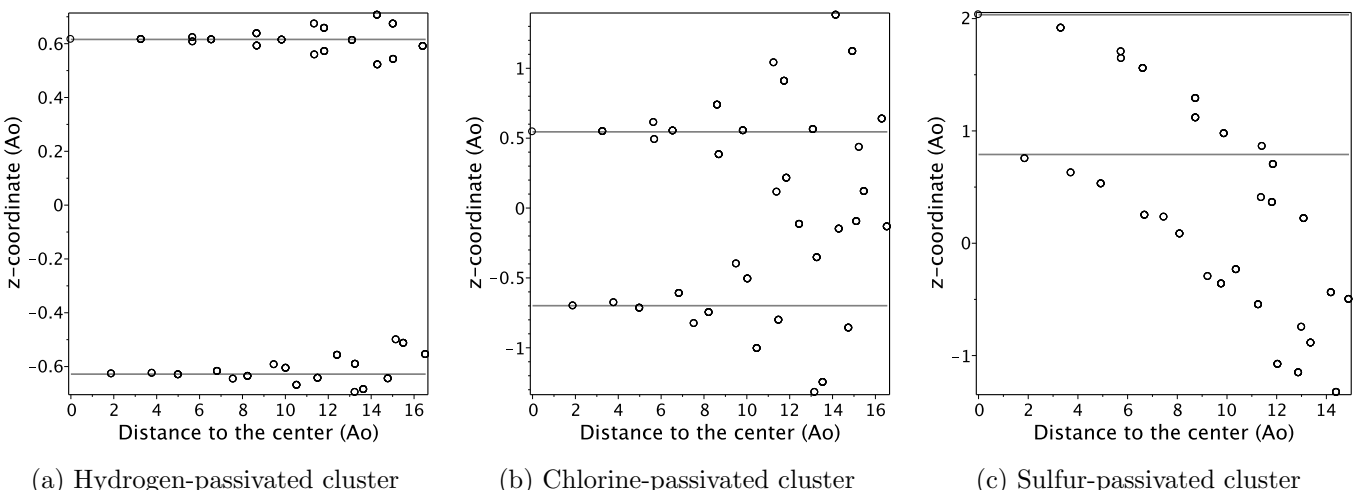


Figure S48: Geometry of the considered clusters (181 atoms): z-coordinate of phosphorus atoms in the orientation of Fig. 1. The gray colored lines show z-coordinates of the infinite monolayer.